Abstracts of the Annual Meeting of Planetary Geologic Mappers, Flagstaff, AZ 2012

Edited by:

James A. Skinner, Jr.
U. S. Geological Survey, Flagstaff, AZ

Kenneth L. Tanaka
U. S. Geological Survey, Flagstaff, AZ

Michael S. Kelley
NASA Headquarters, Washington, DC

NOTE: This is a preliminary posting in advance of the final volume to be published as a NASA Conference Paper. Abstracts in this volume can be cited using the following format:

Graupner, M. and Hansen, V.L., 2012, Structural and Geologic Mapping of Tellus Region, Venus, *in* Skinner, J.A., Jr. and others, eds., Abstracts of the Annual Meeting of Planetary Geologic Mappers, Flagstaff, AZ, June 18-20, 2012.

Report of the Annual Meeting of Planetary Geologic Mappers
Astrogeology Science Center
U.S. Geological Survey
Flagstaff, Arizona
June 18 to 21, 2012

The construction of cartographic products to illustrate the surface characteristics of planetary bodies beyond our own has historically been met with particular challenges. These challenges can be overcome through innovative adaptation to burgeoning data sets and analytical technologies as well as a focused forum within which to present, critique, and discuss both technical approaches and scientific results. To assist, the Annual Meeting of Planetary Geologic Mappers (PGM) provides a unique forum for planetary scientists to address these challenges through the exchange of ideas and experiences relating to the creation, publication, and promotion of planetary geologic maps. PGM 2012 was convened by NASA's Planetary Geology and Geophysics (PG&G) program Geologic Mapping Subcommittee (GEMS) Chair Jim Skinner (U.S. Geological Survey (USGS) Astrogeology Science Center), USGS Geologic Map Coordinator Ken Tanaka, and PG&G Program Scientist Mike Kelley (NASA Headquarters) on June 18 to 21, 2012. The meeting was hosted by the USGS Astrogeology Science Center in Flagstaff, Arizona. This volume contains summaries of PGM 2012 events and discussions, as schedule of presentations, and submitted abstracts (attending and in absentia).

The meeting began with two geologic mapping-based workshops. On Monday, June 18, Trent Hare and Corey Fortezzo (both from USGS) led a GIS workshop and round-table discussion that focused on outlining the recommended workflow for using GIS to complete, submit, and refine planetary geologic maps for USGS publication. The workshop was attended by 17 people, who either shared one of 8 dual-screen computer workstations provided by USGS or used their own laptop computer. This year's installment included discussions of geologic map finalization, line smoothing and topological editing, constructing PDF layouts for printed maps and posters, and additions to the 2010 planetary geologic mappers handbook. On Tuesday, June 19, Thomas Platz and Greg Michael (both from Freie Universität Berlin) led a workshop on crater counting techniques, dubbed "CraterStats Boot Camp." The workshop was attended by 23 people and included discussions on the theory of crater counting, GIS-based tools that facilitate crater counting, methods of determining and interpreting crater statistics, and the role that spatial randomness plays in determining reliable crater-based model ages. Presentations for both workshops can be viewed at http:/astrogeology.usgs.gov/facilities/mrctr/gis-tutorials.

Scientific, programmatic, and technical presentations were held on Wednesday, June 20 and Thursday, June 21. Presentations began with welcoming comments and GEMS remarks by Jim Skinner, an update on the status of mapping projects and publications by Ken Tanaka, and a summary of the current state of the PG&G program generally and PG&G-funded map projects specifically by Mike Kelley. In addition, Justin Hagerty (USGS) gave a presentation encouraging the geologic mapping community to use the resources provided by the Regional Planetary Image Facility (RPIF) network. Trent Hare also gave a report summarizing new functions in GIS and providing an update to renovations to the Planetary Geologic Mapping website, hosted by USGS.

Twenty nine abstracts were submitted to this year's meeting (10 Mars, 5 Venus, 3 Moon, 3 Vesta, 1 Mercury, 1 Europa, and 6 technical). In addition, there were 2 abstracts submitted by Mars Exploration Student Data Teams (MESDT). Of the abstracts submitted, 19 were scheduled for presentations, which focused on ongoing, variously scaled map-based science investigations. Detailed discussions of particular projects were augmented by accompanying hard-copy maps and posters, which were viewed on poster boards set up adjacent to the meeting area. Breaks and poster sessions were planned accordingly. Presentations on Wednesday, June 20 focused primarily on reports of Vesta, Mercury, and Venus mapping projects. A BBQ dinner was

organized by Jim Skinner at Thorpe Park in downtown Flagstaff on Wednesday evening. Presentations on Thursday, June 21 focused on reports of Mars and Moon mapping projects. Attendees also heard summaries of MESDT projects, including details of Martian “cryptic” terrains as indicators of sub-surface water (presented by students from Kickapoo High School, Springfield, MO) and a characterization of Hebes Chasma, Mars as scientifically interesting landing site for a future landed mission (presented by students from Orting High School, Orting, WA).

Science discussions on Thursday were followed by a discussion on various aspects of the current state of the planetary geologic mapping program, including (1) encouraged use of the Mapping, Remote Sensing, Cartography, Technology, and Research (MRCTR) GIS Lab at USGS, (2) means to promote the use of published geologic maps, (3) the general health and status of the planetary geologic mapping program. Locations and dates for the 2013 meeting were offered and tabled for future discussion by GEMS. The meeting ended in the afternoon of Thursday, June 21, 2012.

-SCHEDULE OF EVENTS-

Monday, June 18 – GIS for Map Completion, Submission, and Refinement

Time	Topic
8:30 am	Arrive/Setup
9:00	GIS presentations and exercises
12:00 pm	LUNCH
1:30	GIS presentations and exercises
5:00	ADJOURN

Tuesday, June 19 – CraterStats "Boot Camp"

Time	Topic
8:30 am	Arrive/Setup
9:00	Technical presentations and exercises
12:00 pm	LUNCH
1:30	Technical presentations and exercises
5:00	ADJOURN

Wednesday, June 20 – Planetary Geologic Mappers Meeting

Time	Planet/Body	Topic
8:00 am		Arrive/Setup
8:30		Welcome/Logistics/GEMS Remarks (J. Skinner)
8:45		USGS Map Coordinator Remarks (K. Tanaka)
9:00		NASA HQ and Program Remarks (M. Kelley)
9:30		Regional Planetary Image Facility (RPIF) Updates (J. Hagerty)
9:50		GIS and Web Updates (T. Hare)
10:10		BREAK
10:20	Vesta	*Overview of Vesta quad mapping* (D. Williams)
10:40	Vesta	*Global Mapping* (A. Yingst)
11:00	Vesta	*Numisia Quad* (Av-9) (D. Buczkowski)
11:30		LUNCH (GEMS Meeting)
1:30 pm	Venus	*Niobe and Aphrodite Quads* (V. Hansen)
1:50	Venus	*Tellus Regio #1* (M. Graupner)
2:10	Venus	*Tellus Regio #2* (A. Slonecker)
2:30	Venus	*Beta-Atla-Themis (BAT) region* (L. Bleamaster)
2:50	Mars	*Margaritifer Terra* (S. Purdy-Wilson)
3:10		POSTER SESSION
4:10~		ADJOURN
5:00 – 8:00		BBQ DINNER AT THORPE PARK (SERVED AT 6:00 pm)

Thursday, June 21 - Planetary Geologic Mappers Meeting

Time	Planet/Body	Topic
8:00 am		Arrive/Setup
8:30	Mars	*Global/Scandia Mapping* (K. Tanaka)
9:00	Mars	*Nili/Mawrth* (L. Bleamaster)
9:20	Mars	*Libya Montes* (J. Skinner)
9:40	Mars	*Olympus Mons* (D. Williams)
10:00	Mars	*Arsia and Pavonis Mons* (B. Garry)
10:20		POSTER SESSION
11:00	Mars	*Daedalia Planum* (D. Crown)
11:20	Mars	*Candor Chasma* (C. Okubo)

11:40	Mars	*Runanga-Jörn basin analog* (J. Skinner)
12:00		LUNCH
1:30	Mercury	*Caloris Basin* (D. Buczkowski)
1:50	Moon	*LQ-10* (T. Gregg)
2:10	Moon	*LQ-29* (F. Chuang)
2:30	Moon	*Mare Imbrium Lava Flows* (B. Garry)
2:50		POSTER SESSION
3:30		GROUP DISCUSSION
5:00		ADJOURN

CONTENTS *(sorted by body, then alphabetically by author)*

Technical

Mars Exploration Student Data Teams

A MAP OF THE INTRA-EJECTA DARK PLAINS OF THE CALORIS BASIN, MERCURY. D.L. Buczkowski and K.D. Seelos, Johns Hopkins University Applied Physics Laboratory, Laurel, MD 20723, Debra.Buczkowski@jhuapl.edu.

Introduction: Two Mercury quadrangles based on Mariner 10 data cover the Caloris basin (Fig. 1): H-8 Tolstoj [1] and H-3 Shakespeare [2]. The dark annulus identified in MESSENGER data corresponds well to the mapped location of certain formations [3], primarily the Odin Formation. The Odin Formation is described in the quadrangle maps as a unit of low, closely spaced knobs separated by a smooth, plains-like material and was interpreted as ejecta from the Caloris impact. Schaber and McCauley [1980] observed that the intra-ejecta plains in the Odin Formation resemble the Smooth Plains unit that was also prevalent in the H-8 and H-3 quadrangles outside of Caloris. They state that these plains were included as part of the Odin Formation for mapping convenience.

Crater counts based on MESSENGER imagery indicate that the Odin intra-ejecta plains are younger than the Caloris floor plains within the basin [4,5]. This is inconsistent with the intra-ejecta plains being Caloris ejecta but is consistent with the plains being fingers of the smooth plains unit embaying the Odin ejecta knobs.

However, the intra-ejecta plains are not the same color as the smooth plains in Mercury Dual Imaging System (MDIS) data [3]; while the smooth plains are bright, the intra-ejecta plains are the same dark color as the ejecta knobs. A possible explanation is that the Odin knobs and intra-ejecta dark plains represent two facies of dark basement material excavated by the Caloris impact. Alternately, the intra-ejecta plains could represent a dark volcanic flow, distinct from the bright smooth plains volcanic flow; however, it would have to be a volcanic flow restricted to a region circumferential to the basin. A third possibility is that the intra-ejecta dark plains are a pre-Caloris smooth material (possibly the Intercrater Plains unit) darkened by a thin layer of superposed dark Odin material.

This abstract outlines the progress associated with a new mapping project of the Caloris basin, intended to improve our knowledge of the geology and geologic history of the basin, and thus facilitate an understanding of the thermal evolution of this region of Mercury.

Previous Caloris basin mapping: A detailed analysis of the Odin Formation performed by [5] noted that the unit is easily recognizable circum-Caloris in the MESSENGER data and concluded that the Odin Formation knobs are Caloris ejecta blocks that have been mostly embayed and buried by younger volcanic deposits. They found that MDIS color data supported this hypothesis and divided the formation into two sub-units: knobby plains and smooth plains.

High-resolution mapping of the intra-ejecta dark plains: We are using high resolution imaging data from the MDIS instrument to create a new geomorphic map of the dark annulus around the Caloris basin. We also utilize a principle component map [3] to distinguish subtle differences in the color data. In the principle component map green represents the second principle component (PC2), which reflects variations between light and dark materials. Meanwhile, red is the inverted PC2 and blue is the ratio of normalized reflectance at 480/1000 nm, which highlights fresh ejecta.

We are mapping all contacts between bright and dark materials within the intra-ejecta plains, as determined in the principle component map, as sub-units of the Odin Formation (Fig 2a). All knobs are mapped individually and their color (either dark or bright) is noted (Fig 2b). Ejecta blankets from local craters (both extent and color) are mapped separately (Fig 2a).

All craters are mapped according to a newly devised crater classification scheme. The crater classification used in the Tolstoj and Shakespeare quadrangles [1,2] and formalized in 1981 [6] was based on degree of crater degradation. Our classification scheme includes both degradation state and level and type of infilling. Current classifications include: 1) blue and pristine, 2) fresh but not blue, 3) intact rim and superposed, 4) intact rim and embayed, 5) degraded rim and superposed, 6) degraded rim and embayed, 7) very degraded and superposed, 8) very degraded and embayed and 9) little to no rim.

Observations: The Odin Formation shows two distinct sub-units: a dark sub-unit and a (relatively) bright sub-unit. The dark sub-unit has a higher concentration of knobs, knobs that are both bright and dark and craters that are both embayed and superposed. Meanwhile, the bright sub-unit has a lower concentration of knobs, knobs that are predominantly bright and craters that are fresh and/or superposed. Outcrops of the bright material can be associated with crater ejecta blankets, but are not always.

There is an inherent difficulty in determining if there is an age difference between the dark and bright sub-units. Crater counts on sub-units may be affected by the relatively small size of craters (< 20 km). Recent work by [7] indicates that secondary craters on Mercury can be as large as 25 km. More of the Caloris intra-ejecta dark plains need to be mapped, to provide a large enough area and crater population for viable counting. However, the observation that dark sub-unit craters encompass all crater classifications while bright sub-unit craters are almost uniformly fresh and superposed does imply that the bright sub-unit is younger.

Ongoing work: We continue to identify all craters within the dark annulus surrounding the basin in the MESSENGER MDIS data. Each primary crater is assigned a classification, as discussed earlier. Secondary craters, which usually have morphologies distinct from primary craters and they tend to occur in either clusters or chains, are mapped separately.

Craters identified while mapping are compared to the resultant geomorphic units. The diameters of craters superposed on each individual surface unit are measured and counted, and the area covered by each geomorphic unit is determined. Crater counts will be normalized to a common area of one million square kilometers in order to generate a crater size-frequency distribution (SFD) for each geomorphic unit. The SFDs are plotted on a log-log graph with crater diameter against the normalized cumulative crater count. Younger surfaces have SFDs that plot to the left and below older surfaces and so the relative ages of multiple units can be determined. Statistical uncertainties and plotting techniques will follow the form outlined by the Crater Analysis Techniques Working Group [8].

References: [1] Schaber and McCauley (1980) USGS Map I-1199. [2] Guest and Greeley (1983) USGS Map I-1408. [3] Murchie et al. (2008) *Science 321*, 73-76. [4] Strom et al. (2008) *Science 321*, 79-81. [5] Fasset et al. (2009) *Earth Planet. Sci Lett 285*, 297-308. [6] McCauley et al. (1981) *Icarus 47*, 184-202. [7] Strom et al. (2011) LPSC abs 1079. [8] Crater Analysis Techniques Working Group (1979) *Icarus 37*, 467-474.

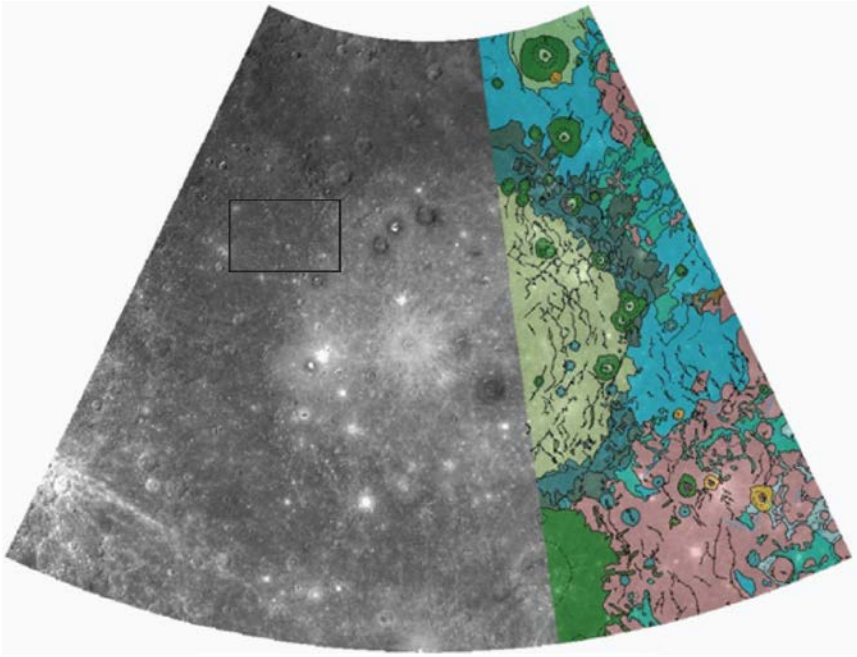

Figure 1. MESSENGER mosaic of the Caloris basin overlain by portions of the H-8 Tolstoj [1] and H-3 Shakespeare [2] quadrangles. Odin Formation is light blue; Smooth Plains are pink. Black box indicates location of Figure 2.

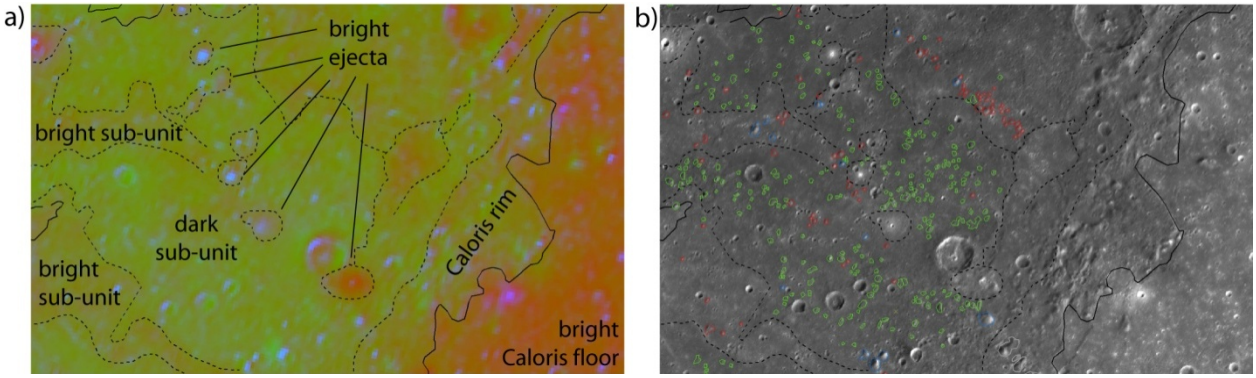

Figure 2. Part of Caloris dark annulus used as Odin Formation example in [5]. a) Principle component map, to demonstrate how bright and dark sub-units were mapped. Sub-units are labeled. b) Odin Formation knobs, shown with sub-unit contacts (dashed lines). Green knobs are dark in the MDIS principle component map; red are light. Note that the majority of knobs are identified in the dark sub-unit.

GEOLOGIC MAPPING OF THE DEVANA CHASMA (V-29) QUADRANGLE, VENUS. L. F. Bleamaster, III[1,2], [1]Planetary Science Institute, 1700 E. Ft. Lowell Rd., Suite 106, Tucson AZ, 85719, [2]Trinity University Geosciences Department, One Trinity Place #45, San Antonio TX, 78212.

Introduction: The Devana Chasma Quadrangle (V-29; 0-25°N/270-300°E) is situated over the northeastern apex of the Beta-Atla-Themis (BAT) province and includes the southern half of Beta Regio, the northern and transitional segments of the Devana Chasma complex, the northern reaches of Phoebe Regio, Hyndla and Nedolya tesserae, and several smaller volcano-tectonic centers and impact craters.

Methodology & Data Sets: Aiming to discover the types of processes that have shaped the Venusian surface, geologic mapping began with the identifciation of major structural and morphologic features (lava flow boundaries, shield fields and edifices, radial and concentric deformation zones) and follows with the formal delineation of geologic map units. Temporal constraints are determined by embayment and cross-cutting relations as well as crater morphology and crater halo modification and degradation [1].

All data used were acquired during NASA's Magellan mission (operational 1989-1994) and includes: Synethic Aperture Radar (SAR; basemap provided by the United States Geoloical Survey at 75 meter/pixel), altimetry and reflectance (~10 x 10 km footprint), and emissivity (~20 x 20 km footprint). Mapping is facilitated with the use of a georeferenced digital synthetic stero (red-blue anaglyph, which merges SAR and altimetry together). ESRI ArcGIS software is used along with a WACOM Cinitiq 21 inch interactive monitor and digitizing pen; important geological features are digitized and attributed in the ArcGIS geodatabase as a location feature (point), linear feature (line), or geocontact (polyline features that will be converted into polygon features at a later time). While the published map scale will be 1:5M, linework is constructed at a scale larger than the published scale. Location features and linear features are mapped at a scale of 1:300,000; geocontacts are mapped at a scale of 1:500,000. Excess linework (i.e., very closely spaced lineament sets) may be edited prior to printed map publication but will be presereved in digital archives. The accuracy of the linework is controlled using streaming (500 map units) and snapping tolerances (set to 250 map units). Upon the completion of mapping, the geodatabase within the ArcGIS will allow for efficient data analysis.

Tessera: Geologic contacts are drawn in order to define individual geologic units. In the case of tessera, geologic contacts mark regions of highly deformed material characterized by intersecting structures. In the Devana Chasma Quadrangle, tessera are typically high standing regions with a polygonal, mosaic-like surface, and are located predominantly to the east of Devana Chasma. Tessera units are easily recognized in the SAR by their distinct polygonal surface and bright radar properties, however, altimetry and derived slop maps, are also useful in defining their boundaries, particularly when isolated as kipuka within the plains. Two major tessera units are defined in V-29 (Nedolya Tessarae and Hyndla Regio), each is part of much larger tessera provinces located outside of the V-29 cartographic boundaries. In addition to the two large tessera units, several smaller outliers, or kipuka, of tessera are found throughout the V-29 quadrangle; structural trends within some kipuka clearly domonstrate a genetic origin to the larger tesserae tracts, hence they represent lateral extensions of tessera underneath embaying plains and flows.

Within the Nedolya and Hyndla tessera units, localized lowlying areas exhibit a dark radar characteristic of intra-tessera plains. We hypothesize two possible scenarios for this dark material. The first possibility is that the material is produced by shields within the tessera. The second is that dark plains material flowed through the troughs seen in the tessera and infilled the low-lying areas. Both of these possibilities require that the dark material be younger than the bright tessera unit. Although timing is clear, identifying pathways for these materials to or from the plains is difficult given the best available radar and tographic resolutions.

Volcanic Features. Contacts have been drawn to define the major volcanic edifices found in the V-29 quadrangle including Beta Regio and the smaller Tuulikki Mons (diameter of approximately 1000 kilometers). The contact around Beta Regio is well defined in places by lobate lava flows that superimpose the surrounding plains units. However, the bright radar charactreristic of Devana and Zverine Chasmata southwest of Beta Regio (due to higher density of structural lineaments) interferes with individual flow boundaries making the contact difficult to follow; the contact here is inferred. The contact to the southeast of Beta is defined by a transition from mottled terrain with fractures, which radiate outward from Beta, to homogenous plains with polygonal lineaments. Shield clusters roughly follow this boundary and may indicate

a transition in the types of volcanic processes at work. The contact around Tuulikki Mons is largely defined by flow aprons that superpose the plains and/or interfingered with flows from other volcanic centers. Flow arrow symbology has been used to indicate where flow margins are clearly visible and can be traced to their source(s).

A variety of small volcanic edifices (< 20 km in diameter) are present in the V-29, including: densely populated shield fields, pancake domes, edifices with scalloped margins and flat-topped relief, edifices with steep margins and concentric flat-topped relief and a cratral center, and edifices where radar backscatter suggests a more conical shape. It is unclear whether there is a relationship between the types of volcanic edifices present and the difference in terrain between the eastern and western regions of the V-29 Quadrangle. However, it is clear that there is a difference in the concentration of small volcanic edifices between these two regions. The concentration to the west of Devana Chasma is ~1.4 volcanoes/10^6 km^2 whereas the concentration to the east is ~0.73 volcanoes/10^6 km^2. Beta Regio and the rift itself have small, localized, densely clustered shield fields but the overall concentration and distribution is difficult to determine because of the lack of radar contrast in these "bright" terrains.

Devana Chasma. The most prominent feature, and hence namesake of the V-29 quadrangle, is Devana Chasma - a narrow (~150 km) 1000 km long, segmented topographic trough (1-3 km deep with respect to the surrounding terrain), which accommodates 3 to 9 kilometers of extension [2]. Devana Chasma is one of three radiating arms of tectonic lineaments that trends south from Beta Regio and marks a physiographic divide between the relatively young Beta-Atla-Themis province to the west and the older highlands and plains to the east according to Average Surface Model Age (ASMA) [3,4]. Near the center of the map area (10°N, 283.7°E), Devana Chasma's northern lineament suite decreases in lineament density and changes trend to the southeast where it meets the southern section of Devana Chasma which trends due north. Preliminary mapping delineated major structural trends (mostly large normal faults, which agreed with previous investigators [5-8]). Although cross-cutting relations between structures and flows are inconclusive with respect to timing, new, detailed structural mapping reveals evidence to support a temporal distincition between between the northern and southern structural segments. Based on the orientiaton of "rift" segments, distinciton between three possible formation scenarios can be tested: 1) the segments formed synchronously creating the bend in the chasma simultaneously, 2) the northern segment formed first, and the southern segment deflected toward the north, by "feeling" the regional stress and pre-existing weaknesses due to earlier rifting from Beta Regio in the north, or 3) the reverse, with the southern section forming first (the preferred interpretation [9]; see below). Extrapolating this interpreatiaon also carries implications for timing of tectonic activity steming from the volcanic centers near

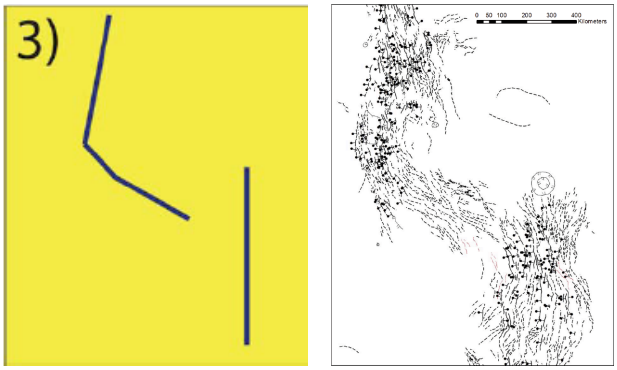

Beta (north) and Pheobe (south) Regiones.

Craters. There are 19 impact craters in the V-29 Quadrangle that range in size from 2.8 km to 102.2 km in diameter [10]. The ejecta from craters is identified by its bright radar characteristics; however, many craters also exhibit more diffuse ejecta with darker radar properties that radiate farther from the center of crater than the bright ejecta and have been assigned to a second ejecta unit. Lava flows, which may have formed during the time of impact are also seen and mapped as crater flow material (i.e., Rosa Bonheur and Boivin Craters.

References: [1] Basilevsky, A.T. et al. (2003), *Geophys. Res. Lett. 30,* doi:10.1029/ 2003GL017504. [2] Keifer, W.S and Swafford, L.C. (2006) *J. Struct. Geo., 28,* p. 2144-2155. [3] Phillips, R.J. and Izenberg, N.R. (1995) *Geophys. Res. Lett., 22*, p. 1517-1520 [4] Hansen, V.L. and Young, D.A. (2007) Geological Society of America Special Paper 419, p. 255-273. [5] Stofan et al. (1989) *GSA Bull. 101*, p. 143-156. [6] Solomon et al (1992) *J. Geophys. Res., 97,* p.13,199-13,255. [7] Foster and Nimmo (1996) *EPSL 143,* p. 183-195. [8] Connors and Suppe (2001) J. Geophys. Res., 106, p. 3237-3260. [9] Shaw, B.G.R., (2012) Senior Honors Thesis, Trinity University. [10] Herrick, R.R. et al., (1997) in *Venus II,* p.1015-1046.

STRUCTURAL AND GEOLOGIC MAPPING OF TELLUS REGIO, VENUS. M. Graupner and V. L. Hansen, Department of Geological Sciences, University of Minnesota, 1114 Kirby Drive, Duluth MN, 55812, USA, graup044@d.umn.edu

Introduction: Tellus Regio, commonly referred to as Tellus Tessera, is one of five prominent crustal plateaus on Venus. Tellus Regio, centered at 42.6N/76.8E, is nearly oval with a slightly smaller and tapered southern part, has a long axis dimension of ~2300 km, is bordered by lowlands, and sits ~2-3 km above the regional plains with the highest elevations in the eastern, western, southern portions, and steep eastern and western margins and gently sloping northern and southern margins [1, 2]. The northern margin of Tellus Regio is not well defined and may represent a transitional area with the lowlands. North-central Tellus is host to a low-lying interior showing complex surface deformation. High resolution SAR data reveals an overall rough surface topography on Tellus Regio marked by ribbon tessera terrain (Fig. 1). In an effort to understand the formation of Tellus Regio geologic and structural mapping of southern Tellus (43N/73-90E, 26N/74-86E) is underway.

Methods: *Mapping*. Mapping of this region employs Magellan SAR and true stereo images in Adobe Illustrator™. Eventually, the georeferenced map result will be imported into GIS space in order to be compared to other map areas, as well as allow for analysis using GIS toolkits.

Wavelength Analysis. Structural wavelengths of suites of folds, ribbons and graben complexes are measured across the region.

Geologic Relations: The eastern and western margins of Tellus Regio are bound by long-wavelength folds (25-150 km) with crests parallel to the plateau margins and lengths up to 750 km (Fig. 1) [3]. The southern margin is dominated by folds with NE-trending crests cut by fold crest-orthogonal graben. Much of the interior of Tellus Regio appears as radar bright surfaces indicating rough surface topography, although several radar-dark basins are distinguishable throughout the plateau. The interior shows complex deformation created by structures such as multiple wavelength folds, ribbons, and graben. Structural lows associated with a wide range of structures are buried (most likely by lava fill), forming basins of variable sizes and shapes (commonly elongated). The majority of large basins (~90-125 km long axes) occur along the boundaries and within the southern portion of the plateau, whereas smaller basins (~50 km long axes) are distributed throughout the interior. Some basins lack post-flooding deformation, whereas others show reactivated and imposed structures. The presence of local basin fill at all structural wavelengths indicates that layer contraction and extension, and flooding occurred broadly synchronously.

Mapping also reveals fold wavelengths that include small wavelengths, <1 km down to the effective data resolution, which have not yet been mapped across Tellus Regio. Small- (<5km), intermediate- (5-25km) and long-wavelength (>25km) folds are consistently distributed throughout Tellus, defining a fluid-like pattern lacking sharply demarked domain boundaries [3]. Extensional structures, which typically trend orthogonal to fold crests, include shear fracture ribbons (1:25 length:width ratio) with wavelengths of 2.5 km. Graben complexes (1:3.5 length:width ratio) show spacing of ~30 km. Ribbon structures typically cross-cut small-wavelength folds; graben complexes dissect long-wavelength folds.

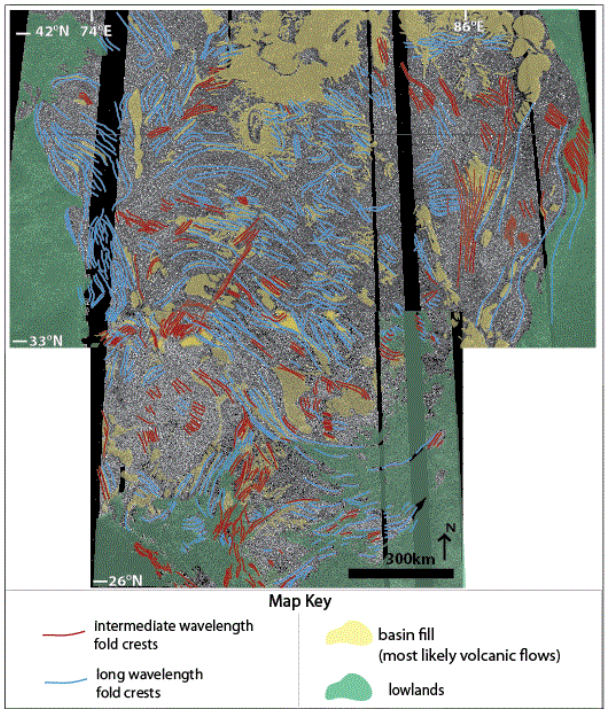

Fig. 1. Preliminary structural geologic map of southern Tellus Regio illustrating the distribution of intermediate- and long-wavelength fold crests, describing a coherent fluid-like pattern across the plateau.

Comparison with previous studies: SW Tellus was previously subdivided into structural domains including an indenter, fold belt, crustal plateau interior, and NW and SE marginal domains (Fig. 2) [4, 5, 6].

However, the results of the current study reveals that areas dominated by a specific type of structural fabric extend beyond the proposed domains (Fig. 2). Distinct regions demarking possible stratigraphic and tectonic domains are not clearly identifiable based on fold and basin trends [4, 5, 6].

Domain A, 'the indenter', shows fewer intratessera basins (ITBs) than the other domains, but ITBs occur across the domain. Intermediate-wavelength fold crests of domain A, B and C are all parallel. Long-wavelength folds in the SE part of domain A parallel long-wavelength folds in the S part of domain B.

Domain B, 'fold belt', includes two regional orientations; the N portion displays structural and ITB trends parallel to those in adjacent parts of domains A and C. The S part of B shows trends parallel to structures in the SE part of A and the NW part of D, both adjacent domains. Ribbons trend normal to fold crests, thus trending NE in the N part of B and NW in the S part of B.

Domain C, 'the plateau interior', is host to ITBs and fold crests that trend NW, parallel to fold crests and ITBs in the adjacent part of B. Short- and intermediate-wavelength folds parallel long-wavelength folds; ribbons trend normal to fold crests.

Domain D shows mostly lowland interaction. Along the boundary with domain B the orientation of fold crests begins to gradually change form parallel to B domain trends (NNE) to more E-trends in the east, marking the dominant trend within domain D, marked by long- to intermediate-wavelength folds. Ribbons general trend normal to local fold crests.

Domain E is characterized by NNW fold trends; the boundary between E and C is at a high angle to all surrounding structural wavelengths. Long-wavelength fold crests depict a change in orientation across the proposed boundary, although not demarcating the proposed boundary in any obvious way.

From these preliminary mapping results it is not clear how the boundaries between domains A-E were defined; no exact correlation between the geologic map and these domains can be made.

Implications: The importance of structural wavelength is related in part to layer thickness, which, in the case of Tellus, increased with time, with subsequent amplification of both contractional and extensional structures. Strain became more partitioned over time, which coincided with an increase in mechanical layer thickness [7, 8], resulting in wider spaced wavelengths. Throughout this time, lava leaked to the surface flooding local structural lows, which formed local basins. The surface evolution (deformation and flooding) point to an extremely high geothermal gradient across all of Tellus Regio, as suggested by other works [5, 6], allowing for the early formation of fold and ribbon structures with wavelengths <1km. With time cooling led to increased layer thickness, yet the surface retained mobility. The size of the area, the coherent pattern of extensional and contractional structures and flooding over the area is consistent with the lava pond hypothesis of crustal plateau evolution [8].

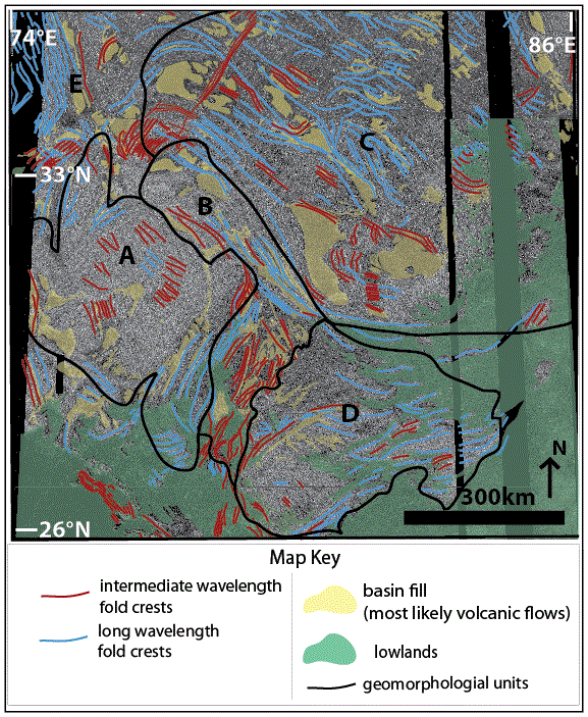

Fig. 2. Subset of SW Tellus Regio with geomorphic domains after [4, 5, 6]. A, Indenter, B, Fold Belt, C, plateau interior, D and E are geomorphic domains to the SE and NW respectively overlain on part of the geologic map of this study.

References: [1] Bindschadler D. L. et al. (1992) JGR 97. [2] Senske D. A. (2010) LPSC XLI, Abstract #1256. [3] Graupner M. (2011) GSA Abstract #191691. [4] Gilmore M. S. (2009) LPSC XL, Abstract # 2015. [5] Gilmore M. S. et al. (2010) LPSC XLI, Abstract #1769. [6] Gilmore M. S. et al. (2011) LPSC XLI, Abstract #2053. [7] Hansen V. L. (2006) JGR 111 [8] Banks B. and Hansen V. L. (2000) JGR 105.

GEOLOGIC MAPPING OF THE NIOBE AND APHRODITE 1:10M MAP AREAS OF VENUS; A PROGRESS REPORT. V. L. Hansen[1] and I. López[2], [1]University of Minnesota Duluth, Duluth, MN 55812 (vhansen@d.umn.edu), [2]Departamento de Biología y Geología. Universidad Rey Juan Carlos. 28933. Mostoles. Madrid (ivan.lopez@urjc.es)

Introduction: Over 15 years ago NASA's Magellan mission revealed that Venus lacks plate-tectonic processes [*1,2*], yet Venus' evolution and operative geodynamic processes remain elusive. Venus' surface likely preserves a rare record of early terrestrial planet evolution given Venus' lack of plate tectonics and a hydrologic cycle, and a dense protective atmosphere that shields the surface from extensive bolide impact. It is critical to recognize the value of even a limited record of ancient planet surfaces. Renewed study of Magellan's spectacular global data sets has the potential to reveal such a history preserved across Venus' surface.

We are conducting a detailed and comprehensive geologic, structural, and volcanic synthesis of Niobe Planitia (0-57°N/60-180°E, *I-2467*), Aphrodite (0-57°S/60-180°E, *I-2476*), and the immediate surroundings, herein referred to as Niobe Map Area (NMA) and Aphrodite Map Area (AMA), respectively. This geologic mapping will help to adress two first-order aspects of Venus evolution: (1) an *early* history recorded by cross-cutting suites of Ribbon Tessera Terrain (RTT) fabric, and (2) the extent and evolution of Artemis, and also evaluate other parts of the geologic history with respect to these two temporal divisions.

Mapping methods: Planetary geologic mapping using remote data sets has evolved significantly over the last decade, driven by improvements on many fronts: digital data formats; high resolution data; versatile and high-powered hardware (processors and monitors); and software development.

Geologic mapping in the NMA-AMA area is being conducted within a GIS framework. Data is being compiled and projected using ArcGIS™ and ArcGLOBE™) accommodating robust nesting and co-registration of data sets, and allowing for: spatial correlation (positive and negative) of layers, quantification of both areas and lengths (thus with limited assumptions, unit thickness and depths can be estimated in some situations), and quantitative spatial comparison of units and structures. All of these criteria can provide critical clues toward the goal of understanding geohistories, and ultimately the discovery of operative geologic processes.

For geologic mapping we follow established planetary mapping techniques [*e.g., 3-10*] in accordance with the Planetary Geologic Mapping Handbook [*11*].

We have found that starting with delineation of location and trends of primary and secondary structures, and major geomorphic features is a good approach toward the goal of discovering geohistories. Primary structures provide clues to the spatial limits and emplacement mechanism(s) of material units. Secondary (or tectonic) structures inform us about the spatial limit of units that formed after these structures, as well as crosscutting/embayment relations between different units and tectonic suites. Geomorphic structures can result from either primary or secondary structures, or a combination of the two. Identification of material units will emerge from reconnaissance mapping focused on geomorphic features and structures.

Niobe and Aphrodite Map Areas: We have two first order goals in mapping the NMA-AMA area: (1) document the detailed regional history of RTT exposures; and (2) document the nature and extent of Artemis-related features. The first goal allow us to define suites of RTT, and to unravel the temporal relations between suites of RTT that emerge from mapping and other units across the region. This analysis in turn will allow us to determine if RTT broadly lies within a basal location across the map area, or if the formation of different RTT suites record a range of temporal relations. Through this part of the study, a picture of both local stratigraphic positions and regional evolution should emerge. It will be important to see if evidence emerges that indicates that RTT formed throughout the recorded history across the NMA-AMA map area, or if RTT formation was confined to a early geologic era. If the later case is true, and RTT represents evolution of an early geologic time, then the relative temporal history of different suites of RTT should allow us to begin to delineate a 'basement history' that will provide new constraints for hypotheses of RTT formation, and in a related though separate vein, hypotheses of crustal plateau evolution. If RTT evolution occurred through the recorded history of the map area, then the temporal relations of the various suites of RTT, and the other geologic units will provide a coherent history across an extensive region of Venus, which will in turn place first-order constraints on any models of Venus' evolution. If a basal history emerges, that basal history can serve as a regional broad temporal framework within which to place younger geologic units and events, as with any basal geologic history. If no basal history

emerges, then the large spatial extend of individual suites of RTT will provide areally-extensive 'marker events' that will contribute to a robustly spatial and temporal defined geologic histroy across nearly one fourth of Venus' surface, and indeed extending beyond this region as individual suites of RTT will almost certainly extending beyond the spatial boundaries of the NMA-AMA area. The second goal will allow us to document the spatial limits of an Artemis 'footprint', and the history of Artemis, both of which will provide constraints for hypotheses of Artemis' evolution. Regional-scale delineation of Artemis-related features should all provide a second type of spatially extensive (i.e., broad regional) timeline with which to compare geologic units and structures. New mapping reveals that Artemis (typically viewed as an ~2400 km diameter structure) could be much larger, including a wide outer trough (>5,000 km dia.), a radial dike swarm (12,000 km dia.), and a concentric wrinkle ridge suite (13,000 km dia.)-collectively affecting *one third to one fourth of Venus' surface* [12]. This possibility is exciting for several reasons: 1) the extent of the radial fracture suite exceeds radial swarms recognized elsewhere, but is proportionally similar to Mars' Tharsis radial dike system as compared to host planet size; 2) such a large spatial footprint means that Artemis could provide a means for relative age comparison across much of Venus—recognizing, of course that Artemis could have formed over a protracted period of time. Detailed mapping across NAMA will help to constrain the evolution of Artemis, and the geologic history of the volcanic plains in relation to Artemis and their possible RTT substrate.

We have compiled existing 1:5M maps, and begun regional mapping of primary and secondary structures with the goal of producing a coherent regional map independent of different mapping styles.

The Niobe map area consists in 10 1:5M geologic maps—6 published (V3, V4, V13, V23, V24 and V25), 2 in review/edit (V11 and V12) and 2 in progress (V10 and V22). Initial work in this area include the compliation and mapping of primary and secondary structures in the central part of the mapping area (V11, V12, V23 and V24) in order to define the different suites of RTT and their temporal relations. Initial results revealed that deformational histories of the various RTT inliers are different; suites of ribbons, folds and graben in different inliers present different orientations and spacing. This initial results also suggest that not all RTT inliers formed at the same time; for example, crosscutting relations and interaction with regional suites of structures on the plains suggest that Shimti Tesserae postdate RTT located in Uni Dorsa.

The Aphrodite map area consists of 10 1:5M geologic maps—4 published maps (V35, V37, V46 and V48), 5 in progress (V34, V36, V47, V57 and V58) and 1 unassigned (V49). Unlike Niobe this area lacks deformation belts and isolated coronae, however it hosts coronae-chasmata chains. This area provides an excellent opportunity to explore the interaction of Artemis-related structures with lowland regions unaffected by these sorts of regional complexities. The comparison of Artemis structures within Aphrodite and Niobe should prove quite informative about possible interactions between the mantle and the lithosphere. Artemis' global-scale manifestation could have implications for wrinkle ridge formation, transfer of heat through the crust and to near-surface environments, mantle flow, mantle-lithosphere coupling, and Venus evolution.

Conclusions and further work: Initial work on the 1:10M geologic mapping of the NMA-AMA area has been carried out. This initial work include the compilation and projection of existing data sets using ArcGIS^{TM} and ArcGLOBE$^{TM)}$, and the compilation of existing published maps of the study area. For the areas where no maps are yet published we have started the mapping of primary and secondary structures together with major geomorphic units. Initial work on the NMA revealed that the deformational histories of the various RTT inliers are different and suggest a diachronous evolution for the basement material.

Future work will include the complete mapping of primary and secondary structures before start with the identification of the material units, and definition of regional units according to the map scale and synthesis of published geologic maps .

References: [1] Solomon, S.C. et al. (1992) JGR, 97, 13199-13255. [2] Phillips, R.J., & V.L. Hansen (1994) Ann. Rev. Earth Planet. Sci., 22, 597-654. [3] Wilhelms, D.E. (1990) Geologic mapping, in Planetary Mapping, R. Greeley & R.M. Batson (eds), 296pp. [4] Hansen, W.R. (ed) (1991) Suggestions to Authors of the reports of the United States Geological Survey, 28pp. [5] Tanaka, K.L., et al. (1994) The Venus geologic mappers' handbook, 2nd edition, 50 pp. [6] Hansen, V.L. (2000) EPSL, 176, 527-542. [7] Skinner, J.A. & K.L. Tanaka (2003) 34th Lunar & Planetary Science Conference, Abstract 2100. [8] McGill, G.E., & B.A. Campbell (2004) Ages of Venusian ridge belts relative to regional plains, 36th LPSC, Abstract 1143.[9] *Zimbelman, J. R. (2001)* Geomorphology*, 37, 179-199.* [10] Tanaka, K. L. et al. (2009) Planetary structural mapping, in Watters, T.R. & Schultz, R.A., eds., Planetary Tectonics, Cambridge University Press, p. 349-394. [11] Tanaka. K.L. et al. (2010) Planetary Geologic Mapping Handbook. USGS [12] Hansen, V.L., & A. Olive (2010) Geology , 38, 467-470.

GEOLOGIC MAPPING OF V-19. P. Martin[1], E.R. Stofan[2, 3] and J.E. Guest[3], [1]Durham University, Dept. of Earth Sciences, Science Laboratories, South Road, Durham, DH1 3LE, UK, (paula.martin@durham.ac.uk), [2]Proxemy Research, 20528 Farcroft Lane, Laytonsville, MD 20882 USA (ellen@proxemy.com), [3]Department of Earth Sciences, University College London, Gower Street, London, WC1E 6BT, UK.

Introduction: A geologic map of the Sedna Planitia (V-19) quadrangle, extending over 25°N - 50°N latitude, 330° - 0° longitude, is being completed at 1:5,000,000 scale as part of the NASA Planetary Geologic Mapping Program. The quadrangle largely consists of the Sedna Planitia lowlands (low-lying plains units, with numerous small volcanic edifices including shields, domes and cones) but also the northernmost portion of western Eistla Regio. The quadrangle also contains several tholi, the large flow-field Neago Fluctūs, the Manzan-Gurme Tesserae, and Zorile Dorsa and Karra-māhte Fossae which run NW-SE through the southwestern part of the quadrangle. In this abstract we provide a comprehensive summary of the geologic history and stratigraphic relationships between the units mapped in V-19 (Table 1).

Geologic history and stratigraphic relationships: The geologic history of Sedna Planitia is dominated by multiple episodes of plains formation and wrinkle ridge formation interspersed in time and space with edifice- and corona-related volcanism. The formation of most of the mapped plains units predates the formation of Eistla Regio to the southwest of this quadrangle, which has resulted in the mapped plains units being deformed by wrinkle ridges and overlaid by corona and volcano flow units.

Seven plains materials units have been mapped in V-19 (from oldest to youngest): Sedna deformed plains material (unit pdS), Sedna patchy plains material (unit ppS), Sedna composite-flow plains material (unit pcS), Sedna homogeneous plains material (unit phS), Sedna uniform plains material (unit puS), Sedna mottled plains material (unit pmS) and Sedna lobate plains material (unit plS). These seven units range from relatively localized, limited extent units (e.g. unit pdS) to the regional plains unit (unit phS) that dominates the northeastern half of the map. The dominance of this regional-scale plains unit is similar to other mapped quadrangles on Venus [1, 2]. The remaining plains units tend to crop out as isolated patches of materials.

The V-19 quadrangle contains a variety of mappable volcanic landforms including two shield volcanoes (Evaki Tholus and Toci Tholus) and the southern portion of a large flow field (Neago Fluctūs): these units are labeled as unit fE, unit fTo and units fNe_{a-d}, respectively. A total of sixteen units associated with volcanoes have been mapped in this quadrangle, with multiple units mapped at Sif Mons, Sachs Patera and Neago Fluctūs. An oddly textured, radar-bright flow is also mapped in the Sedna plains (unit fu), which appears to have originated from a several hundred kilometer long fissure.

The six coronae within V-19 have a total of eighteen associated flow units. Several edifice fields are also mapped (unit ef), in which the small volcanic edifices both predate and postdate the other units. Impact crater materials are also mapped. In addition, highly deformed materials have been mapped as tessera (unit t), including the Manzan-Gurme Tesserae which are made up of several individual outcrops distributed along the eastern edge of this quadrangle.

Conclusions: The stratigraphy of V-19 reveals a number of interleaved units of volcanic origin, including plains units with no apparent sources, edifice fields, flows from in-

termediate and large volcanoes, and flows from coronae. No distinct pattern of activity can be identified from these relationships. The region instead was affected by early tectonism (unit t) and plains forming volcanism (unit pdS), followed by both regional and local-scale volcanic activity, some of which was related to the formation of the Eistla rise.

Table 1. Stratigraphic relationships of V-19.

Deposit type	Unit label	Older units	Younger units
Volcanic and edifice flow materials	fE	phS, pcS	
	fTo	phS, plS	
	fNea	phS	fNeb
	fNeb	phS, fNea	fNec, fNed
	fNec	phS, fNeb	fNed, ef
	fNed	fNeb, fNec	
	fSia	phS, fNi2	fNi3, fNi4
	fSib	pcS	fSic, fSid
	fSic	phS, pcS, fSia, fSib	
	fSid	pcS, fSib	
	fG	fNi1	fIc
	fp	phS	
	fu	phS, pcS	
	fSa1	phS, puS	fSa2
	fSa2	fSa1	
Corona flow materials	fNi1	phS	fNi2, fNi3, fNi4, fG, c
	fNi2	phS, fNi1	fNi3, fSia, fIc, c
	fNi3	fNi1, fNi2, fSia	fNi4
	fNi4	fNi1, fNi3, fSia	
	fIa		phS, fIc, fId
	fIb	phS	fId
	fIc	phS, fIa, fNi2, fG	c
	fId	phS, fIa, fIb	
	fIe	phS	
	fPa	pcS	fPb, fPc
	fPb	pcS, fPa, fMc	fPc, fMd
	fPc	fPb	
	fMa	phS	fMc
	fMb	phS	fMc
	fMc	phS, fMa, fMb	fMd, fPb
	fMd	fMc, fPb	
	fTu	pcS, ppS	ef
	fB	phS, ef	
Plains materials	pdS		pcS, phS, puS, pmS
	ppS		pcS, phS, fTu
	pcS	t, pdS, ppS	phS, puS, pmS, plS, fE, fu, fSib, fSic, fSid, fMa, fMb, fMc, fPa, fPb, fPc, fTu, c
	phS	t, pdS, ppS, pcS	puS, plS, fSa1, fTo, fE, fp, fu, fNea, fNeb, fNec, fSia, fSic, fNia, fIa, fIb, fIc, fId, fIe, c
	puS	pdS, phS, pcS	pmS, fSa1, fB, ef, vc
	pmS	pdS, pcS, puS	c
	plS	phS, pcS, fTo	

References: [1] Bender, K. C. et al., 2000, Geologic map of the Carson Quadrangle (V-43), Venus. [2] McGill, G. E., 2000, Geologic map of the Sappho Patera Quadrangle (V-20), Venus.

STRUCTURAL AND GEOLOGIC MAPPING OF NORTHERN TELLUS REGIO, VENUS. A. J. Slonecker and V. L. Hansen, Department of Geological Sciences, University of Minneosta, 114 Kirby Drive, Duluth MN, 55812, USA slone014@d.umn.edu

Introduction: Crustal plateaus and volcanic rises, classes of large surface features on Venus, are both circular in planform, with similar diameters ~1,000-2,500 km, rising ~0.5–4 km above the surrounding terrain; however crustal plateaus and volcanic rises differ in topography, isostatic support, interpreted ages, and surface features [1]. These differences indicate that crustal plateaus formed from different processes than volcanic rises, which mark surface expressions of mantle upwellings [1,2]. In contrast, crustal plateaus represent ancient features and record ancient geodynamic processes, although the nature of those processes is unknown. Tellus Regio, one of two isolated crustal plateaus, lies centered at 42.6N/76.8E. Its eastern, southern, and western margins are well defined, compared to its poorly defined northern margin. To understand the geologic history and evolution of the northern margin of Tellus Regio geologic mapping is underway using Magellan high-resolution SAR and altimetry data.

Background: Four main hypotheses address crustal plateau formation: mantle downwelling [2], mantle upwelling [3], pulsating continents [4], and lava-pond and bolide impact [5]. All four hypotheses include an initial thin global lithosphere, however, they differ in timing of structures formed and processes responsible for crustal plateau formation and support. Each hypothesis makes predictions for structures present at the margins of crustal plateaus and surface histories; however few previous studies have considered the geologic relations recorded at plateau margins, and the implications of margin geologic history for crustal plateaus evolution hypotheses. The southern part of Tellus Regio has been the subject of numerous studies [6-12] however northern Tellus Regio, which has been mostly ignored, provides an excellent area for focused mapping of crustal plateau margins.

Methods: Magellan SAR and altimetry data allow for detailed geologic mapping of Venus' surface. Geologic mapping of surface lineations and radar backscatter domains allows for the interpretation of geologic units, identification of tectonic structures, and construction of geohistories and surface evolution scenarios. Mapping of this portion of Tellus Regio uses SAR, altimetry, and synthetic stereo data with mapping conducted using in Adobe Illustrator™.

Structural Descriptions: The northern part of Tellus Regio can be divided into seven domains (Fig. 1). Domains A, C, E, and F are each dominated by a radar-bright (rough) surface and high topography. Domains B, D, and G are radar-dark (smooth) regions, that lie at relatively lower elevation. A suite of NE-trending radar-bright single lineaments that appear to occur in bundles cuts across most, if not all, of the domains. The bundles are more dense in certain domains and seem to be more sporadic in others. These lineaments cross-cut structures in other domains and appear to be younger in age, and formed after each of the domains was in its current spatial location.

Domain A is dominated by ribbon tessera terrain (RTT) fabric with long-wavelength folds trending E-W. Short-to-medium-wavelength folds parallel long-wavelength folds. Ribbons trend perpendicular to fold crests. Intratessera basins (ITBs) cover parts of this domain, mostly filling troughs of long-wavelength folds, although, local ITBs occur perpendicular to fold crests. A sharp boundary separates domains A and B.

Domain B is dominated by a suite of E-trending radar-bright paired lineaments. The lineaments are long and straight, and the spacing between pairs is consistent throughout the domain. Toward domain A, the pairs are harder to distinguish and get covered by the bundles of NE-trending lineaments. Domain B includes patches of radar-bright surfaces that could be inliers of RTT.

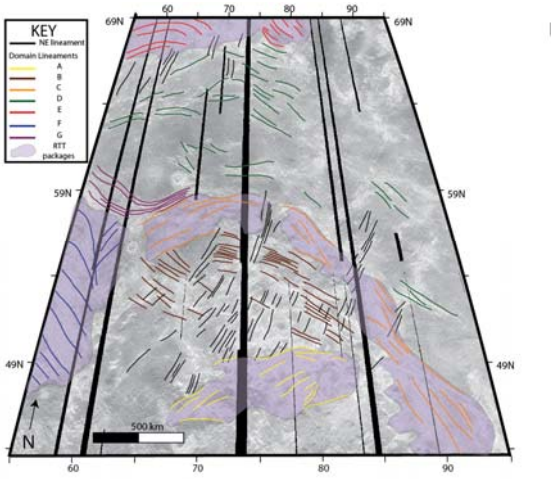

Fig. 1. Northern area of Tellus Regio illustrating structural domains.

Domain C includes two regions of RTT fabric with similar trends. The northern region has long-wavelength folds trending E-W, whereas the eastern region contains long-wavelength folds trending NW. Both regions have short-to-medium-wavelength folds parallel to long-wavelength folds, and ribbon structures oriented perpendicular to long-wavelength fold crests. ITBs lie in troughs of long-wavelength folds, but also occur in different orientations to fold crests. In the SE portion there is a gradational boundary between the RTT and the lowlands, with a sharp boundary in the north between domains B and D. The late NE-trending lineaments separate the two regions of domain C, which is also marked by a topographic low.

Domain D is dominated by a radar-dark region that lies at relatively low elevation marked by radar-bright paired lineaments. These lineaments are similar to the lineaments in domain B, with trends E-W; however the spacing between lineaments and the shapes are different. Lineaments in domain D are less periodic in spacing, and appear to occur in bundles. They also appear wispy and tend to curve, unlike the straight lineaments in domain B. Like domain B, domain D hosts local radar-bright patches that sit higher than their surroundings, and which may be inliers of RTT.

Domain E is dominated by RTT fabric. Long-wavelength folds generally trend E–W, with ribbons oriented perpendicular to fold crests. Folds tend to curve south toward the middle of the domain. Short-to-medium-wavelength folds are parallel to long-wavelength folds. In general linear ITBs trend parallel to and lie localized along long-wavelength fold troughs; although some ITBs are small and have a different orientation than long-wavelength folds. The RTT in domain E is extremely organized and shows consistent trends for each suite of structures. The southern boundary is sharp, whereas the eastern boundary is gradational.

Domain F is dominated by RTT fabric with long-wavelength folds that trend NW. Parallel to long-wavelength folds are short-to-medium-wavelength folds. Ribbons trend perpendicular to fold crests. The RTT fabric in the western part of the domain is well organized and shows consistent trends of structures. Toward the north the long-wavelength folds begin to curve more to the west, whereas folds in the northeast portion trend to the NE. The eastern boundary is poorly defined.

Domain G is dominated by a distinct suite of radar-bright, long and skinny, lineaments that are broadly U-shaped. In the western portion the lineaments trend NW and in the eastern portion they trend NE. The single lineaments are evenly spaced and show a general straight character. The northern boundary is well defined, while the southern boundary is poorly defined.

Implications: Questions arise from mapping the domains in the northern area of Tellus Regio including the limit of northern Tellus Regio? Are the domains from the same crustal plateau, or are they parts of multiple crustal plateaus? If the domains are from the same plateau were the domains formed as a coherent package and later rifted from one another after plateau formation, with the low regions representing rift zones or thinned lithosphere? Or perhaps the domains record progressive accretion to the north with the lower, more radar-dark domains preserving 'captured' terrain between separate tracts of RTT? If the domains represent parts of different plateaus, what are their relative temporal relations, and what can the interaction of one or more plateaus tell us about plateau formation? Perhaps these domains record a progressive evolution of material 'added' to the Tellus Regio 'core' and indicate that crustal plateaus need not all be plateau-shaped. Mapping the northern area of Tellus Regio hopes to address these questions relating to the mapped domains and their spatial and temporal relationships, leading to further understanding of crustal plateau margin evolution.

References: [1] Phillips R. J. and Hansen V. L. (1994) *Annu. Rev. Earth Planet. Sci., 22*, 597-654. [2] Bindschadler D. L. et al. (1992) *JGR, 97*, 13,495-13,532. [3] Phillips R. J. and Hansen V. L. (1998) *Science*, 279, 1492-1497. [4] Romeo I. and Turcotte D. L. (2008) *EPSL*, 276, 85-97. [5] Hansen V. L. (2006) *JGR*, 111, E11010 [6] Straley B. L. and Gilmore M. S. (2007)*LPS XXXVIII*, Abstract #1657. [7] Gilore M. S. (2009)*LPS LXXI*, Abstract #2015. [8] Gilmore M. S. et al. (2010)*LPS LXXII*, Abstract #1769. [9] Gilmore M. S. et al. (2011)*LPS LXXIII*, Abstract #2053. [10] Senske D. A. (1999)*LPS XXX*, Abstract #1668 [11] Graupner M. (2011)GSA Abstract # 100-7. [12] Banks B. K. and Hansen V. L. (2000) *JGR*, 105, 17,655-17,667.

GEOLOGIC MAPPING OF THE LUNAR WEST SOUTH POLE AITKEN QUADRANGLE (LQ29). F. C. Chuang[1], R. A. Yingst[1], and D. C. Berman[1], [1] Planetary Science Institute, 1700 E. Fort Lowell Rd., Suite 106, Tucson, AZ 85719 (e-mail: chuang@psi.edu).

Introduction: The nature and stratigraphy of the Moon's impact record and volcanic activity are not well understood. To this end, we are currently producing a 1:2,500,000 scale geologic map of Lunar Quadrangle 29 (LQ29) covering an area between 30°-60° S latitude and 120°-180° E longitude (Figure 1) that encompasses the western portion of South-Pole Aitken (SPA) Basin. This region has diverse volcanic materials and has excavated deep into the lower crust, providing the greatest stratigraphic cross-section on the Moon. Our objectives in mapping LQ29 are to 1) provide constraints on models of lunar volcanic generation and evolution by characterizing volcanic units along this portion of SPA Basin, 2) provide constraints on the timing and sequence of impact events by characterizing the spatial relationships and boundaries between impact-related surface materials and features found uniquely clustered in this region (lower crustal material, structures antipodal to Imbrium Basin, compositionally-distinct Th-rich and Fe-rich terranes, and ancient cratered highlands), and 3) characterize the extent and distribution of units that are important for future lunar missions, including potential sample sites that may have high science return, as well as mineral resources derived from pyroclastic deposits. For more details on the general setting, impact structures, and volcanic materials in western SPA, see [1] and the references therein.

Mapping Status: In early 2011, the region in and around crater Jules Verne was completed as a starting point for mapping [1]. Several geologic units were identified along with various structures and preliminary crater count ages. We commenced mapping of the entire quadrangle in mid-to-late 2011, starting with the eastern half that lies inside the SPA Basin rim. With the completion of the eastern half, we will next shift to the western half. Crater counting of the entire quadrangle is currently underway and these will be used to age constrain all geologic units in the full map.

Data Sets and Methods: During the initial stages of geologic mapping, including that of Jules Verne, a 200 m/pixel Clementine UVVIS 750 nm band mosaic was used as our basemap, primarily for morphology. In 2011, a 100 m/pixel global mosaic from the wide-angle camera (WAC) on the Lunar Reconnaissance Orbiter was made available to the scientific community and we have integrated this as our new basemap. This new base also provides seamless coverage across LQ29 (Clementine base contained gaps). In conjunction with morphology, we used Clementine UVVIS 415-750 nm band-ratio data to provide soil maturity information in defining mapped units (see [1]), particularly those associated with mare lavas and crater ejecta deposits. We will also use 100 m/pixel Lunar Orbiter Laser Altimeter topographic data with ~1 m vertical resolution in our stratigraphic analysis of units. All of the datasets have been processed and ingested into a geodatabase for ArcGIS Desktop, a Geographic Information System (GIS) software package used to display, query, map, and analyze both raster and vector datasets.

Mapping Results: For the eastern half of LQ29, excluding Jules Verne, 18 geologic units were identified along with structural features and 750 primary craters for crater count age estimates. For consistency, all mapping was done at no more than 1:250,000 scale.

Geologic Units. The following units were identified from our mapping (no ages assigned): Mare Ingenii rim materials (AI1), Mare Ingenii floor materials (AI2), Leibnitz rim materials (AL1), Leibnitz floor materials (AL2), Poincare rim materials (AP1), Von Karman rim materials (AV1), Von Karman rim and Leibnitz rim materials (AV2), sharp-rimmed bowl craters (c1), sharp-to-subdued rimmed craters (c2), complex craters with central peak (cc), crater and ejecta (ce), ejecta (e), mare 1 materials (m1), mare 2 materials (m2), cratered plains (p1), plains with Leibnitz ejecta materials (p2), surficial 1 materials (s1), surficial 2 materials (s2).

Structures. For impact-related structures, we have mapped the rim crests (sharp and subdued) of craters with $D \geq 10$ km. Several craters (D= ~30-60 km) have well-developed sinuous channels along portions of their interior walls. Several wrinkle ridges are apparent near the center of crater Poincare. Individual to branching systems of linear to arcuate rilles (well-defined to approximate) (1-100 km) occur mainly on the floors of craters Poincare, Garavito, and Jules Verne.

Crater count ages. Impact craters larger than 1 km in diameter were counted on all mapped units as a first step in relative age dating of geologic units. Areas with secondaries, secondary chains or clusters were avoided. We have derived preliminary N(1) and N(20) count values [2] with the latter used to compare the recent results by [3] for major terrain types on the Moon. The N(20) values (Table 1), combined with the mapped geology, shows that Mare Ingenii and Poincare have some of the oldest geologic surfaces in the region. These N(20) values are comparable to those by [3] for heavily cratered highland regions where high N values exist. This result is reasonable considering that the

eastern half of LQ29 is within SPA, one of the oldest features on the Moon, and has likely been exposed to a similar degree of impact cratering as in the lunar highlands.

References: [1] Yingst et al. (2011) *NASA/CP-2011-xxxxxx*. [2] Wilhelms et al. (1978) *Proc. LPSC 9th*, 3735-3762. [3] Head et al. (2010) *Science, 329*, 1504-1507, doi:10.1126/science.1195050.

Table 1. Preliminary N(20) values for geologic units in the eastern half of LQ29.

Unit	Area (km^2)	n(20)	N(20)
AI1	33717.23	6	178±73
AI2	3042.19	1	329±329
AL1	18128.64	1	55±55
AL2	2925.63	0	----
AP1	25991.46	5	192±86
AV1	8230.82	1	121±121
AV2	15156.62	0	----
c1	20722.19	1	48±48
c2	42984.39	1	23±23
cc	41994.86	2	48±34
ce	30007.63	0	----
e	12361.93	2	162±114
m1	33752.09	3	89±51
m2	55350.30	3	54±31
p1	----	--	----
p2	43997.01	3	68±39
s1	3533.35	0	----
s2	1070.77	0	----

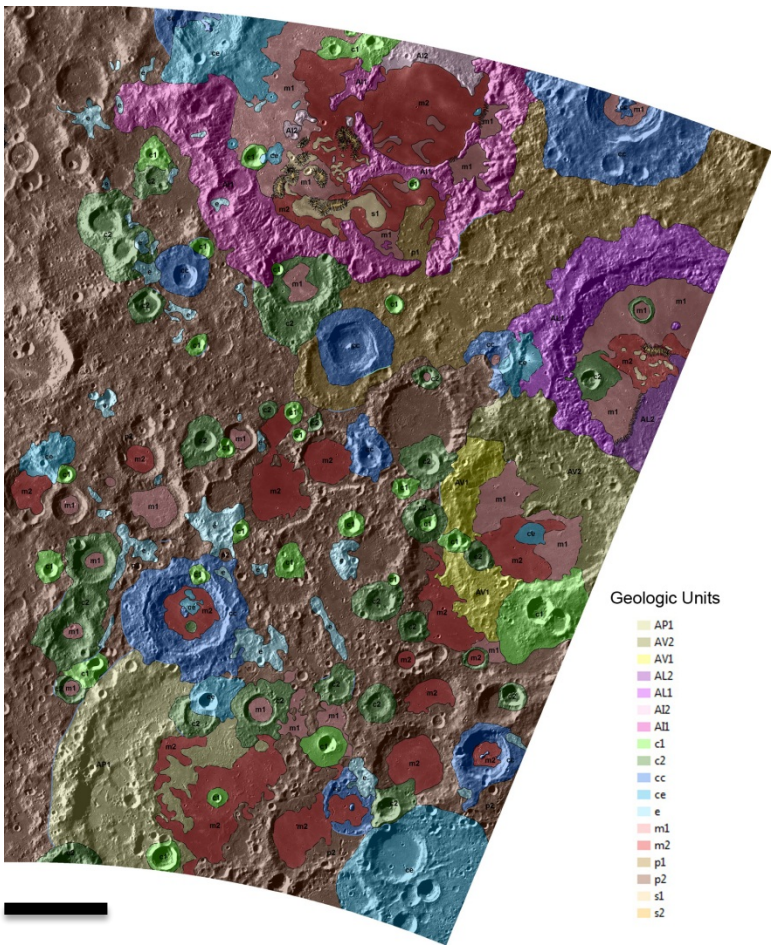

Figure 1. Preliminary map of the geologic units in the eastern half of LQ29. Geologic structures not shown. Contact types: certainty (solid), approximate (dashed), and gradational (hachure). See text for full description of the abbreviated unit names. Scale bar is 100 km.

MORPHOLOGIC MAPPING OF MARE IMBRIUM LAVA FLOWS ON THE MOON. W.B. Garry[1]. [1]Planetary Science Institute, Tucson, AZ (wbgarry@psi.edu).

Introduction: Lava flow margins on the Moon are scarce [1,2], and the best preserved examples are observed in Mare Imbrium [3-5]. The Mare Imbrium lava flows are unique to the lunar surface in that they have well-defined flow margins, levees, and channels that are traceable from the source region to the flow front. These flows have been mapped and measured by *G.G. Schaber* using images from the Apollo 15 and 17 Metric cameras (Figs. 1,2) [4,5]. These studies conclude the flow field was erupted in three phases (I-III) from 3.0±0.4 to 2.5±0.3 Ga with flow lengths of 300 km, 600 km, and 1200 km [4,5]. Lava flow margins, 10 to 63 m thick, are observed in the younger Phase II and III lavas, while the older Phase I lavas are primarily defined by a color and albedo boundary with the surrounding mare [4-7]. No flow lobes or margins related to the Phase I flows have been identified in previous data sets.

Recent missions have provided unprecedented data sets of the Moon with more consistent coverage and a variety of viewing angles and incidence angles. Here, a new study is presented that will focus on refining the morphologic mapping of the Mare Imbrium lava flows based on new data sets from the Lunar Reconnaissance Orbiter (LRO) [8], supplemented by data from Kaguya, Moon Mineralogy Mapper (M3), Clementine [9], Lunar Orbiter, and Apollo. The goal of this study are to analyze the morphology of the Mare Imbrium lava flows and provide a qualitative and quantitative description of the emplacement of the flow field.

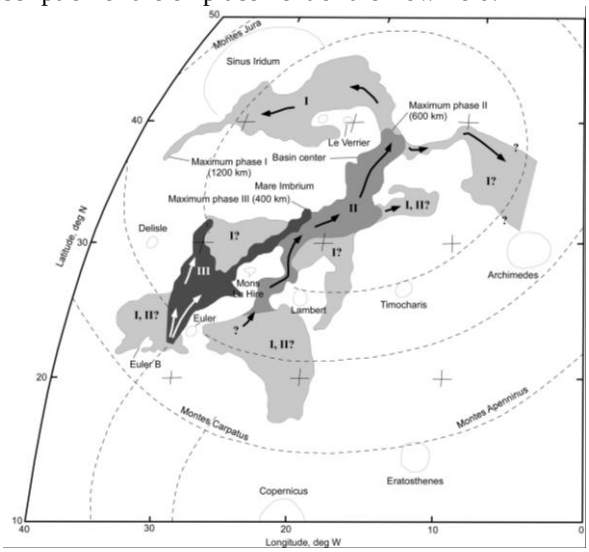

Figure 1. Map of the lava flows in Mare Imbrium showing the eruption Phases I-III. Redrawn from Figure 30-14 in *Schaber* (1973) [4].

Data: The current basemap is an *LRO Wide Angle Camera (WAC)* mosaic (50 m/pixel, incidence angle of ~70°) processed in ISIS. A separate, initial project of only *Clementine* basemaps has also been produced, but not merged with the LROC project yet. Preliminary mapping is being completed in Canvas X, a graphic design software package. The final map will be completed in an ArcGIS 10 project with the following data sets: LRO WAC, LRO WAC DTM, LOLA DTM, and Clementine, incorporating image frames from LROC NAC and Kaguya as needed. By completing the final map in ArcGIS, layers can be exported and viewed in different programs and overlain on additional lunar data sets.

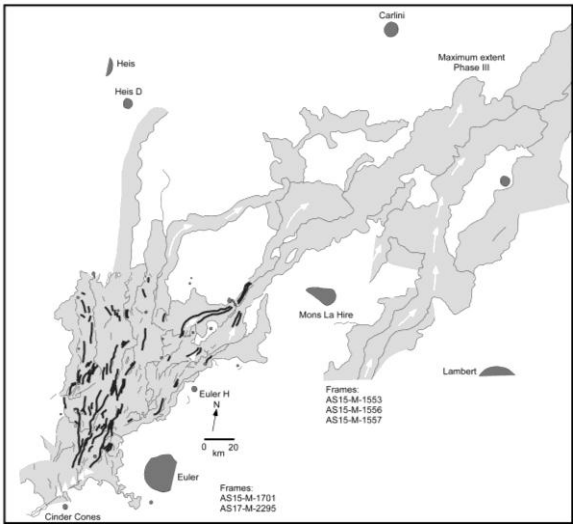

Figure 2. Detailed map of the Phase II and III lava flows in Mare Imbrium. Redrawn from Figures 30-15 and 30-21 in *Schaber* (1973) [4].

Progress and Initial Observations: The morphology mapping is still in the early stage (Fig. 3,4) with preliminary maps being completed on *LROC WAC* mosaic to get the morphology and *Clementine* basemap which provides context for the boundary of the lava flow.

Flow path: The flow maps by *Schaber* [4] (Fig. 1) show the Phase I flows going around Le Verrier crater. Initial mapping of the flow field with more recent data shows that the Phase I does not follow this path and instead, flows to the south of Le Verrier crater.

Phase I Flow Lobes: Observations of LROC NAC images and LOLA topographic data indicate that flow lobes are present in northern region of the Phase I flows, with thicknesses ~5-7 m and a few kilometers

wide. Potential flow lobe margins are being mapped in on the LROC WAC mosaic (Fig. 3). LOLA profiles across additional areas of Phase I flows (Fig. 1) do show positive relief that corresponds to mapped flow boundaries and possible flow margins are also observed along these boundaries.

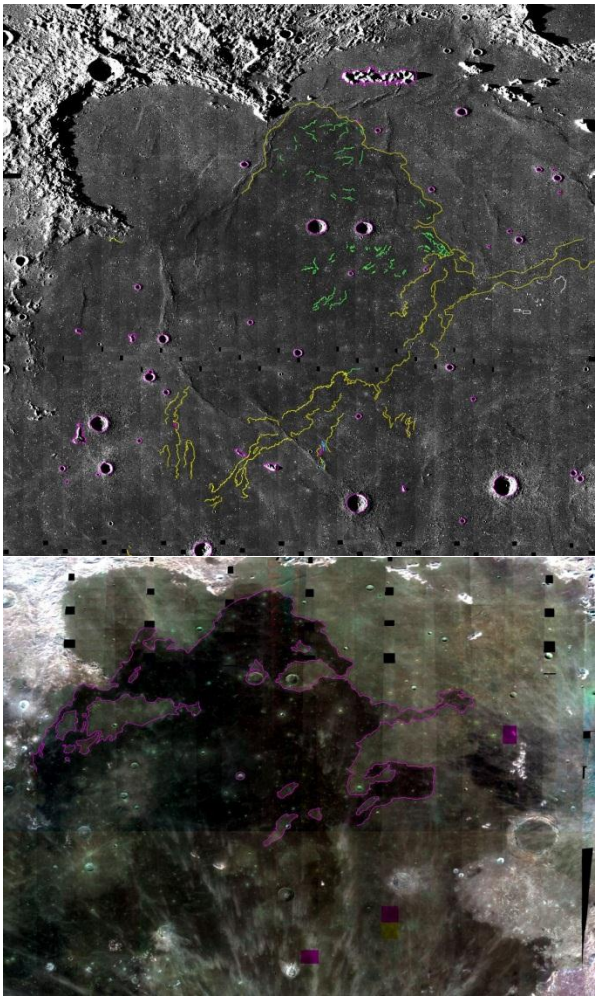

Figure 2. (Top) Preliminary morphologic map of the Mare Imbrium flow field on LROC WAC mosaic. (Bottom) Preliminary map of the flow field boundary on the *Clementine* NIR basemap.

Future Plans: 1) Create ArcGIS 10 project with registered basemaps and data sets to complete final mapping; 2) Finalize morphologic mapping; 3) Create topographic profiles across flow lobes in each eruption phase; 4) obtain crater count ages for individual flow lobes in Phase II and III lava flows using LROC NAC (Fig. 3) and Kaguya images, 5) field work at Askja volcano in Iceland, studies of potential analogs for the flow, and quantitative modeling [10-12].

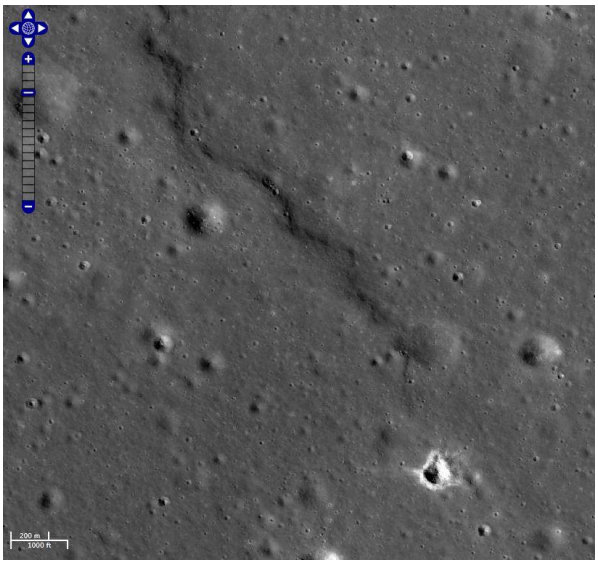

Figure 3. LROC NAC image of flow margin in a Phase III lava flow.

References: [1] Schaber G.G. et al. (1976) *Proc Lunar Sci Conf 7th*:2783-2800. **[2]** Gifford A.W. and El Baz F. (1981) *The Moon and the Planets* 24:391-398. **[3]** Fielder G. and Fielder J. (1968) *Boeing Science Research Laboratory Document* D1-82-0749:1-36. **[4]** Schaber G.G. (1973) *Proc Lunar Sci Conf 4th*, 73-92. **[5]** Schaber G.G. (1973) *Apollo 17 Prelim. Sci. Report*, 30-17 – 30-25. **[6]** Schaber G.G. et al. (1975) *The Moon* 13:395-423. **[7]** Bugiolacchi R. and Guest J.E. (2008) *Icarus*, 197, 1-18. **[8]** Robinson M.S. et al. (2005) LPSC XXXVI, Abs. 1576. **[9]** Eliason E. et al. (1999) The Clementine UVVIS Global Lunar Mosaic. **[10]** Hulme G. and Fielder G. (1977) *Phil Trans R Soc Lond A* 285:227-234. **[11]** Wilson L. and Head. JW. (2008) *LPSC XXXIX*, Abs. 1104. **[12]** Walker G.P.L. (1991) *Bull. Volcanol.*, 53, 546-558.

Acknowledgements: This research is funded by NASA LASER (NNX11AH44G).

SINUOUS RILLES IN THE MARIUS HILLS QUADRANGLE (LQ10) Tracy K.P. Gregg and Carolyn E. Roberts, Department of Geology, 411 Cooke Hall, University at Buffalo, 14260-1350, tgregg@buffalo.edu

Introduction: Lunar Quadrangle 10, informally known as the "Marius Quadrangle," extends from 0° - 30°N and 270° to 315°E. This region includes some of the most volcanologically diverse terrain on the Moon, including Aristarchus plateau and the Marius hills [1-5]. These two regions have the highest concentration of sinuous rilles on the lunar surface [6]. Although lunar sinuous rilles have been studied for decades, relative roles of construction, thermal erosion and mechanical erosion, remain debateable [7 – 10].

Quantifying lunar sinuous rille morphologies, and detailed examination of a few specific rilles within LQ10 may shed light on this continuing debate. Aristarchus plateau and the Marius hills are distinct geologic and geographic regions within Oceanus Procellarum; by comparing rille morphologies (and ultimately stratigraphies) between these different areas, we can begin to unravel external controls (such as the affect of the pre-existing surface) from the internal controls (such as eruption rates and durations) on final rille behavior and morphology.

Methods: All rilles within the Marius hills (n = 41) and Aristrachus plateau (n = 40) regions were measured. In addition, 3 highland rilles were examined, as were 3 rilles near Struve-Eddington craters and Rimae Brayley, Diophantus, and Mairan located to the east of LQ10. Sinuous rille length, width and sinuosity measurements were performed in ArcGIS 10 on a Lunar Orbiter IV and V frame mosaic base map (~20– 1000 m/pixel), because it provided total coverage. All parameters were measured repeatedly until at least 3 consecutive values within 5% of each other were obtained.

Rille lengths were measured along central axes from visible origins (irregular depressions, or the first location rilles become visible on relative topographic highs) to visible termini (last location both rille walls are discernible). Where available, Lunar Reconnaissance Orbiter-Narrow Angle Camera (LRO-NAC) frames (0.5 m/pixel [11]) were consulted as needed and as available.

Sinuosity measurements were obtained from the ratio of total rille length to the straight-line length connecting the origin and the terminus of a rille [12, 13]. Twenty width measurements were collected, evenly spaced, along the length of each rille.

Fractal dimenions were obtained using ArcGIS 9.3 and the central axis of each rille. Radius of curvature was measured for each bend in each rille by fitting a circle in ArcGIS 10.0 to the inside of the curve to the wall of the rille. The radius of this circle was recorded, as was the number of circles required to measure the entire rille.

The kernal density analyses tool in ArcGIS 10.0 was used for analyzing the spatial distribution of sinuous rilles around Aristarchus plateau and the Marius hills region.

Finally, Rima Marius was selected for detailed terrain mapping, using newly aquired Lunar Reconnaissance Orbiter Narrow Angle Camera (LRO-NAC) images to search for geologic clues about the origin and evolution of this rille. It should be noted that the great length of this rille (almost 325 km) make it perhaps not the most representative of all lunar rilles; however, we assert that this same length suggests a rich emplacement history that might be lacking for some of the shorter lunar rilles.

Results: The spatial density analysis reveals distinct clusterings of rilles, confirming visual observations of both the Marius hills and Aristarchus plateau regions (Fig. 1). Detailed mapping of Rima Marius (Fig. 2) confirms that this long rille (and others outside of LQ10) have many shallow "rillettes" that are crosscut by the main rille, and follow the same general trend as the main rille. This suggests that at least the long rilles, such as Rima Marius, have a complex history: they appear to have begun as more of a sheet-like flow prior to lava channelization.

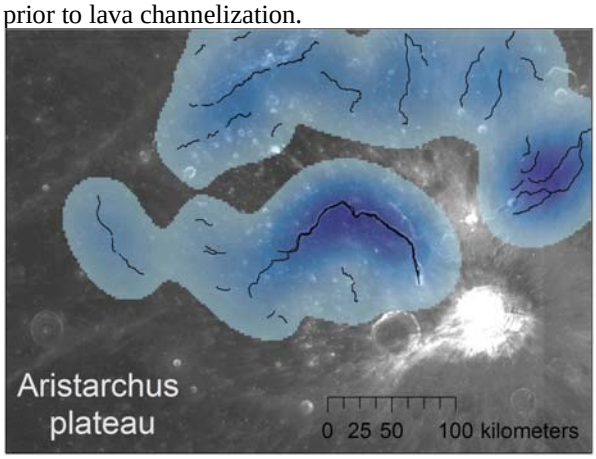

Figure 1. Distribution of sinuous rilles (black) around Aristarchus plateau. Dark blue indicates a high spatial density of rilles; light blue indicates a low spatial density.

We suspected that longer rilles would tend to be more sinuous than shorter rilles, because of the greater volume of lava required to generate them as compared with shorter rilles, and therefore possibly greater amounts of time as well. However, there is no strong correlation with rille length and sinuosity (Fig. 3). In

fact, of all parameters examined, only one relationship displayed a weak correlation (Fig. 4): sinuosity and fractal dimension.

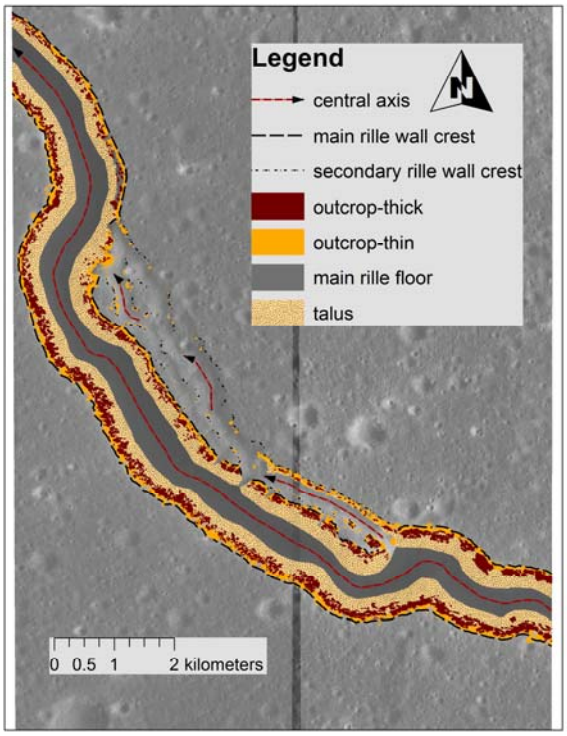

Figure 2. A reach of Rima Marius. Note the red arrows to the north of the main rille; we have termed these shallow, cross-cut rilles to be "rillettes" and they likely represent early phases of the flow that ultimately generated Rima Marius. (LRO-NAC images courtesy of NASA/JPL/ASU.)

Interpretations: As of this writing, the preponderance of evidence for most rilles is more supportive of a constructional origin for most of the rilles within LQ10. Currently, the focus is on geologic mapping of individual rilles using available LRO-NAC images, and it is possible that conclusion will change as we analyze and interpret these data.

References: [1] Wilhelms (1987) *The Geologic History of the Moon*, USGS Prof. Paper 1348. [2] Hiesinger et al (2000) *JGR*, *105*, 29,239-29,275. [3] Adams et al. (1974) *Proc. Lunar Plan. Conf. 5*, *1*, 171-186. [4] Gaddis et al. (1985) *Icarus*, *61*, 461-489. [5] Weitz et al. (1998) *JGR 103*, 22,725-22,759. [6] Hiesinger H. and Head J. W. (2006) *Rev. Min. & Geochem.*, *60*, 1-81. [1] Oberbeck V. R. et al. (1969) *Mod. Geology*, *1*, 75-81. [2] Greeley R. (1971), *Science*, *172*, 722-725. [3] Schubert G. (1970) *Rev. Geophys. & Space Phys.*, *8*, 199-224. [4] Hulme G. (1973), *Mod. Geology*, *4*, 107-117. [11] Robinson M. S. et al. (2010) *Space Sci. Rev.*, *150*, 81-124. [12] Chen L. J. (2008) *LPS XXXIX,* Abstract #1713. [13] Roberts, C.E. and T. Gregg (2012), *LPSC XLIII,* Abstract #1685.

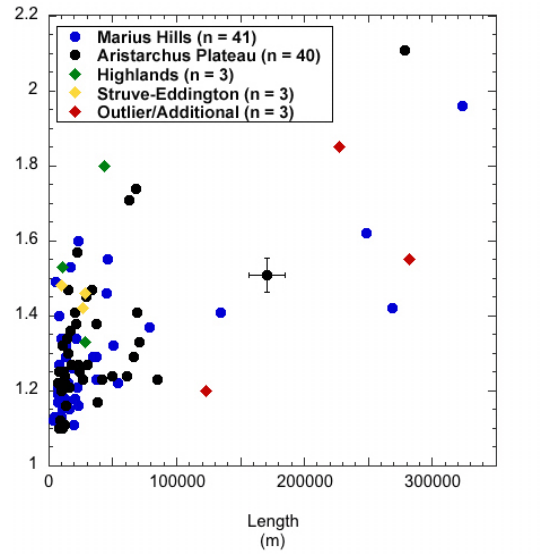

Figure 3. Rille length (x axis) and sinuosity (y-axis). There is no strong correlation.

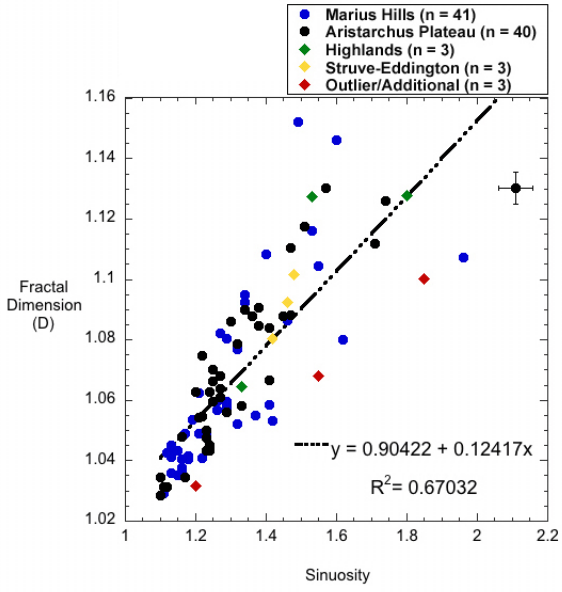

Figure 4. Rille sinuosity and fractal dimension display a weak correlcation.

GEOLOGIC MAPPING OF NILI FOSSAE AND MAWRTH VALLIS, MARS. L.F. Bleamaster, III[1,2], F.C. Chuang[1], and D.A. Crown[1], [1]Planetary Science Institute, 1700 E. Ft. Lowell Rd., Suite 106, Tucson AZ, 85719; [2]Trinity University Geosciences Department, One Trinity Place #45, San Antonio TX, 78212; lbleamas@psi.edu

Introduction. Geologic mapping at 1:1 million-scale of Nili Fossae and Mawrth Vallis is being used to assess geologic materials and processes that shape the highlands along the Arabia Terra dichotomy boundary. Placing these landscapes, their material units, structural features, and unique compositional outcrops into broad spatial and temporal context along the dichotomy (red dashed line = topographic dichotomy) and with other highland-lowland transitions (like the Hellas basin rim) (***Fig. 1***) may help to: a) constrain paleo-environments and climate conditions through time, b) assess fluvial-nival modification processes related to past and present volatile distribution and their putative reservoirs (aquifers, lakes and oceans, surface and ground ice) and c) address the influences of nearby volcanic and tectonic features on hydrologic systems and processes, including possible hydrothermal alteration, across the region and d) further evaluate the origin and subsequent modification of the Martian crustal dichotomy. The identification of broad geologic/ geomorphic units (12 map units for Mawrth Vallis and 27 for Nili Fossae; ***Figs. 2 & 3***) at scales significantly higher than previously available [1] constrain the distribution, stratigraphic position, and crater model age of units across these areas providing regional and temporal context for larger-scale and more focused studies looking at mineralogic signatures from orbit. Anticipated submission for these maps is August 2012.

Data and Methods. Datasets for geologic mapping include Viking and THEMIS day & night IR basemaps, MOLA topographic data (128 pixel/deg; ~462 m/pixel), and HRSC and CTX images. Mineralogy maps are derived from CRISM and OMEGA data and have been extracted from multiple literature sources [2, 3, and references therein]. These mineralogy maps, show outcrops and deposits of olivine, pyroxene, hydrated silicate, phyllosilicates, carbonate and sulfate detections. Using GIS and digital methods, manual geo-rectification of published mineralogy is compared with the newly generated geologic maps, and crater counts provide temporal context.

Nili Fossae (MTM quadrangles 20287, 20282, 25287, 25282, 30287, 30282; ***Fig. 2***) is located west of Isidis basin and north of Syrtis Major volcano. Nili Fossae contains several regional plateau and plains sequences from the Noachian to late Hesperian as constrained by crater counts (***Fig. 2***) and several localized occurrences of landslides, alluvial fans, dunes, and dust mantles from the Amazonian. Nili

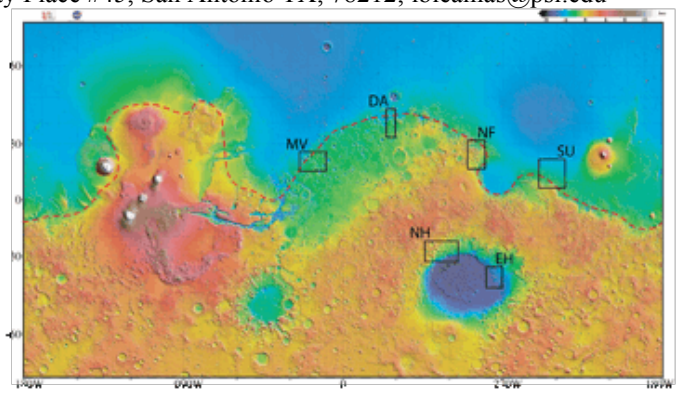

Figure 1. *Global MOLA map showing locations of various highland-lowland mapping efforts: MV=Mawrth Vallis, NF=Nili Fossae, DA=Deuteronilus/Arabia [12], EH=Eastern Hellas [13], SU=Southern Utopia [14], NH=Northwest Hellas [15].*

Fossae itself and a series of other small curved depressions related to the Isidis basin cut both the plateau and plains sequences revealing a window into the local stratigraphy provided they have not been completely filled with eolian deposits (particularly in the northeast portion of the trough), which mask the underlying bedrock. Minerals identified in the Nili Fossae region include: smectites, chlorite, prehnite, serpentine, kaolinite, potassium mica, high and low-FE olivine, high and low-Ca pyroxene, and traces of dunite [2]. Outcrops of phyllosilicate-bearing materials (likely Noachian in age) have been discovered by both the OMEGA and CRISM instruments; these lie mostly within the plateau sequences of the highlands, but mostly in exposures along trough walls. The presence of these phyllosilicates provides evidence for the stable presence of water for extended periods of time in Mars' ancient history. In contrast, low calcium pyroxene outcrops are also observed in the plateau sequences (brown and green units) and make up the majority of the Isidis plains unit (blue unit). These mineral signatures, if broadly correlated with morphology and geologic units may reveal a break in aqueous alteration. Lastly, many of the Amazonian surface deposits also contain phyllosilicate materials; these likely represent redistribution of previously altered and weathered rock.

Mawrth Vallis, (MTM quadrangles 20022, 20017, 20012, 25022, 25017, and 25012; ***Fig. 3***) is one of the oldest preserved outflow channels on the surface of Mars. This sinuous channel cuts across the western surface of the Arabia Terra plateau and is a possible manifestation of past catastrophic outflow of a subterranean aquifer or persistent groundwater sapping. Few bed forms are preserved indicating the

channel has undergone significant modification since its formation. There are three primary units along and within Mawrth Vallis: the Noachian cratered terrain, Hesperian channel floor materials, and Amazonian deposits near the northwest boundary of the channel.

Three principal clay types are present: Fe, Mg, and Al-rich smectites. The Al-rich phyllosilicates, in the form of montmorillonite clays, are located in eroded light-toned outcrops along the flanks of Mawrth Vallis [4]. The Al-rich unit is minimally hundreds of meters thick [4, 5, 6], layered down to the meter-scale [4-8] with moderate thermal inertia signatures [5, 6], and eroded into knobby and flat mesa-like cliff forms [7, 8], typical of the dark blue map unit. In some locations along the walls of Mawrth Vallis, the Al-rich unit appears to lie stratigraphically between Fe or Mg-bearing smectite units (e.g., nontronite) [8, 9]. A transitional unit with spectral signatures of both Al-bearing and Fe/Mg clays is also observed. The Al-bearing unit has meter-scale polygonally fractured surfaces while the darker-toned Fe/Mg-bearing clay units have larger polygonal surfaces that are tens of meters wide [5, 10]. These surfaces may have formed as a result of thermal and/or desiccation contraction [5, 10]. Other dark-toned materials present throughout the region are identified as pyroxene-rich materials (i.e., basaltic sand and dust) that mantle the surface (and clay-bearing units) [6, 8, 9]. The presence of clays in Mawrth Vallis is important as they imply a past aqueous environment in this region of Mars. It is argued that the clay-bearing units were formed early in the history of Mars (also prior to the formation of Mawrth Vallis) as aqueous deposits of sedimentary or pyroclastic materials, or a combination of both [4-11].

References: [1] Greeley and Guest (1987) USGS Geo. Inv. Ser. Map 1802-B. [2] Ehlmann et al., (2009) JGR 114, doi:10.1029/2009JE003339 [3] Noe Dobrea et al., (2010) JGR 115, doi:10.1029/2009JE003351 [4] Poulet et al. (2005) Nature 438, 623-627; [5] Loizeau et al. (2007) JGR 112, doi:10.1029/ 2006JE002877; [6] Michalski and Fergason (2009) Icarus 199, 25-48; [7] Bibring et al. (2006) Science 312, 400-404; [8] Michalski and Noe Dobrea (2007) Geology 35, 951-954; [9] Bishop et al. (2008) Science 321, 830-833; [10] Wray et al. (2008) GRL 35, doi:10.1029/ 2008GL034385; [11] Howard and Moore (2007) LPSC 38, abstract #1339; [12] Chuang and Crown (2009) USGS SIM #3079; [13] Bleamaster and Crown (2010) USGS SIM #3096; [14] Skinner and Tanaka (2010) Ann. Meet. Plan. Geo. Mappers, abstract p. 42; [15] Crown et al., (2010) Ann. Meet. Plan. Geo. Mappers, abstract p. 26.

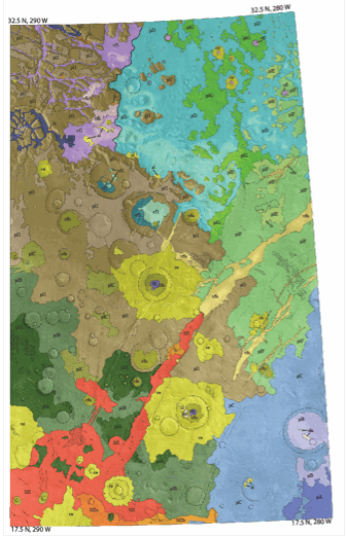

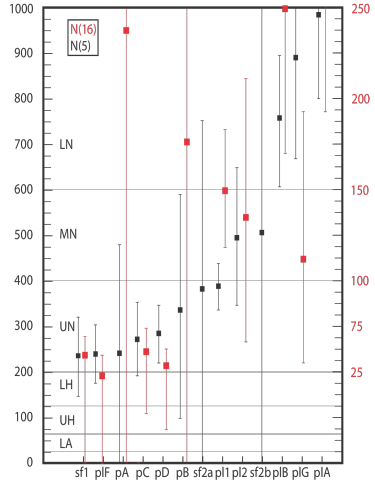

Figure 2. *Nili Fossae (left). Current mapping and cumulative crater count (N5 and N16) of spatially significant map unit*

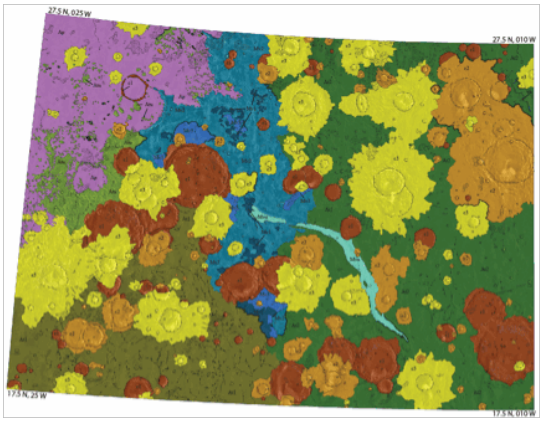

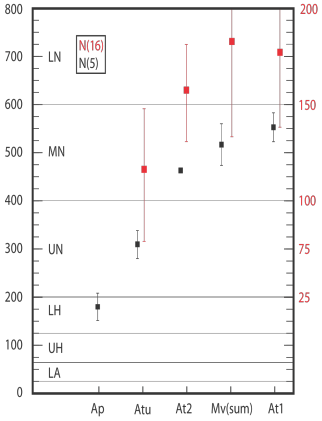

Figure 3. *Mawrth Vallis (below) Current mapping and cumulative crater count (N5 and N16) of spatially significant map units.*

GEOLOGIC MAPPING INVESTIGATIONS OF MTM -35137 QUADRANGLE: DAEDALIA PLANUM REGION OF MARS. David A. Crown, Daniel C. Berman, and Frank C. Chuang, Planetary Science Institute, 1700 E. Ft. Lowell Rd., Suite 106, Tucson, AZ 85719, crown@psi.edu.

Introduction: Geologic mapping and related analyses are being used to characterize the geologic and volcanic histories of the southernmost extent of the Tharsis region on Mars. SW Daedalia Planum exhibits a extensive complex of volcanic flows and plains that embay and fill low-lying regions in the highlands. Detailed geologic and flow field mapping is designed to a) characterize the styles of volcanism in southern Tharsis, b) identify potential local and regional sources for the observed flows and plains, c) determine the timing of flow emplacement and overall volcanic chronology, d) examine interactions between volcanic and tectonic processes, and e) evaluate the degradational history of the highlands.

Study Area: Flat-lying volcanic flows and plains units that embay degraded remnants of Terra Sirenum dominate MTM -35137 quadrangle [32.5°-37.5°S, 135°-140°W]. Previous regional and global mapping studies that included this area identified the Tharsis Montes Formation, mountains, and highland terrain [1] and Arsia Mons flow units, older flows, smooth plains, and highlands [2] along the southern margin of Tharsis in the study area.

Geologic and Flow Field Mapping: In this investigation, traditional geologic mapping of the 1:500K-scale MTM quadrangle is combined with detailed flow field mapping at 1:50K-scale to take full advantage of new high-resolution datasets for Mars and to document observations important for interpreting volcanic processes and geologic history. Context Camera (CTX; ~5 m/pixel) images imported into ArcGIS form the primary image base; also used are the Thermal Emission Imaging System (THEMIS) global mosaic and infrared multi-band images (~100 m/pixel), High Resolution Imaging Science Experiment (HiRISE; ~1 m/pixel) images, and Mars Orbiter Laser Altimeter (MOLA; 128 pixel/deg) DEMs and PEDR profiles.

Mapping Results: Preliminary mapping for MTM -35137 quadrangle, including identification and definition of the major geologic units, has been completed [3-5] (Figure 1). Ongoing efforts include mapping of geologic structures and volcanic features and flow surface textures, as well as estimating flow thicknesses.

Preliminary crater counting results provide constraints on the geologic history of the map area, which includes: a) eroded Noachian cratered terrain (highlands) that stabilized in the Early Hesperian Epoch, b) an early episode of volcanism (volcanic plains) that embayed the highlands in the Early Hesperian (~3-3.5 Gy), and c) recent volcanism emplacing vast sheet flows during the Middle Amazonian Epoch (0.5-1 Gy) [4-5].

Highlands occur as locally highstanding and rugged remnants of heavily cratered terrain. Highlands appear to have been extensively degraded, with surfaces exhibiting numerous fluvial channels and erosional troughs. Distinct embayment relationships are evident between the highlands and adjacent plains and flows.

Two plains units have been mapped: 1) a smooth unit with mottled appearance in THEMIS IR images that covers a low-lying region at the SW corner of the map; the origin of this unit is unclear and its surface textures suggest the presence of mid-latitude mantling deposits; and 2) a smooth-surfaced unit that also exhibits numerous small impact craters as well as some wrinkle ridges and graben; this unit is covered by younger flows but clearly embays the highlands and is interpreted to be volcanic in origin.

The majority of the quadrangle consists of young lava flows forming a large sheet complex that inundates the region [3-5]. The flows typically have strongly ridged surfaces but also display knobby, platy, and smooth textures. Impact craters on the pre-flow surface influence flow emplacement as indicated by changes in surface ridge patterns. Formation of sheet flows partly by coalescense of large lobes is suggested in local zones where flow converges.

Sheet flow margins display various morphologies. Sheet flows that embay highlands develop complex frontal shapes due to topographic irregularities in the older, degraded terrain. Sheet flows emplaced over volcanic plains exhibit lobate margins suggesting lobe coalescence or differential flow at the front. A series of smooth plateaus is observed along sheet flow margins. The plateaus have steep sides and some appear to have small breakout flows at their edges. These smooth plateaus are interpreted to be due to flow inflation as the front stagnates. This is consistent with their smooth surfaces, as low-velocity emplacement may limit the ability to form surface ridges. MOLA PEDR profiles indicate sheet flows range in thickness near the front from 18 to 96 m, with an average of ~51 m.

References: [1] Scott, D.H. and K.L. Tanaka (1986), *USGS Map I-1802A*. [2] Scott, D.H. et al. (1981), *USGS Map I-1275*. [3] Crown, D.A. et al. (2011), *AGU*, abstract V31A-2514. [4] Crown, D.A. et al. (2012), *LPSC XLIII,* Abstract 2138. [5] Crown, D.A. and D.C. Berman (2012), *LPSC XLIII,* Abstract 2055.

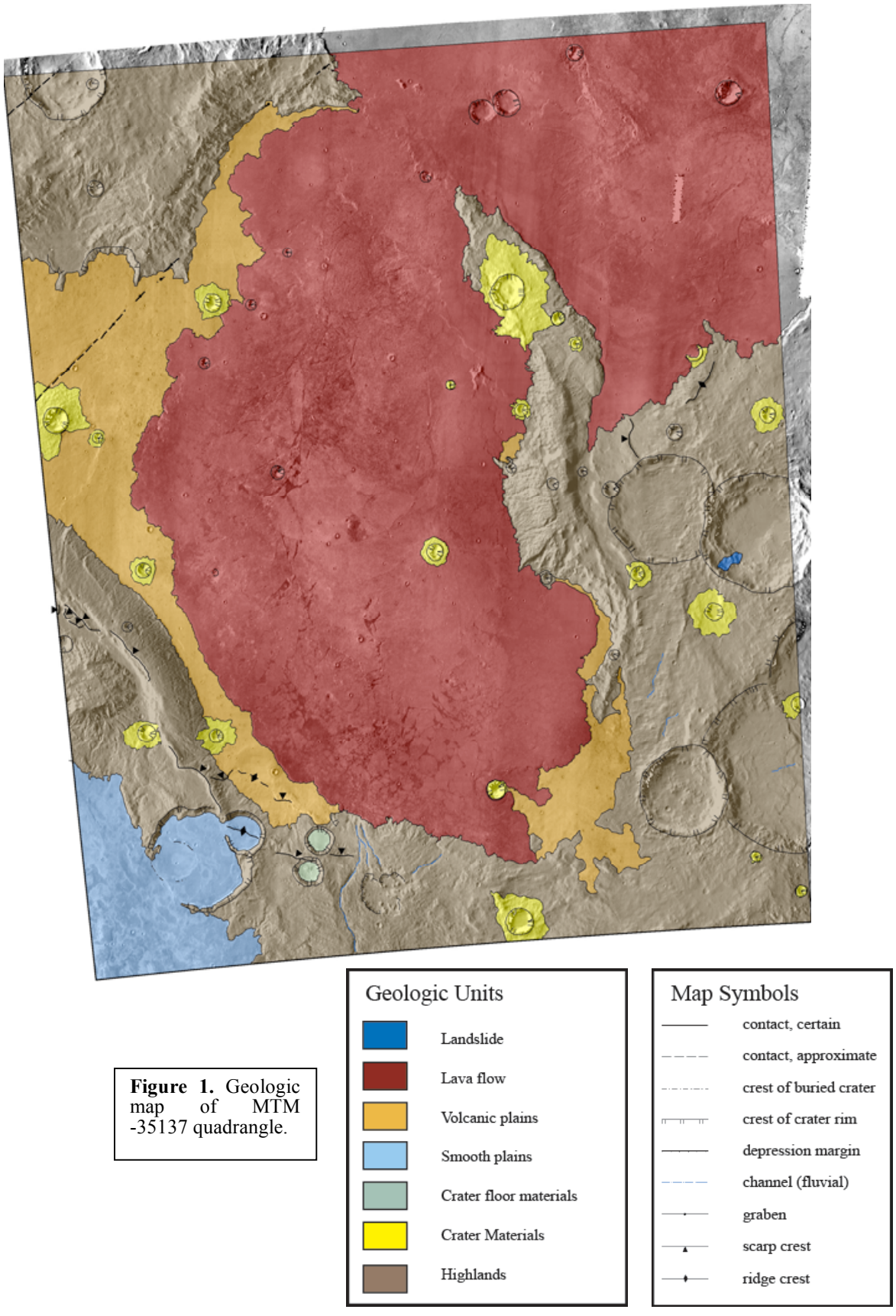

Figure 1. Geologic map of MTM -35137 quadrangle.

GEOLOGIC MAPPING INVESTIGATON OF THE ARGYRE AND SURROUNDING REGIONS OF MARS. J. M. Dohm[1], S. J. Robbins[2], B. M. Hynek[2,3], M. R. El Maarry[4], T. M. Hare[5], [1]Department of Hydrology and Water Resources, University of Arizona, Tucson, AZ (dohm@hwr.arizona.edu), [2]LASP, UCB 600, University of Colorado, Boulder, CO, [3]Geological Sciences Department, UCB 399, University of Colorado, Boulder, CO, [4]Physikalisches Institut, Universität Bern, 3012, Bern, Switzerland, [5]United States Geological Survey, Flagstaff, AZ

Introduction: Argyre is the best preserved of the large multi-ringed impact basins on Mars, comparable to the Orientale Basin of the Moon when viewed at resolutions less than a kilometer per pixel. However, even at Viking Orbiter image resolutions, the basin has been distinctly modified by erosional and depositional processes. The Argyre impact was one of several large impact events (including Hellas and Isidis) that occurred relatively early in the geologic history of Mars; based on a new global crater data base [1], [2] indicates that the Argyre impact event took place 3.93±0.02 Ga based on fitting the Hartmann isochrons [3] or 3.94±0.03 Ga based on fitting Neukum isochrons [4]. Though it is difficult to establish whether Argyre formed prior to or concurrent with the incipient development of Tharsis, the multi-ringed impact structure appears to have influenced the geophysical and geological development of a large part of Mars. This includes the southeast part of the Thaumasia plateau (i.e., impact-induced basement structures partly controlled plateau development [5]) and the Uzboi drainage system and other systems of surface and subsurface movement of liquid water and water-ice [6,7].

A post-Viking-era geologic mapping investigation of the Argyre impact basin and surroundings at 1:5,000,000 scale is ongoing to address important questions concerning the impact event and its subsequent influence on the geology and hydrology of the region. Questions include: What was the extent of flooding and glaciation in and surrounding the ancient impact basin [6,7]? Was the basin occupied by a large lake, and did this hypothesized lake source the Uzboi Vallis drainage system during the Noachian Period, as hypothesized during Viking-era investigation [8]? What was the extent of Argyre-related tectonism and its influence on the surrounding regions [e.g., 5,9]? How did the narrow lowland ridges in the southeastern part of the basin form [e.g., 10]?

Map status: The geologic map, which includes detailed stratigraphic and structural (fluvial and tectonic) information, has been completed (poster). A total of 20 map units have been delineated and respective crater statistics compiled using the dataset of [1] (poster). A spectroscopic/stratigraphic investigation of the map information is underway, which includes construction of cross sections [e.g., 11].

Impact crater investigation: All impact craters [1] were extracted for the map units. Cumulative size-frequency diagrams (SFDs) were created [12] and isochrons were fit from both the Hartmann [3] and Neukum [4] chronologies. These provide minimum ages of the map units. Variations in the differences in the model crater-retention ages are due to fitting different parts of the crater size-frquency distributions where there are different levels of agreement between the two systems.

All impact craters in the map region with diameters $D \geq 1$ km were manually examined to identify only those superposed (i.e., those impact craters that display pristine rims and ejecta blankets, and well-defined basins with little to no infill that have no visible evidence of resurfacing).

Focusing solely on the Argyre basin mateirals (units Ab1-4 of Table 1), and based on the isochron ages, there is a distinct time separation between Ab1, Ab2-3, and Ab4(a,b). In addition, the superposed-only craters indicate Middle Amazonian surfaces that have not undergone major modification since that time.

Preliminary mapping highlights: Detailed geologic mapping of the Argyre basin and surroundings reveal significant findings, including: (1) sequence stratigraphy indicating environmental change, (2) lakes occupying the Argyre basin, including one of largest extent that may have formed as a result of the impact event, feeding the Uzboi drainage system [8,13], (3) crater statistics corroborating the mapped sequence strigraphy, (4) and glacially, periglacially, and fluvially etched landscapes [7,13]. More work, which includes spectroscopic/stratigraphic (including cross sections) investigation of the map information, is necessary to better understand the geologic and hydrologic histories of the Argyre basin and surroundings. This includes the spatial and temporal relations among the four major stratigraphic sequences identified in the basin (units Ab1-4).

References: [1] Robbins, S.J., and Hynek, B.M., 2012. JGR-P 117, E05004, doi: 10.1029/2011JE003966. [2] Robbins, S.J., and Hynek, B.M., 2012. LPSC 43, # 4039. [3] Hartmann, W.K., 2005. Icarus 174, 294-320. [4] Neukum, G., et al., 2001. In Chronology and Evolution of Mars (R. Kallenbach, J. Geiss, and W. K. Hartmann, eds.), Kluwer Academic Publishers, 55-86. [5] Dohm, J.M. et al., 2001. USGS Map I-2650. [6] Kargel, J.S., and Strom,

R.G., 1992. Geology, 20, 3-7. [7] Kargel, J.S., 2004. Praxis-Springer, 557 pages. [8] Parker, T.J., and Gorsline, D.S., 1993. Am. Geophys. Union Spring Meeting, 1pp. [9] Scott, D.H., et al., 1986-87. USGS Map I-1802-A-C. [10] Banks, M.E., et al., 2008. J. Geophys. Res., 113, E12015, doi:10.1029/2007JE002994. [11] Buczkowski, D.L., et al., 2010. J. Geophys. Res., 115, E12011, doi: 10.1029/ 2009JE003508. [12] Crater Analysis Techniques Working Group, 1979. Icarus 37, 467-474. [13] Dohm, J.M. et al., 2011. LPSC 42, #2255. [14] Hartmann, W. K., and Neukum, G., 2001. Space Sci. Rew. 96, 165-194.

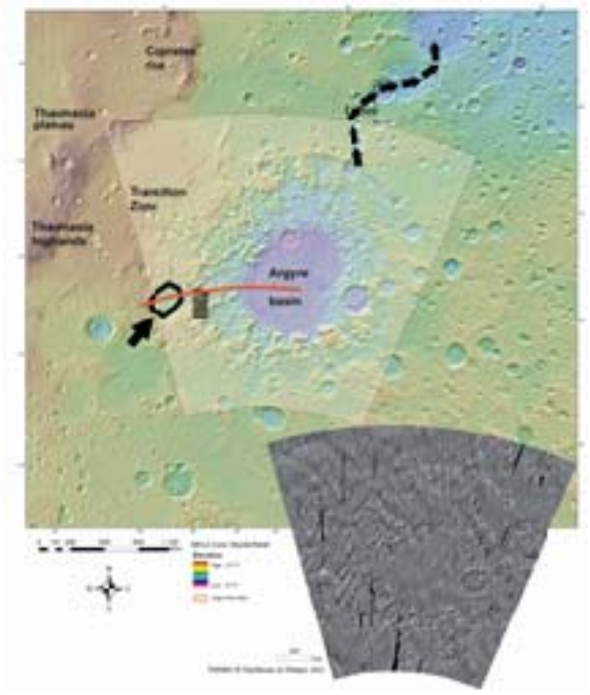

Fig. 1. MOLA color shaded relief map centered on the Argyre region (lighter shaded region). The image on the bottom right shows a 256 pixels/degree THEMIS IR day mosaic. The regional 1:5,000,000-scale mapping investigation includes the Argyre floor and rim, transition zone, and the southeast margin of the Thaumasia plateau. Also shown is a possible paleolake basin (wide arrow) located on the western margin of the Argyre impact basin and the Uzboi drainage system (narrow arrows) and possible spillway separating AWMP from the Argyre basin at a present-day topographic interval nearing 1.5km (dashed line).

Table 1. Cumulative crater densities and unit ages of the Argyre basin units in the map region (see poster for complete list and corresponding geologic map).

		Area (km^2)	Total Craters	$N(3)$ Age, Ga	$N(5)$ Age, Ga	$N(16)$ Age, Ga	Isochron Age, Ga/ Epoch based on [14]
Ab1 All	Hartmann	85635	34	$3.36^{+0.05}_{-0.17}$	$3.52^{+0.05}_{-0.09}$	$3.89^{+0.04}_{-0.05}$	$3.94^{+0.05}_{-0.07}$ / **MN**
Ab1 All	Neukum	85635	34	$3.74^{+0.03}_{-0.04}$	$3.79^{+0.03}_{-0.04}$	$3.95^{+0.04}_{-0.05}$	$3.99^{+0.05}_{-0.07}$ / **EN**
Ab2 All	Hartmann	214370	107	$3.46^{+0.04}_{-0.05}$	$3.57^{+0.03}_{-0.04}$	$3.72^{+0.05}_{-0.07}$	$3.82^{+0.06}_{-0.11}$ /**MN-LN**
Ab2 All	Neukum	214370	107	3.78±0.02	3.80±0.02	$3.79^{+0.04}_{-0.06}$	$3.89^{+0.06}_{-0.10}$ /**MN**
Ab2 Superposed	Hartmann	214370	13	0.68±0.19	0.51±0.26	0.29±0.20	0.53±0.21/**MA**
Ab2 Superposed	Neukum	214370	13	$2.44^{+0.29}_{-0.67}$	1.52±0.76	0.83±0.58	$1.77^{+0.60}_{-0.70}$ /**MA**
Ab3 All	Hartmann	208081	127	3.54±0.03	$3.65^{+0.03}_{-0.03}$	$3.79^{+0.04}_{-0.05}$	$3.78^{+0.05}_{-0.07}$ /**LN**
Ab3 All	Neukum	208081	127	$3.81^{+0.01}_{-0.02}$	3.86±0.02	$3.85^{+0.03}_{-0.04}$	$3.87^{+0.03}_{-0.04}$ /**MN**
Ab3 Superposed	Hartmann	208081	10	0.61±0.19	0.55±0.25		0.55±0.24/**MA**
Ab3 Superposed	Neukum	208081	10	2.16±0.67	1.73±0.77		1.76±0.74/**MA**
Ab4a All	Hartmann	341500	124	$3.30^{+0.06}_{-0.09}$	$3.44^{+0.05}_{-0.07}$	$3.50^{+0.06}_{-0.10}$	$3.52^{+0.06}_{-0.10}$ /**LH**
Ab4a All	Neukum	341500	124	3.72±0.02	$3.74^{+0.03}_{-0.03}$	$3.61^{+0.06}_{-0.11}$	$3.70^{+0.04}_{-0.05}$ /**EH**
Ab4a Superposed	Hartmann	341500	14	0.47±0.12	0.64±0.21		0.73±0.29/**MA**
Ab4a Superposed	Neukum	341500	14	1.67±0.45	1.98±0.66		1.92±0.74/**MA**

POSSIBLE SOURCES OF WATER FOR LATE ALLUVIAL FAN ACTIVITY IN SOUTHERN MARGARITIFER TERRA, MARS J. A. Grant[1] and S. A. Wilson[1], [1]Center for Earth and Planetary Studies, National Air and Space Museum, Smithsonian Institution, 6th at Independence SW, Washington, DC, 20560, grantj@si.edu.

Introduction: The distribution, age and morphology of alluvial deposits within impact craters on Mars provide insight into past hydrologic and climatic conditions [1-10]. Many of these deposits occur as alluvial fans within large craters in and around USGS quadrangles -20037, -25037, -30037 and -30032 (Fig. 1) where mapping is underway. A recent study of alluvial fans within large craters in southern Margaritifer Terra [10] using crater statistics coupled with regional stratigraphic context showed that deposition of exposed surfaces occurred into the early Amazonian. Hence, understanding fan morphometry (Table 1) as it relates to water sourced locally by impacts [e.g., 11-14] vs. synoptic climatic events [e.g., 10, 15] has implications for the nature of late water activity and habitability of Mars.

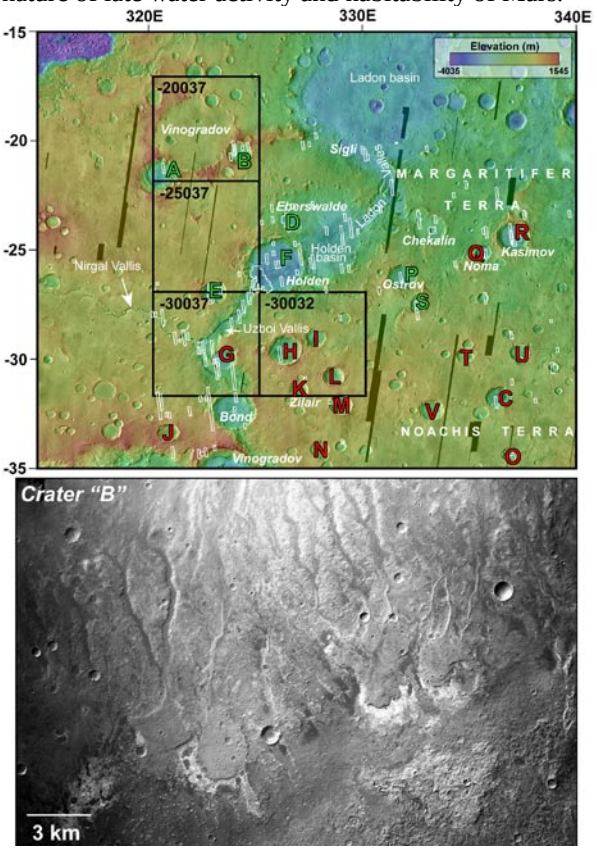

Figure 1. (Top) Craters in southern Margaritifer Terra included in study; color of label indicates crater with (green) or without (red) alluvial fans. MOLA over THEMIS daytime IR. Black and white boxes indicate USGS quadrangles being mapped and HiRISE footprints, respectively. (Bottom) Fans in crater "B" are crossed by valleys and ridges inferred to be the expression of channels. Lobes at the termini of the deposit are somewhat rounded, positive-relief features that are suggestive of deposition into shallow standing water. CTX image P17_007692_1590_XN_21S035W (5.2 m pixel scale). North is up.

Label (Fig. 1)	Crater Name	Lat. (°S)	Lon. (°E)	Diam. (km)	Min. Elev. (m)	Crater Depth (m)	Location of Fans	Nature of Crater Floor
A	none	21.8	320.6	99	-1800	3250	N (best), E, S, W	playa (?), LTD, fans, central peak, landslide
B	none	20.65	324.28	69	-680	2810	N (best), S	playa, LTD, fans
D	Eberswalde	23.76	326.7	65.3	-1500	1060	W (best), N, SW*	LTD, deltas
E	none	27.2	323.1	64	-1400	2405	N, E, W	playa, LTD, fans, landslide
F	Holden	26.14	326	154	-2370	3233	N, S, W	playa (?), LTD, fans
P	Ostrov	26.54	331.8	73	-1532	2059	N, S, E, W	playa (?), fans, central peak
S	none	27.8	332.6	43	-1117	1678	N, E, S (best), W	LTD, fans
C	none	32.2	336.4	72	-1217	1651	none	channels, playa (?) LTD, filled/mantled
G	none	30.4	323.55	58	-1500	2078	none	LTD, filled/mantled
H	none	29.9	326.4	80	-1072	2435	none	playa (?), LTD, filled/mantled
I	none	29.4	327.9	55	-1052	1947	none	LTD, filled/mantled
J	none	33.8	321	50	-6	1497	none	filled/mantled
K	Zilair	31.8	327	48	-228	1264	none	filled/mantled
L	none	31.2	328.7	49	-919	2182	none	filled/mantled
M	none	32.5	329	57	-880	1943	none	filled/mantled
N	none	34.6	328	57	-23	834	none	filled/mantled
O	none	34.8	336.9	38	-1164	1585	none	channels, filled/mantled
Q	Noma	25.4	335.6	42	-1733	1695	none	playa (?), LTD, channels, mantled
R	Kasimov	24.9	337.1	91	-1629	1975	none	playa, LTD, channels, mantled
T	none	30.2	334.8	49	-448	1208	none	channels, LTD, filled/mantled
U	none	30	337.4	47	-796	980	none	filled/mantled
V	none	32.7	333.3	59	-759	1672	none	channels, LTD, filled/mantled

Table 1. Characteristics of deposits identified in craters included in this study. Craters A through V correspond to labels in Figure 1. Minimum elevation (Min. Elev.) is relative to MOLA datum. Crater depth for craters without fans is the difference between the average rim elevation and the lowest elevation of the crater floor. For craters with fans, the crater depth is the difference between the height of the rim(s) adjacent to the best-preserved fans and the lowest elevation of the crater floor. Interpreted playa surfaces are characterized by scabby, light toned deposits (LTD) that are typically higher in thermal inertia and occur on the crater floors. They are often somewhat circular in plan view and are located at the terminus of fluvial channels or fans.

Possible Impact-Related Water Sources: Various studies [e.g., 11-14] have suggested that water released during and after crater formation may cause runoff, thereby incising valleys and contributing to the formation of fluvial and alluvial landforms. Such a mechanism for fan formation would not require broader changes in Mars climate. Athough the broad distribu-

tion (Fig. 1) and similar age [10] of the fans is not consistent with multiple impact events [16], impact-related sources of water resulting in fan formation cannot be completely ruled and is thus considered below.

Valleys incised into the ejecta around Hale crater south of the map area (35.7S, 323.6E) were interpreted as an example of impact-induced activity [12]. Because the Hale impact occurred in the Amazonian or near the Hesperian-Amazonian boundary, its formation may overlap with nearby fan formation and represents one possible mechanism for triggering fan development [e.g. 11, 12]. Hale does not appear responsible for the alluvial fans, however, because: many valleys appear confined to the ejecta, whereas some alluvial fans are in craters 700-800 km away; craters containing fans vary in azimuth from Hale and may not be consistent with downwind transport of volatiles under prevailing winds [e.g., 13]; and many of the craters without fans are closer to Hale than those with fans [10] (Fig. 1).

The impact event forming Holden crater, dating to the middle-to-late Hesperian [16], is another potential trigger of fan formation. However, like at Hale, craters with alluvial fans are up to hundreds of km from Holden and are found at a range of azimuths (though there is a general paucity of fans south of Holden). Some valleys incising Holden's ejecta source the Eberswalde delta complex [14], and while some alluvial deposition nearby (e.g., in Eberswalde) and within Holden could be related to the Holden impact [13, 14], there is additional evidence from the rim and fans around Holden that there was a gap in time between the Holden impact and when exposed fan materials were emplaced, suggesting these two events are not contemporaneous.

Six degraded craters in the higher relief near-rim of Holden suggest a gap in time between the Holden impact, formation of these six craters, and late fan activity. In addition, fans on the north wall of Holden are excavated by a crater (325.8E, 25.3S) that was later filled by younger fan alluvium. Older fans near the southwest wall of the crater (325.0E, 26.7S) are cut by Uzboi overflow channels and were later filled by younger fan sediments. In addition, deposits near the south wall of Holden (325.5E, 26.9S) were cut by fractures before being buried by younger fan sediments. Hence, any fan activity associated with crater formation was apparently followed by later fan deposition.

Possible Synoptic Water Sources: A latest Hesperian or Amazonian emplacement age for the widely distributed fans likely requires precipitation (rain or snow [5, 15]) relatively late in Martian history, after most precipitation-driven fluvial activity ended [e.g., 5, 18, 19]. Late intervals of water-driven erosion on Mars have been suggested [e.g., 19-23] and a possible source of water includes precipitation derived from redistribution of outflow channel discharge [e.g., 20, 22, 24] into the highlands [25]. The distribution of the fans implies late occurring precipitation was possibly snow whose accmulation and melting could have been modulated over time by season and (or) orbital cycles [26]. Concentration of snow into existing depressions and (or) pre-existing alcoves along crater rims would have allowed it to accumulate and facilitate physical weathering to produce the fine-grained sediments transported onto the fans [5, 10, 26]. If correct, this interpretation suggests the fans were formed during a globally occurring late period of water activity on Mars, perhaps accentuated by volcanic activity [27], topography, and/or orbital variations. [e.g., 4, 5, 15, 19]. This activity may have enabled at least locally habitable conditions relatively late in Martian history.

References: [**1**] Cabrol, N. A., and E. A. Grin (2001), *Geomorph.*, *37*, 269. [**2**] Malin, M. C., and K. S. Edgett (2003), *Science*, 302, 1931, doi:10.1126/ science.1090544. [**3**] Moore, J. M., et al. (2003), *GRL*, 30, 2292, doi:10.1029/2003GL019002. [**4**] Crumpler, L. S., and K. L. Tanaka (2003), *JGR*, 108, 8080, doi:10.1029/2002JE002040. [**5**] Moore, J. M., and A. D. Howard (2005), *JGR*, 110, doi:10.1029/ 2005JE002352. [**6**] Irwin, R. P. III, et al. (2005), *JGR*, 110, doi:10.1029/2005JE002460. [**7**] Weitz, C. M., et al. (2006), *Icarus*, 184, 436. [**8**] Kraal, E. R., et al. (2008), *Icarus*, 194, 101, doi:10.1016/ j.icarus.2007. 09.028 [**9**] Williams, R. M. E., et al. (2010), *Icarus* doi:10.1016/j.icarus. 2010.10.001. [**10**] Grant, J. A. and Wilson, S. A., 2011, *GRL*, 38, L08201, doi:10.1029/2011GL046844. [**11**] Maxwell, T. A., et al. (1973), *Geology*, *1*, 9. [**12**] Jones, A.P., et al. (2010), *Icarus*, doi: 10.1016/j.icarus.2010.10.014. [**13**] Kite, E. S., et al. (2011), JGR, 116, doi:10.1029/ 2010JE003783. [**14**] Mangold, N. (2011), *LPSC 42*, Abs. 1378. [**15**] Howard, A. D., and Moore, J. M. (2011), *JGR*, 116, doi:10.1029/2010JE003782. [**16**] Irwin, R. P. III, and J. A. Grant (2012), *USGS Sci. Invest. Map 3209* (in press). [**18**] Grant, J. A., et al. (2010), *Icarus*, doi:10.1016/j.icarus.2010.11.024. [**19**] Fassett, C. I., and J. W. Head (2008), *Icarus*, 195, 61, doi:10.1016/j.icarus.2007.12.009. [**20**] Carr, M. H. (2006), *The Surface of Mars*, 307p, Cambridge Univ. Press, Cambridge, UK,. [**21**] Gulick, V. C., and V. R. Baker (1990), *JGR*, 95, 14,325, doi:10.1029/ JB095iB09p14325. [**22**] Mangold, N., et al. (2004), *Science*, 305, 78, doi: 10.1126/science.1097549. [**23**] Fassett et al. (2010), *Icarus*, 208, doi: 10.1016/j.icarus. 2010.02.021. [**24**] Rotto, S., and K.L. Tanaka (1995), *USGS Map I-2441*. [**25**] Luo, W., and Stepinski, T. F. (2009), *JGR*, 114, doi:10.1029/ 2009JE003357. [**26**] Grant, J. A. and Wilson, S. A., 2012, *PSS* (in press). [**27**] Caudill, C. M., et al. (2012), *Icarus* (in review).

HIGH-RESOLUTION STRUCTURAL MAPPING IN WEST CANDOR CHASMA, MARS: 2012 STATUS REPORT. C. H. Okubo[1], J. A. Skinner Jr., and C. M. Fortezzo, Astrogeology Science Center, U.S. Geological Survey, 2255 N. Gemini Dr. Flagstaff, AZ 86001. [1]cokubo@usgs.gov.

Introduction: Much work has been directed toward understanding the geologic evolution of Valles Marineris and the layered sedimentary deposits that are exposed within its chasmata. The majority of this earlier work focused on structures and processes that operated at length scales of a few kilometers to thousands of kilometers. Although invaluable for establishing an initial framework for understanding the broader geologic history of this region, the finer details of these interpretations need to be further tested and refined through investigations at outcrop scales. Such insight can be gained through new, high-resolution structural mapping at length scales of 100 m or less using DEMs derived from HiRISE data.

The goal of this project is to use high-resolution structural information to test and refine current interpretations and their corollaries, address outstanding questions, and define new structural relationships, in the geologic history of the layered deposits exposed in west Candor Chasma. The standards and procedures developed over the course of this mapping effort will also help to establish new protocols for the publication of future high-resolution maps.

DEM production: The HiRISE DEMs are built following the methodology of [1,2]. These DEMs have 1 m/post spacings. The HiRISE image pairs are orthorectified using their corresponding DEMs and are output at both 0.25 m/pixel and 1 m/pixel. HiRISE DEMs and orthoimagery for map areas 1 and 2 (Fig. 1A) were constructed in early 2011. Progress in mapping these two areas is detailed below. Preliminary DEMs for map areas 3 and 4 were constructed in April 2012 and both are currently being edited. Editing of both DEMs will be complete and the corresponding imagery will be orthorectified by June 2012.

During the DEM generation process, one HiRISE stereo pair (ESP_019719_1750/ESP_020075_1750; Fig. 1A) was found to have poor stereo correlation and the extraction of a DEM from these data ultimately failed. Dejittering of both stereo images was conducted, but this degraded rather than improved the stereo correlation. This correlation problem has been observed in other HiRISE stereo pairs and its cause is not well understood. An alternate stereo pair (ESP_024967_1755/ESP_024822_1755), the current map area 4, was therefore selected.

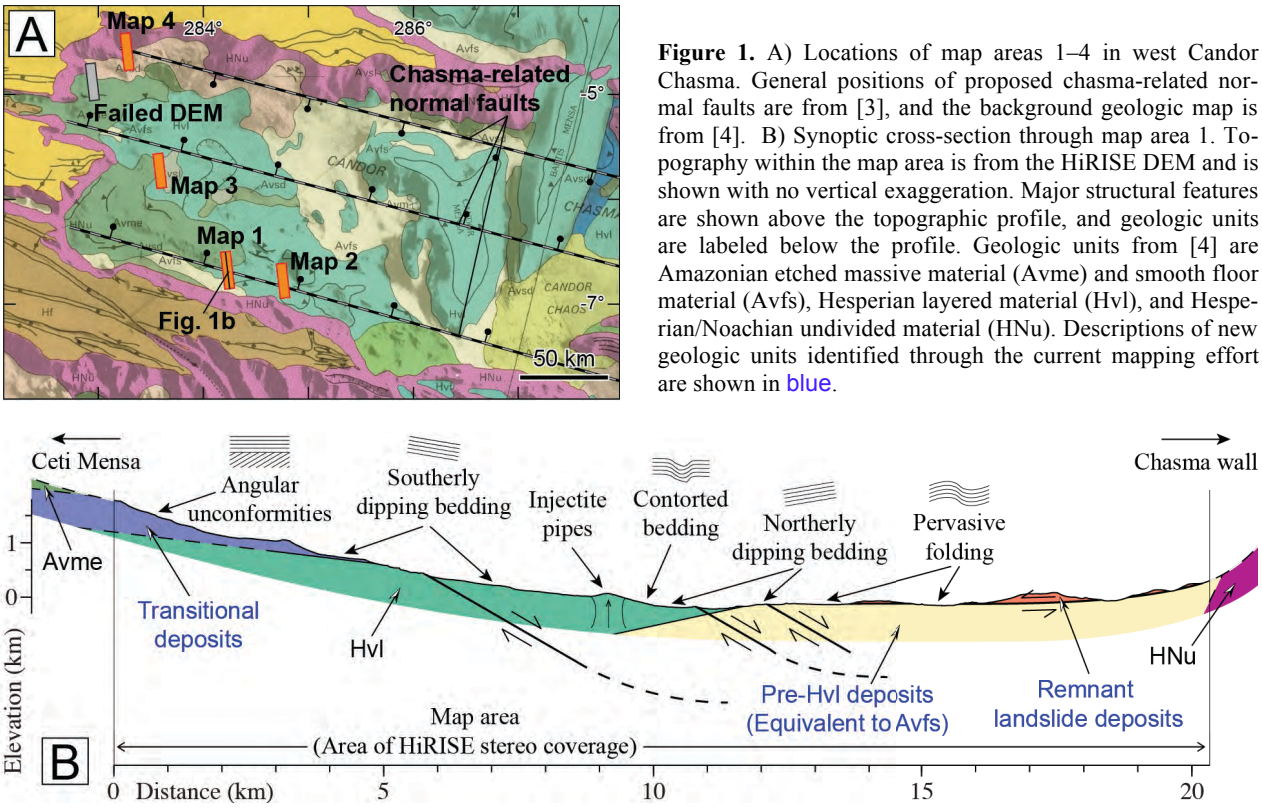

Figure 1. A) Locations of map areas 1–4 in west Candor Chasma. General positions of proposed chasma-related normal faults are from [3], and the background geologic map is from [4]. B) Synoptic cross-section through map area 1. Topography within the map area is from the HiRISE DEM and is shown with no vertical exaggeration. Major structural features are shown above the topographic profile, and geologic units are labeled below the profile. Geologic units from [4] are Amazonian etched massive material (Avme) and smooth floor material (Avfs), Hesperian layered material (Hvl), and Hesperian/Noachian undivided material (HNu). Descriptions of new geologic units identified through the current mapping effort are shown in blue.

Orientation measurement tools: Orientations of bedding, fractures and other structures in map area 1, as well as in the two predecessor high-resolution structural maps in this area [5], were made with the commercial software Orion (® Pangaea Scientific). While Orion provides reliable measurements, these data must be manually exported to a text file and then imported into ArcGIS. In order to follow a more efficient workflow, and to allow multiple project members to work without purchasing multiple licenses of Orion, we have adopted an ArcGIS, Layer Tools [6], to make these measurements.

To ensure continuity between measurements made with Orion and measurements made with Layer Tools, we compared results of both for the same features in map area 1. We analyzed the calculated orientations of bedding, fractures and unconformities. Orientations were defined by x, y, z coordinates taken at five points on each feature along a 50-100 m chord length. We found that both methods yielded consistent orientation measurements for all feature types. Accordingly, we transitioned to using Layer Tools exclusively for any additional measurements in map area 1 and for all measurements in map area 2 and beyond.

Results of Map 1: The majority of the orientation measurements for this map area have been obtained and much of the km-scale structure has been inferred from these data. The most notable structural feature is a previously unrecognized array of normal faults that exhibit generally down to the south displacements (Fig. 1B). These faults displace the deposits interpreted to be of Hesperian age by [4] (Hvl) and extend ten kilometers or more to either side of the map area. These faults may extend into the adjacent map 2.

Angular unconformities are found within the upper-most section of Hvl. These angular unconformities occur in a distinct stratigraphic interval between the areas of Hvl and Avme as mapped by [4]. Layers of Hvl can be traced up into this interval, where they become truncated by the unconformities or become indistinct. Similarly, layers of Avme can be traced down into this interval until they terminate against unconformities or become indistinct. The angular unconformities are discontinuous and appear grade into disconformities and paraconformities in some places. These unconformities can also cross-cut each other. Based on these cross-cutting relationships, this unconformity-rich stratigraphic interval between Hvl and Avme is here defined as a new unit of "transitional deposits" (Fig. 1B). This unit records a period of both erosion and deposition between the accumulation of Hvl in the Late Hesperian and the accumulation of Avme in the Middle Amazonian.

The structure of Hvl is also notable for the abundance of previously unrecognized structures indicative of soft sediment deformation (Fig. 1B). The most prominent of these structures are megapipes, which are formed by upward injection of liquefied sediments [c.f. 7]. These megapipes have diameters on the scale of many hundreds of meters to a kilometer. Also present are several examples of contorted bedding, with wavelengths on the order of several hundred meters. These features record dynamic loading (e.g. seismicity from fault rupture or impact cratering) of the sediments while they were unconsolidated and water-saturated.

Mapping also reveals that the local Avfs unit of [4] is actually conformable to the lower-most layers of Hvl. This means that these deposits are Late Hesperian or older, instead of being Middle Amazonian in age. This finding presents a notable simplification of the geologic history preserved in this area. According to [6], the local Avfs would have represented a separate depositional environment that was contemporaneous with that of Avme, but occurred in a moat between Ceti Mensa and the chasma's south wall. These "pre-Hvl" deposits (Fig. 1B) are pervasively folded within a few km of their contact with Hvl. The pre-Hvl deposits are also covered by remnants of a large landslide that originated from along the south wall of the chasma. These "remnant landslide deposits" are discontinuous in aerial extent, and the pre-Hvl deposits are exposed where the landslide deposits are absent.

Results of Map 2: Orientation measurements of the layers, fractures and unconformities in map area 2 are currently underway. Approximately 200 measurements of bedding have been made to date.

Future work: Maps 1 and 2 are expected to be complete by the end of 2012 and submitted for peer review soon thereafter. Both maps 1 and 2 will be submitted as a single publication in order to reduce the associated costs. Mapping in areas 3 and 4 will commence in 2013, with anticipated completion by the end of the year. Map areas 3 and 4 will be submitted as a single publication as well. Progress on this project is expected to accelerate with the assistance of J. Skinner and C. Fortezzo in FY12 and T. Gaither in FY13.

References: [1] Kirk, R. L., et al. (2008), *JGR*, *113*, E00A24. [2] USGS (2011), http://webgis.wr.usgs.gov/pigwad/tutorials/socetset/SocetSet4HiRISE.htm. [3] Schultz, R. A., and Lin, J. (2001), *JGR*, *106*, 16549–16566. [4] Witbeck, N. E. et al. (1991), *USGS Map I-2010*. [5] Okubo, C. H. (2010), *Icarus*, *207*, 210–225. [6] Kneissl, T. et al. (2010), *41st LPSC*, Abstract #1640. [7] Chan et al. (2007), *AAPG Memoir 87*, 233–244.

EFFICIENCY OF SCALE IN PHOTOGEOLOGIC MAPPING USING THE RUNANGA-JÖRN BASIN, MARS AND THE VERDE BASIN, ARIZONA: PROJECT INTRODUCTION AND TECHNICAL APPROACH. J. A. Skinner, Jr. and C. M. Fortezzo, Astrogeology Science Center, U.S. Geological Survey, 2255 N. Gemini Drive, Flagstaff, AZ, 86001 (jskinner@usgs.gov).

Introduction: The process of photogeologic mapping using remotely-sensed tonal variation, texture, and first-order cross-cutting relationships has proceeded largely unaltered for nearly two decades. Concurrently, the diversity and spatial range of planetary data sets and the software used for their analysis has sidelined some fundamental photogeologic concepts. For example, static cartographic schemes dictate boundaries, projection, and scales that may not efficiently accommodate modern areas of interest. Furthermore, variable coverage of diverse data sets within and across map boundaries means adjacent geologic maps may have relied on starkly different base information. Lastly, digital data sets and analytical software allow for unit definitions at scales wholly incompatible with the final, hard-copy map. The result is divergence in the consistency of geologic maps and, ultimately, the potential deterioration of their utility as contextual products for subsequent research. A refinement and modernization of photogeologic mapping strategies is long overdue.

This abstract introduces the regional settings and technical approaches of a recently-funded 3-year mapping proposal that seeks to address not only the geologic history of Martian basin-related stratigraphic sequences (Runanga-Jörn basin, Mars) but also the accuracy of photogeologic mapping methods using a terrestrial analog location (Verde Basin, Arizona). The primary objectives of this new investigation are (1) detail the geologic evolution of basin-related deposits located within the Martian intercrater highland plains, and (2) identify and reconcile the scale-based limitations of current photogeologic mapping techniques. The proposed work will result in the production of a planetary geologic map of understudied stratified materials on Mars at a scale not currently employed for USGS support, review, and publication. In addition, the work will help modernize photogeologic mapping methods by establishing strategic "best practices."

Regional Settings: This investigation will focus on mapping well-exposed basin-related layered sequences on both Earth and Mars, leveraging one against the other in order to improve our understanding of local and regional geologic processes as well as photogeologic mapping techniques and approaches.

Runanga-Jörn basin, Mars. Clarity in the ancient processes that sculpted the Martian cratered highlands can be achieved by relating vertical and lateral changes in intercrater layered sequences to evolving depositional environments [1-5]. The informally named Runanga-Jörn basin (RJB) is located in Noachian- and Hesperian-age terrains on the northern margin of Hellas basin, west of Hadriaca Patera (Fig. 1).

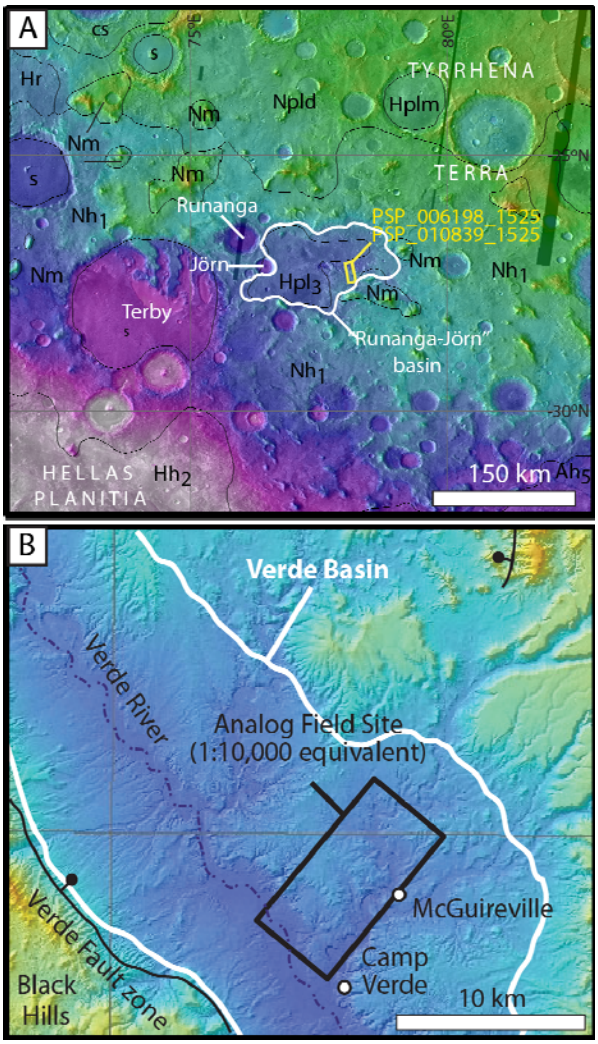

Figure 1. Regional setting of each study. (A) The Runanga-Jörn basin (RJB), Mars in MOLA shaded-relief, showing northern rim of Hellas basin. Contacts and units from [6]. RJB is located in an intercrater basin, adjacent to uplifted crustal massifs and west-flowing drainages. (B) The Verde Basin (VB), Arizona in NED shaded-relief, showing bounding faults and drainages. VB is located in a Transition Zone sub-basin, adjacent to higher-standing Paleozoic rocks of the Colorado Plateau. Field site and local municipalities noted.

RJB is roughly ovoid in planimetric shape and 160 km long by 80 km wide (**Fig. 1A**). The basin's eastern margin is dissected by channels with implied drainage of the Noachian-age cratered plains from the north,

east, and south. The basin surface ranges in elevation from -2450 to -2700m, with a very slight west-southwest slope (<0.1°). The western margin of RJB is generally un-dissected except for a single groove-like channel that debouches into 171.5-km-diameter Terby crater. The region is characterized by Noachian-age mountains (mountainous material – unit Nm of [6]), which rise >1500 m above adjacent basin-filling plains. These mountains are vestige crustal blocks that were uplifted and exposed by the Hellas forming giant impact [7]. Inter-montane regions are defined by topographic and structural basins that are occupied by smooth to rugged and locally dissected Noachian-age cratered plains (Hellas Assemblage, basin rim material – unit Nh1 of [6]).

We will focus on deciphering the geologic character of layered sequences exposed along the southeastern margin of RJB. A HiRISE stereo-pair shows complex sequences of light- and dark-toned units exposed within the margins of eroded buttes and mesas of RJB deposits, including (from bottom to top): (1) dark-toned units with superposed channel-like valleys, (2) medium-toned basal units with meter-scale columnar joints, (3) multiple asymmetric channels located in light-toned wall-rock, and (4) dark-toned capping strata and interbeds. Vertical and lateral variations in exposed materials suggest a level of detail commensurate with that required to discern the stratigraphic architecture of these rocks and sediment [1-5].

Verde Basin, Arizona. We will help elucidate the geologic evolution of the RJB on Mars by using equivalent methods and data sets to analyze the undifferentiated units of the Verde Basin (VB), Verde Valley, Arizona (**Fig. 1B**). The VB is located in the southern Transition Zone province of north-central Arizona (~40 miles south of Flagstaff), which demarcates the structural and tectonic transition between the southern Basin and Range and the Colorado Plateau. The VB is approximately 50 km long and 35 km wide and is drained by the Verde River, which runs to the southeast, sub-parallel to the southern edge of the Colorado Plateau. The VB formed by 2-3 km of normal offset along the Verde fault zone, forming a half graben (down to the northeast) that is filled with Miocene and Pliocene strata [8-11], likely accumulated due to volcanic eruptions east of VB that repeatedly blocked the southeast-flowing ancestral Verde River [8,12].

We will focus on deciphering the geologic character of the basin-related strata of the Verde Formation, which consists of well-exposed sedimentary sequences that are overlain and interfingered with volcanic rocks [12]. Sediments are primarily alluvial, lacustrine, and fluviatile in origin, though the internal characteristics and lateral variability of these rocks remain poorly defined [8-12]. From an analog mapping perspective, the lack of information regarding the vertical and lateral gradation of VB units and facies provides an excellent comparison to RJB on Mars. In both instances, the regional geologic setting has been established while the local geologic characteristics remain unresolved.

Technical Approach: Our approach to detailing, reconstructing, and conveying the geologic evolution of the RJB on Mars centers on integrating both contextual mapping (1:10,000 scale) and local observations (1:1,000 scale) to produce a balanced 1:5,000 scale geologic map of the layered deposits. Map refinement and production will be augmented by scientific and quality assessments of the VB terrestrial analog site. Both the Mars and Earth sites site will be mapped using high-resolution image stereo-pairs (HiRISE and GeoEye, respectively; 0.5 m/px resolution) and digital elevations models derived using SOCET Set® software (1.5 m/px resolution). Guided by 1:10,000-scale geologic context mapping, we will define and divide surface and wall rock materials in locations that target geologic and stratigraphic type localities. Both observed and interpreted outcrop characteristics will be portrayed in vertical section using 1:1,000-scale full resolution images. Sections will be constructed and correlated as fence diagrams using RockWorks® software. We will assess the quality of remotely-determined geologic and stratigraphic relations and interpretations using the VB site. We will identify not only the specific locations where remote-based information may be scale-limited but also the type of information that is either lost or inaccurately conveyed (*e.g.*, contact fidelity, stratigraphic characteristics, absolute material thickness). Quality assurance tasks will also include assessment of the accuracy of bed orientation measurements determined through remote datasets and how these might affect geologic interpretations. The final 1:5,000 scale geologic map of RJB will be submitted for review as a USGS SIM series map.

References: [1] Wilson, S.A. et al. (2007) *JGR*, 112, E08009. [2] Hynek, B.M. and Phillips, R.J. (2001) *Geology*, 29, 407-410. [3] Lewis, K.W. et al. (2008) *JGR*, 112, E05S02. [4] Pondrelli, M et al. (2008), *Icarus*, 197, 429-451. [5] Ansan, V. et al. (2011) *Icarus*, 211, 273-304. [6] Greeley, R. and Guest, J.E. (1987) *USGS I-1802-B*, 1:15M scale. [7] Schultz, P.H. et al. (1982) *JGR*, 87, 9803-9820. [8] Twenter, F.R. and Metzger, D.G. (1963) *USGS Bulletin*, 1177, 132 p. [9] Weir, G..W. et al. (1989) USGS I-1896, 1:100K scale. [10] Karlstrom, T.N.V. et al. (1983) *USGS MF-1567-A*. [11] Ulrich, G.E. et al. (1983) USGS MF-1558-A. [12] Nations, J.D. et al. (1981) *AZ Geo. Soc. Digest*, 13, 133-150.

FINALIZING THE NEW GLOBAL MAP OF MARS. K.L. Tanaka[1], J.M. Dohm[2], C.M. Fortezzo[1], R.P. Irwin, III[3], E.J. Kolb[4], J.A. Skinner, Jr.[1], T.M. Hare[1], T. Platz[5], G. Michael[5], and S. Robbins[6], [1]U.S. Geological Survey, Flagstaff, AZ, ktanaka@usgs.gov, [2]U. Arizona, Tucson, AZ.

Introduction: We are nearing the completion of a global geologic map of Mars at 1:20M scale that will represent the most thorough characterization of global stratigraphic units since the Viking-based 1:15M-scale maps. Here, we describe how post-Viking data sets and our comprehensive, digital, team-based mapping approach have resulted in more robust unit identification, stratigraphic analysis, and understanding of geologic materials and features planet-wide.

Data: The new mapping is primarily based on post-Viking topographic (the Mars Orbiter Laser Altimeter (MOLA) digital elevation model at 460 m/pixel spatial and ~1 m vertical resolution) and image (Thermal Emission Imaging System (THEMIS) infrared images at 100 m/pixel) data. The MOLA topographic data are critical for determining pathways of lavas, fluvial runoff, ice, and mass-wasting debris; for detecting tectonic deformation and exposed and buried impact structures; and for measuring thicknesses and volumes. Because Viking-based topography was largely inadequate for meaningful global assessments of this kind, this data set alone yields substantial refinements for geologic mapping. Although Viking visible range images were generally of similar to somewhat lower (100 to 300 m) resolution than that of THEMIS images, greater detail could be mapped using THEMIS. Additional image data sets (e.g., THEMIS visual range, Viking, High Resolution Stereo Camera, and Context Camera) as well as transparent overlay of image data onto MOLA topography were also employed for enhanced geologic perspectives, based largely on factors such as landform orientations, camera pointing, sun angle, atmospheric conditions, etc. [1].

Approach: Material units are discriminated mainly by relative age, as supported by stratigraphic relations and crater densities. Additional distinguishing criteria include geographic setting and primary geomorphic characteristics indicative of process origins. In addition, feature mapping assists with documenting geological and hydrological processes, geometries of tectonic deformation, and transport pathways.

The use of GIS software enables and facilitates scale-based methodologies of drafting, editing, and embedding ancillary information into the map, providing enhanced capabilities to the mappers.

Crater Counting: The effort put forth in dating units in this global map is unprecedented. First, more so than in the Viking geologic map [2], we focus on discriminating units based on their ages according to the Martian epoch system [3]. This results in more definitive and precise characterization of the surface chronology. Second, type areas are selected and crater counted down to ~100 m and fitted to the Neukum-Ivanov crater production function [4]. These data validate the stratigraphic ages tentatively assigned according to their geomorphic appearance, define the crater size ranges accumulated and preserved from each unit's formation, and characterize timing and amount of resurfacing produced by the unit and post-unit resurfacing. Third, a recent global crater database enables determination of crater densities ≥1 km for every outcrop [5]. The database is used to determine cumulative densities for crater diameters of 1, 2, 5, and 16 km as a simple way to assign stratigraphic epochs. The size-frequency distributions generally fit well with derived formulations (in some cases after removing buried craters and merging crater material to improve accuracy) [3, 6].

Age Assignments: The combined mapping and crater dating approach results in different kinds of age assignments. Some assignments correspond to single epochs (where the Noachian (N), Hesperian (H), and Amazonian (A) are divided into Early (e), Middle (m), and Late (l) episodes). Although these units have the best constrained ages, the crater counts are capable of providing only mean ages. As such, our epoch assignments apply to the majority of the exposed unit outcrops, though in many cases minor amounts of the units likely range in age beyond the assigned epoch and/or may include some amount of other units of similar or differing age. Other units have broader age constraints spanning two or more epochs. This results from units that developed discontinuously in time and space such that averaging is unavoidable at map scale. In addition, broader ages are applied to units that are comprised of co-mingled materials of disparate ages (e.g., knobs of N material surrounded by H or A plains).

Geologic Interpretation: Here, we summarize the major types of geologic terrains and processes as they affected the planet's surface in space and time.

Impact basins: Large impact basins >150 km in diameter formed mostly in the eN, including Hellas. Argyre and Isidis formed in the mN, and others formed in the lN, H, and eA. N basins and craters are degraded and variously infilled with slope debris, fluvial/lacustrine and eolian sediments, and volcanic flows throughout Martian history

Highland strata: Layering is evident in N materials virtually wherever they are eroded, including steep scarps of Valles Marineris and in fluvial and outflow

terrains. The layers likely include mixtures of volcanic flows, fluvial/lacustrine and other types of sediments, and impact ejecta blankets. The eN outcrops generally have high local relief and are more extensive than previously recognized, particularly in higher-elevation regions--especially surrounding Hellas basin but are less common in lower-standing Arabia Terra. The eN highland materials include large scarps that represent structures formed by impact basins and early tectonics. Embaying much of the eN outcrops are mN and to a lesser extent lN and eH outcrops of progressively lower relief and crater density indicative of highland and midland regolith development. Fluvial valleys are common in eN and mN outcrops, but lN and eH outcrops form planar, undissected deposits likely comprised of fluvial and aeolian sediments.

Volcanic edifices. Recognizable volcanic edifices date back to the N, perhaps as early as the eN, and their activity extends to the lA. The majority of N edifices occur peripheral to the southern part of Tharsis. Some 20 denuded N mountains south of 30° S. may be volcanic, but lava flows or caldera structures are not recognized on them--possibly due to water/ice denudation. All N edifices except Ceraunius Tholus, which is marginally Noachian, occur in the southern hemisphere. Circum-Hellas volcanic edifices appear to be lN in age, whereas more central shields and domes of Tharsis and Elysium are H to A. Edifice ages largely indicate when the volcanoes went extinct and generally do not reflect when the volcanoes originated.

Volcanic flows. Volcanic flow morphologies are susceptible to obliteration by processes such as impact gardening, and the earliest recognizable flows on Mars are lN. Earlier flows likely exist but are difficult to identify. We mapped prominent flow directions based on the trends of lobate margins.

We differentiate where possible discrete outcrops of flow materials according to their mean crater densities, where stratigraphic relations and/or crater distributions indicate that most exposed and near-surface flows are of similar age. However, we felt compelled to map the majority of the Tharsis and Elysium rises as a broad mix of ages (AH) because of their high spatial variability in crater density but lack of mappable boundaries within the outcrops. This result is in contrast to previous global mapping that distinguished such boundaries [2]. Outside of these rises, extensive flows formed Malea (lN), Hesperia (eH), and Syrtis Major Plana (eH) on the margins of Hellas and Isidis basins.

We also mapped volcanic fields consisting of groups of low, relatively small vent features and their flows in Tharsis and Elysium of lH and lA ages. The lA fields are among the youngest recognized eruption sites on Mars.

Transition zone. We define the transition zone to include temporally and spatially intermediate areas between highlands and lowlands. This zone is typified by slopes that were modified by mass wasting, outflow and fluvial activity, and subsidence and collapse, mostly between the lN and lH but locally into the A. The transition zone includes the highland/lowland boundary, chaotic terrains north and east of Valles Marineris (including Margaritifer Terra) and higher-standing N materials between Elysium rise and Amazonis Planitia. In these areas, N material was eroded during the H to A, resulting in channels, debris aprons, landslides, and plains deposits. Between Gale crater and Olympus Mons, we remap the Medusae Fossae Formation [2] and delineate a younger (lH to A) unit from an older unit (eH), which are separated by a hiatus indicated by exhumed craters, wrinkle ridges, and inverted channels. In Valles Marineris, light-toned layered deposits infilled canyon floors during the lH, then landslides occurred along canyon walls in the A.

Lowland materials. The majority of the northern lowlands are covered mainly with sediments derived from outflow channels, mud volcanism, and degradation of the north polar plateau. While the lowlands were likely infilled throughout the N and H by volcanic rocks and sediment, the majority of the lowlands have a lH crater retention age. Pedestal-type craters and thumbprint terrains attest to continued regional to local plains activity during the A.

Polar regions. Resurfacing by icy materials as indicated by their albedo, volatility, and radar transparency has occurred in the polar regions since the H. Both regions have a field of vent-like features that may be volcanic or cryovolcanic eruptive centers. The youngest, lA polar deposits are finely layered and include local and perhaps regional truncation surfaces.

Tectonic features. Wrinkle ridges are the most common structure mappable at global scale. However, they appear more prominent in lN to eH materials, especially in volcanic flows and surrounding the Tharsis rise. Wrinkle ridge development was minor during the A. Grabens are common in N and H parts of the Tharsis rise, especially surrounding the Thaumasia plateau and Alba Mons and on Tempe Terra, as well as extending SW from the Tharsis rise.

References: [1] Dohm J.M. and Hare T.M. (2009) *LPSC XXIX,* Abs #1949. [2] Scott D.H. et al. (1986-87) *USGS Maps I-1802-A-C.* [3] Tanaka K.L. (1986) *JGR, 91,* E139-E158. [4] Hartmann W.K., and Neukum G. (2001) *Space Sci. Rev., 96,* 165-194. [5] Robbins S.J. (2011) PhD Thesis, CU-Boulder. [6] Werner S. and Tanaka K. (2011) *Icarus, 215,* 603-607.

THE SCANDIA REGION OF MARS GEOLOGIC MAP. K. L. Tanaka[1], J. A. P. Rodriguez[2], C. M. Fortezzo[1], R. K. Hayward[1], and J. A. Skinner, Jr.[1] [1]U. S. Geological Survey, Flagstaff, AZ (ktanaka@usgs.gov), [2]Planetary Science Institute, Tucson, AZ.

Introduction: We are in the final year of a four-year project to produce a geologic map of the Scandia region of Mars at 1:3,000,000 scale for publication in the USGS Scientific Investigations Map series. The primary objective of the map is to reconstruct the geologic history of this region of Mars using post-Viking image and topographic data [1-2]. We rely mostly on Mars Orbiter Laser Altimeter (MOLA) digital elevation models, Thermal Emission Imaging Spectrometer (THEMIS) infrared and visual range, and Context Camera images for mapping and topographic analysis.

The study region includes (1) a broad swath of the Vastitas Borealis units [1] (where the Phoenix landing site is located); (2) part of the margin of the north polar plateau, Planum Boreum; and (3) the northern margin of the immense Alba Mons volcanic shield.

Science results: Previously we presented a preliminary geologic map of the study region consisting of 20 map units and various features [3] (Fig. 1). Our mapping results provided geologic context for evaluation of geomorphic features, including the distribution and potential origin of (a) >17,000 knobs throughout the study region and concentrated in Scandia Colles, (b) the Scandia Tholi and Cavi field of round plateaus and irregular depressions, and (c) pronounced, channeled flows emanating from fissures radial to Milankovič crater.

We postulated that the location of Scandia down-slope of Alba Mons could explain formation of Scandia features due to Alba Mons volcanism, which was active during the Late Hesperian (and perhaps earlier) and Early Amazonian. The associated crustal heating may have resulted in a zone of partial volatile melt [4]. Farther north the zone of partial volatile melt transitioned into a zone of permafrost, which would account for the accumulation of older, ice-rich materials making up the base of Planum Boreum. Scandia Tholi and Cavi occur within a sub-basin within the northern lowlands that would have preferentially accumulated ices, sedimentary fines, and evaporites related to outflow channel activity and perhaps groundwater emergence. We inferred that these conditions led to (a) enhanced surface collapse and gradation to explain many of the knob fields (including Scandia Colles), (b) sedimentary diapirism to form Scandia Tholi and Cavi, and (c) impact-induced mobilization of surface material that resulted in associated flow deposits. In another study, Rodriguez and Tanaka [5] investigated the only extensive northern plains region that does not comprise a topographic sub-basin within the northern lowlands. The region occurs south of Gemini Scopuli on Planum Boreum and north of a zone of highland collapse along the margin of Arabia Terra, and it is *not* located down-slope from outflow channel discharges from the highlands. Widespread landforms in that region include knob fields, degraded wrinkle ridges, and pedestal craters, as well as an area of older plains materials, which contains channels and possible thermokarst features. The geomorphology indicates relatively less dramatic surface gradation than for Scandia; this also occurred during the Late Hesperian and into the Amazonian. The authors postulated that emergence along tectonic fabrics of excess pressured groundwater led to extensive resurfacing of a Late Hesperian cratered landscape. These resurfacing stages contributed to the generation of northern plains sediments and volatile deposits within them. Aquifer pressurization resulted from an elevated hydraulic head produced by aquifers extend across the regional highland-lowland boundary (HLB).

A third investigation of chaotic terrains within the southern circum-Chryse outflow channels [6] indicates that the Martian cryosphere may contain lenses of briny fluids (cryopegs). Just like in the investigated chaotic terrains, no channels emerge from the similar-sized Scandia Cavi [4], which suggests that both features share a history of gradual devolatilization of upper crustal materials that was not driven by overpressured water systems. In addition, the finding of gypsum aeolian deposits on nearby dunes is consistent with existence of salt deposits within the regional upper stratigraphy (which would facilitate cryopeg formation).

Summary and implications: These studies indicate that at least two distinct cryo-hydrospheric settings, which likely contributed a previously recognized complex history of sedimentary and volatile accumulation in the Martian northern lowlands, as well as to the subsequent modifications of these materials. These include: (I) zones where eruptions of groundwater and fluidized sediments in the lowland occurred over trans-HLB aquifers and (II) zones where volcanic heating partially melted permafrost within the cryosphere. The existence (or formation) of fluid lenses within a cryospheric setting could have facilitated some types of volatile-driven resurfacing that apparently affected the northern plains and particularly during low obliquity (colder) conditions.

Next steps: During this final year we will accomplish three tasks. First, we will incorporate modifications resulting from a focused mapping study of the Scandia Tholi and Cavi, given that our regional analysis [4] noted but did not reconstruct complex details in the development of these features. Evident were multiple stages of tholi/cavi development and attendant

feature development, including narrow sinuous ridges, polygonal troughs, remnants of paleosurfaces (as elevated pedestals), and moats. We are also interested in documenting the duration, timing and stages of this activity. Second, we will incorporate at scale a new geologic unit, the Middle Amazonian lowland unit being incorporated in the global geologic map of Mars [7]. development of Scandia region features, thereby testing. Finally, we will assemble our results and revisit and update our preliminary geologic map [3] and complete it for submission following mappers' handbook guidelines [8]. We plan to follow a more objective approach to line-feature mapping that is being developed for the global map of Mars [8].

References: [1] Tanaka K.L. et al. (2005) *USGS SIM-2888*. [2] Tanaka K.L. et al. (2003) *JGR, 108,* 8043. [3] Tanaka K.L. et al. (2010) *in* Bleamaster et al. (eds.), *Abs. Ann Mtg. Planet Geol. Mappers, Flagstaff, AZ, 2010, NASA/CP—2010-217041*, p. 48-49. [4] Tanaka K.L. et al. (in press) *Planet. Space Sci.*, doi:10.1016/j.pss.2010.11.004. [5] Rodriguez J.A.P. et al. (2010) *Icarus, 210,* 116-134. [6] Rodriguez J.A.P. et al. (2010) *Icarus, 213,* 150-194. [7] Tanaka K.L. et al. (this vol.). [8] Tanaka K.L. et al. (2010) *in* Bleamaster et al. (eds.), *Abs. Ann Mtg. Planet Geol. Mappers, San Antonio, TX, 2009, NASA/CP—2010-216680, Appendix,* 21 p.

Figure 1: Geologic map of the Scandia region with units and symbols. North is at top and vertical meridian is 230ºE.

GEOLOGIC MAPPING OF ARSIA AND PAVONIS MONTES. D.A. Williams[1], W.B. Garry[2], J.E. Bleacher[3], D. Shean[4], R. Greeley[1*]. [1]School of Earth & Space Exploration, Arizona State University, Tempe, AZ 85287 (David.Williams@asu.edu); [2]Planetary Science Institute, Tucson, AZ; [3]Planetary Geodynamics Division, NASA Goddard Spaceflight Center, Laurel, MD; [3]Malin Space Science Systems, Inc., San Diego, CA. [*]Deceased.

Introduction: We are funded by the NASA Mars Data Analysis Program (MDAP) to produce 1:1,000,000 scale geologic maps of Arsia Mons and Pavonis Mons, as well as conduct mapping of surrounding regions. In this abstract we discuss progress made during years 1 and 2 of the 4-year project.

Objectives: The *scientific objectives* of this mapping project include: 1) Determining the areal extent, distribution, and age relationships of different lava flow morphologies (**Fig. 1, next page**) on the main flanks, rift aprons, and associated small-vent fields of Arsia and Pavonis Montes to identify and understand changes in effusive style across each volcano, and to provide insight into Martian magma production rates. This work builds on a preliminary study performed by Co-I Bleacher as part of his Ph.D. dissertation [1]. Results will provide insight into the overall volcanic evolution of each structure, enable comparisons between volcanoes, and determine the extent of each shield's contribution to the Tharsis plains; 2) Determining the areal extent and distribution of purported glacial and aeolian deposits on the flanks of each shield and their relationship to the lava flows. Results will establish a volcano-wide understanding of the nature of potential lava-ice interactions and the contribution of aeolian cover to the current form of the shields, enabling comparison among the shields potentially in different stages of development; and 3) Characterizing erosional and tectonic features, such as rift zone graben, flank terraces, and channel networks present on the flanks, rift aprons, and small-vent fields (**Fig. 2, next page**), to determine their relationships to volcanic materials and processes.

Results: We are completing our year 2 objectives on schedule. Our objectives for year 2 include: 1) Review and refine the mapping of structural features over both Arsia and Pavonis Montes volcanoes (**Fig. 3a,b, next page**); 2) Determine the material units to be mapped on Arsia and Pavonis Montes, using the mapping of Olympus Mons as a template [2]; and 3) Begin mapping long lava flows throughout the map area and develop criteria to determine the stratigraphy of overlapping lava flows. In Fall 2012 we will apply the material unit definition and characterization methodology for the Olympus Mons to the Tharsis Montes, and begin unit mapping. Material unit mapping will be the primary tasks of years 3 and 4.

Long Lava Flow Mapping on Arsia Mons: The southwest rift apron on Arsia Mons is comprised of several lava flows tens to hundreds of kilometers. One aspect of this project is to map the length and area of these lava flows (Fig. 4). Thirty-five lava flows have been mapped to date. They range in length from 21 to 228 km and area from 65 to 2685 km^2. These values represent a minimum because the flows are partially buried by other flows, concealing their true dimensions and source areas. From our preliminary mapping, these flows are typically leveed flows, and the flows with shorter length and lower area are observed closer to the chasmata on the flank of Arsia Mons, a potential source area for lava flows on the apron.

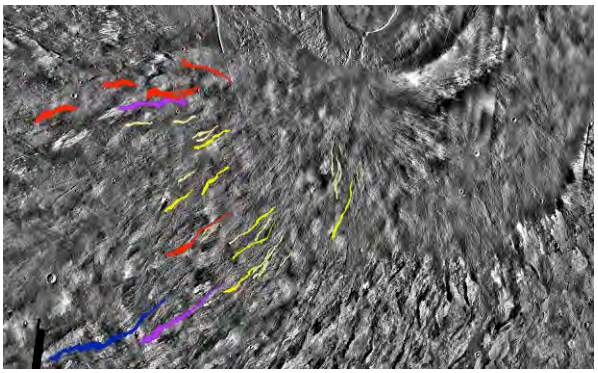

Figure 4. Lava flows mapped on the southwest rift apron of Arsia Mons, color coded by polygon area. Light Yellow: 65-271 km^2, Dark Yellow: 272-491 km^2, Red: 492-968 km^2, Purple: 969-1596 km^2, Blue: 1597-2685 km^2.

References: [1] Bleacher, J.E., R. Greeley, D.A. Williams, S.R. Cave, and G. Neukum (2007), Trends in effusive style at the Tharsis Montes, Mars, and implications for the development of the Tharsis province, *J. Geophys. Res., 112,* E09005, doi:10.1029/2006JE 002873. [2] Bleacher et al. (2012), this meeting 1805.

Figure 1 (next page). Type examples of volcanic units mapped in the Tharsis Montes, using HRSC and THEMIS data. From left to right, top to bottom: A) channel-fed flows (CFF), B) tube-fed flows (TFF), C) raised ridges, D) tabular flows, E) fissure-fed flow fields, F) low shields, G) cones, H) a mottled unit, I) a hummocky unit, J) a smooth unit, K) collapse of non-impact origin, and L) channel network terrain. Modified from [1].

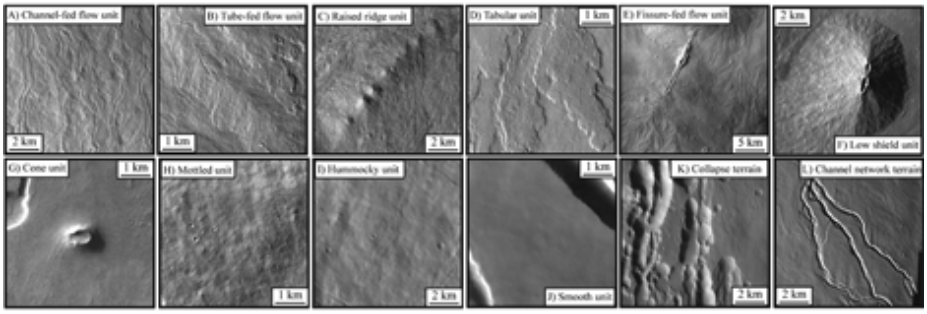

Figure 2 (below). Color-coded altimetry map of the central Tharsis region of Mars showing our mapping regions and the area of our mapping coverage (derived from the ArcGIS™ project provided by the USGS). This map shows superposed CTX coverage (6 m/pixel, bottom image), which almost fully covers the primary mapping regions (smaller solid black rectangles). Supplemental mapping regions include the rift aprons and shield fields (solid white rectangles) and a region of long lava flows (dashed white rectangle).

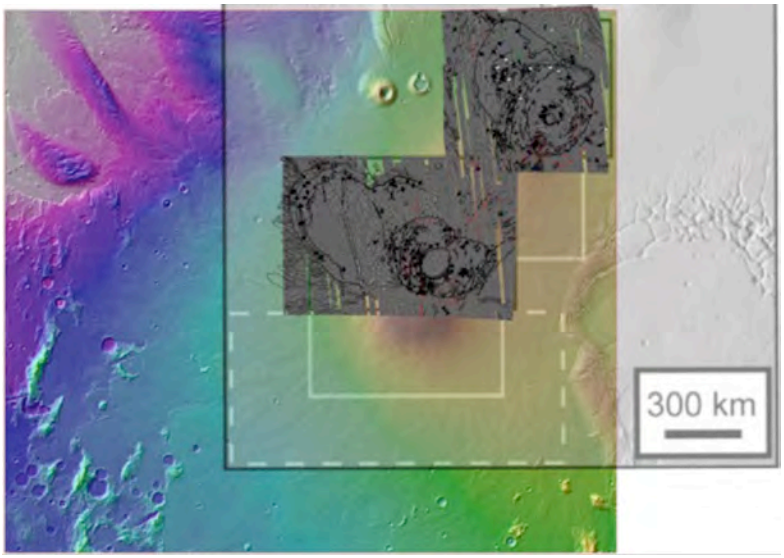

Fig. 3a (below, left). Structural mapping of Arsia Mons superposed on CTX coverage (6 m/pixel) and MOLA color map. **Fig. 3b (below, right).** Structural mapping of Pavonis Mons on same basemap. Red lines mark the trace of volcanic lava channels and/or the traces of lava tubes. Linear features with the white diamond symbols mark the locations of eskers in glacial terrains, and possible dikes in volcanic terrain. Figures derived from the ArcGIS™ project provided by the USGS.

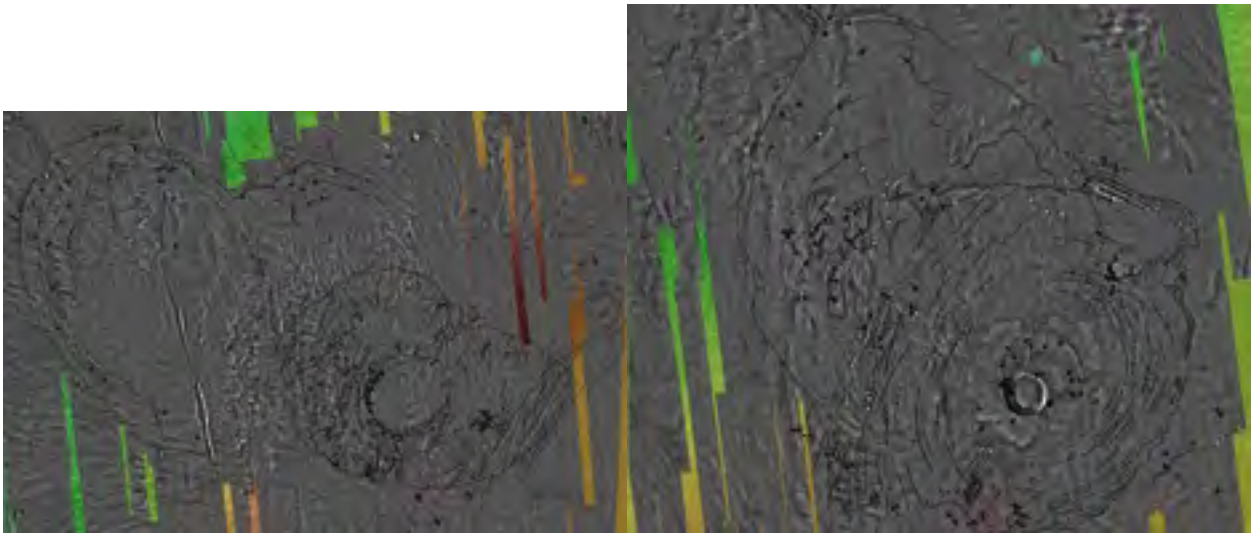

GEOLOGIC MAPPING OF THE OLYMPUS MONS VOLCANO, MARS. D.A. Williams[1], J.E. Bleacher[2], D. Shean[3], R. Greeley[1*], [1]School of Earth & Space Exploration, Arizona State University, Tempe, AZ, 85282, David.Williams@asu.edu, [2]Planetary Geodynamics Laboratory, Code 698, NASA GSFC, Greenbelt, MD, 20771, [3]Malin Space Science Systems, Inc., San Diego, California. [*]Deceased.

Introduction/Background: We are in the third year of a three-year Mars Data Analysis Program project to map the morphology of the Olympus Mons volcano, Mars, using ArcGIS by ESRI. The final product of this project is to be a 1:1,000,000-scale geologic map. The scientific questions upon which this mapping project is based include understanding the volcanic development and modification by structural, aeolian, and possibly glacial processes.

The project's scientific objectives are based upon preliminary mapping by Bleacher et al. [1] along a ~ 80-km-wide north-south swath of the volcano corresponding to High Resolution Stereo Camera (HRSC) image h0037. The preliminary project, which covered ~20% of the volcano's surface, resulted in several significant findings, including: 1) channel-fed lava flow surfaces are areally more abundant than tube-fed surfaces by a ratio of 5:1, 2) channel-fed flows consistently embay tube-fed flows, 3) lava fans appear to be linked to tube-fed flows, 4) no volcanic vents were identified within the map region, and 5) a Hummocky unit surrounds the summit and is likely a combination of non-channelized flows, dust, ash, and/or frozen volatiles. These results led to the suggestion that the volcano had experienced a transition from long-lived tube-forming eruptions to more sporadic and shorter-lived, channel-forming eruptions, as seen at Hawaiian volcanoes between the tholeiitic shield building phase (Kilauea to Mauna Loa) and alkalic capping phase (Hualalai and Mauna Kea).

Methods: To address our science questions we are conducting flow morphology mapping on the Olympus Mons main flank at ~ 1:200,000 scale using the Context Camera (CTX) image mosaic as our base data. This scale enables a distinction between sinuous rilles and leveed channels, which is fundamental for interpreting abundances among, and changes between, tube- and channel-forming eruptions. We identify Channeled, Mottled, Hummocky, Smooth, Tabular, and Scarp Materials morphology units. We do not uniquely interpret a mapped unit as tube-fed flows as was done by [1]. Instead, we map sinuous rilles and chains of depressions as linear features. We identify fans as location features forming topographic highs surrounded by radiating flow patterns. We distinguish elongate topographic ridges as surface features. To assist in the identification of ridges and fans we derive local contour maps at 25, 50 and 75 meter intervals from the HRSC DTMs and MOLA DEMs.

Primary science issues driving this research project are identifying where the volcanic materials were erupted from, and determining if rift zones are present. In order to address these issues we separate the Channeled and Mottled units into 1) caldera-sourced, 2) fan-sourced, and 3) flank units. We also map as linear features boundaries between significant flow fields. Often we observe two distinctly different channelized flow fields that would be mapped singularly as the Channeled unit. However, distinguishing between these flow fields might provide insight into eruption recurrence rates.

Results: After conducting 1:1,000,000 structural mapping of the volcano [2], we are now focused on the morphology mapping on the flank of the volcano.

Our mapping of CTX data at ~ 6 m/pixel shows that surfaces that would have been mapped as lava tubes by [1] from HRSC data (12-20 m/pixel) can be divided into several other units (typically Mottled, Smooth, and Channeled). This is shown in Figure 1 where a topographic ridge with sinuous rille and fan is seen to be dominated by the mottled unit and some small channels. As such, we now infer the presence of tube-fed flows by a combination of at least two of the following criteria: rilles or pit chains, topographic ridges with smooth or mottled surfaces, fans, and/or non-impact raised rim depressions. As such, a tube-fed flow can comprise several Olympus Mons morphologic units. These criteria are also based upon field work funded by the Moon & Mars Analog Missions Activities Program and a Hawaiian analog is demonstrated in Figure 1 [3]. We will conclude our morphologic mapping by interpreting which flow surfaces are tube-fed and adding this information as a surface feature.

Our observations also suggest that an inference by [1] that tube-fed flows are embayed by younger channel-fed flows is not always consistent. If in fact a number of major tube systems are observed to be the locally youngest flow features, then based on comparison with the Hawaiian volcanoes, Olympus Mons might be in an evolutionary stage similar to Kilauea and Mauna Loa (tholeiitic shield building) as opposed to Hualalai and Mauna Kea (alkalic capping).

The Mottled and Hummocky units of [1] were noted as difficult to distinguish, in other words, a possible over-interpretation. The distinction between the units was based on surface roughness, Mottled being rough at the 10s-100s m scale and Hummocky at the 100s-1000s m scale. The CTX mosaic confirms that these two units are unique. The Mottled unit is now seen to represent the development, or near development, of small channeled flows (not detectable at the mapping scale of 1:200,000 but at full resolution), whereas the Hummocky unit appears to be a mantled lava flow surface, or a location where channels did not form near the caldera.

Along the base of the volcano, particularly to the N and SE, are several flat topped plateaus that are unique from the apparently normal faulted cliffs of the basal scarp. We infer these features to be analogous to the Ninole Hills of Mauna Loa, HI [5,6]. These features are thought to represent an older volcano surface that remains after flank collapse. As such, these locations provide a window into older Mauna Loa flank construction [4] or possibly even Hualalai [5]. The Olympus Mons plateaus are similar in that they preserve lava flow textures on the upper surfaces, stand above the younger, embaying lava flows, and might be associated with large flank collapses expressed as the aureole deposits [6]. If these martian features are similar to the Hawaiian Ninole Hills, then they would be an ideal location to assess possible changes in magma composition for the Olympus Mons volcanic system.

Ongoing Mapping: We have identified map units and features that appear to remain consistent across Olympus Mons and provide insight into the development of the volcano. We are currently continuing our mapping from the south flank, clockwise around the volcano. The northwest flank does show a surface mantle similar to that of the Hummocky unit near the summit [7]. This region might prove to require the addition of new map units. Otherwise, our unit identification and mapping efforts suggest that the current approach will be sufficient to complete the project and to provide new insight into the current science questions outlined in our proposal.

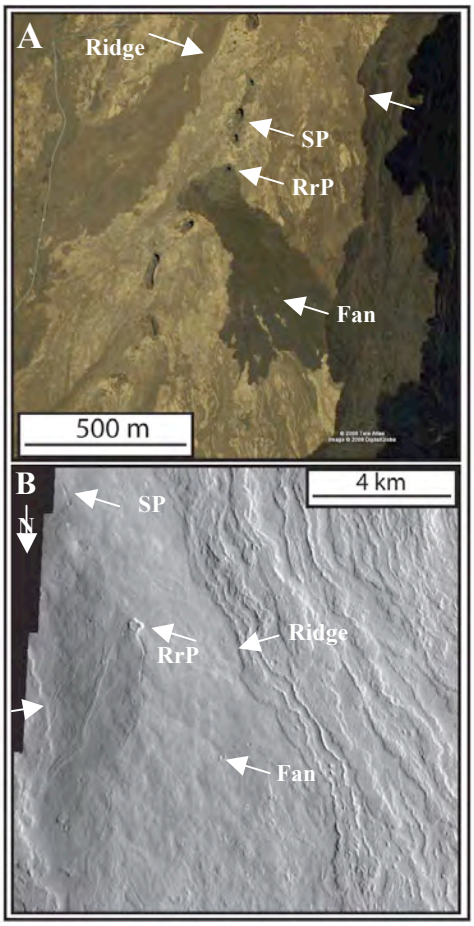

Figure 1. A) Landsat image (Google) showing the Pōhue Bay lava flow with several rimless pits that are sinuously aligned (SP) along the axis of a raised ridge (Ridge). Some pits also display raised rims (RrP), with one as the source for a ~750 m ʻaʻā flow (Fan). B) Themis image showing an Olympus Mons lava tube with rimless pits that are sinuously aligned (SP) along the axis of a ridge (between arrows marked "Ridge"). A raised rim pit (RrP) also is located at the apex of a lava fan (Fan). Although the ridge typically shows a mottled surface it also displays minor channels.

References: [1] Bleacher et al., (2007), JGRE 112, doi:10.1029/2006JE002826. [2] Williams et al., (2010), LPSC 41, #1053. [3] Bleacher et al., (2011), LPSC 42, #1805. [4] Lipman et al., (1990), Bull. Vol. 53, 1-19. [5] Holcomb et al., (2000), Geology, 28, doi:10.1130/091-7613(2000)28. [6] McGovern et al., (2004), JGRE 109, doi:10,1029/2004JE002258. [4] Basilevsky et al., (2005), Solar System Research, 39, 2, 85-101.

THE AV-9 NUMISIA QUADRANGLE OF VESTA. Buczkowski, D.L.[1], Wyrick, D.Y.[2], Scully, J.E.C[3], Williams, D.A.[4], Hiesinger, H.[5], Garry, W.B.[6], Yingst, R.A.[6], Le Corre, L.[7], Nathues, A.[7], Schenk, P.M.[8], Jaumann, R.[9], Raymond, C.A.[10], Pieters, C.M.[11] Roatsch, T.[9], Preusker, F.[9], Russell, C.T[3]. [1]JHU-APL, Laurel, Maryland, USA; [2]SwRI®, San Antonio, Texas, USA; [3]UCLA, Los Angeles, California, USA, [4]ASU, Tempe, Arizona, USA; [5]Wilhelm Westfalisch University, Münster, Germany; [6]PSI, Tucson, Arizona, USA; [7]Max Planck Institute, Katlenburg-Lindau, Germany, [8]LPI, Houston, Texas, USA; [9]DLR, Berlin, Germany; [10]JPL, California Institute of Technology, Pasadena, California, USA; [11]Brown University, Providence, Rhode Island, USA

Introduction: NASA's Dawn spacecraft arrived at the asteroid 4Vesta on July 16, 2011, and is now collecting imaging, spectroscopic, and elemental abundance data during its one-year orbital mission. As part of the geological analysis of the surface, the Dawn Science Team has begun geologic mapping of Vesta's surface at the global scale [1,2] and as a series of 15 quadrangle maps that are being produced based on Framing Camera (FC) images , along with Visible & Infrared Spectrometer data (VIR) obtained during the High-Altitude Mapping Orbit (HAMO). We here concentrate on our geologic analysis and mapping of quadrangle Av-9 Numisia.

Geologic Setting: Av-9 Numisia quadrangle is located in the equatorial region of Vesta, extending from ±22° latitude and from 216º - 288º E longitude (Fig. 1). The region is dominated by Vestalia Terra, a distinct region of Vesta. Many of the impact craters in Av-9 have both bright and dark layers in their walls and also distinct ejecta lobes.

Data: Clear filter (monochrome) FC HAMO images (spatial resolution of ~70 m/pixel) were mosaicked to make a base for this quadrangle (Fig. 2a). Topography of Av-9, is observed in a colororized Digital Terrain Model (DTM) derived from Survey orbit FC data [3-5] (Fig 2b). Variations in surface compos tion are revealed by VIR hyperspectral images from Survey (700 m/pixel) and HAMO (200 m/pixel) orbits and FC color ratio images (250 m/pixel) from Survey orbit (Fig. 2c).

Compositional Information: FC color ratio images using standard *Clementine* ratios [Red (750/430 nm); Green (750/920 nm); Blue (430/750 nm)] [6] show compositional variations within the Numisia quadrangle (Fig. 2c). Several of the craters on Vestalia Terra have "colorful" ejecta, indicating spectral and possibly compostional diversity. Further study with VIR data is underway to investigate the significance of these color variations observed in the FC color ratio data. VIR data analysis thus far has concentrated on determining the band depth of the 1 μm and 2 μm a sorptions associated with iron-bearing pyroxene minerals [7,8].

Geologic Units and Features: Three of the global geologic units are present in Av-9 Numisia: cratered highlands material (chm), northern cratered trough terrain (nctt) and cratered plains material (cpm) [1].

Vestalia Terra: Vestalia Terra is a distinct, topographically high region of Vesta bound by steep scarps (Fig.1). The region is albedo-bright in clear filter FC images, compared to surrounding terrains. The large number of craters with "colorful" ejecta on Vestalia Terra implies that the region have a diverse composition.

Numisia Crater: Centrally located at 7ºS, 247ºE, the 33 km diameter Numisia crater is the largest impact crater in the Av-9 quadrangle. It has a sharp rim and shows both bright and dark layers in its walls. The object that formed Numisia impacted into an older crater to its northeast; this older crater appears to be buried by a ribbon of dark material (see description below). The dark material evident in the crater wall may thus be exposures of the "dark ribbon".

Cornelia Crater: Although significantly smaller than Numisia (15 km), Cornelia crater shows greater color diversity. In clear filter FC data, Cornelia's interior shows large deposits of albedo-dark material. There are two distinct lobes of ejecta: the smaller, inner lobe albedo-dark and the larger, outer lobe albedo-bright. This two-toned ejecta is also evidenced in the FC color ratio data (Fig. 2). In addition, Cornelia diplays an extensive ray system, that extends beyond the boundaries of the Av-9 quadrangle, to the south and west.

"Dark ribbon": The so-called "dark ribbon" is primarily evident in FC color ratio data (Fig. 2) but is also discernable in clear filter data as a roughly linear unit of albedo-dark material crossing Vestalia Terra from the northwest to the southeast. This dark material seems to fill a locally low region cutting across top of the regionally high Vestalia Terra. The ribbon is cut by Numisia crater, whose wall stratigraphy thus may display the thickness of the dark material. The origin of this material has yet to be determined, but possibilities include impact ejecta flow and/or volcanism.

Pit crater chains: While the other equatorial quadrangles on 4Vesta display the numerous wide and flat-floored troughs of the equatorial ridge and trough terrain (ertt) [1], Av-9 does not. There are, however, three long pit crater chains. The merged pits show signs of collapse but distinct fault faces can also be observed. A

strong correlation between pit crater chains and fault-bounded graben has been observed on other planetary bodies [9]. These pit crater chains are roughly aligned with the equatorial flat-floor troughs of unit ertt [10].

Elongate hill: The topography of Av-9 reveals the presence of an elongate hill in the southeast of the quadrangle (Fig. 2b). Merged pits appear in line with the elongate hill to both the west and east. FC color data shows material of a distinct composition which appears to be moving downslope on the northern flank of the hill. A crater impacted into the northern face of the hill has albedo-bright and "colorful" ejecta Other potential flow features include a linear arrangement of elongate pits.

References: [1] Yingst et al. (2011) Fall AGU, #P43B-0248. [2] Yingst et al. (2012) 43rd LPSC, this volume. [3] Preusker et al. (2011) Fall AGU, #U23B-02. [4] Jaumann et al. (2012) *Science*, in review. [5] Preusker et al. (2012) 43rd LPSC, this volume. [6] Nathues et al. (2011) Fall AGU, #U22A-01. [7] [7] De Sanctis et al., this meeting. [8] Capaccioni et al. (2012) EGU. [9] Wyrick et al (2004) JGR doi:10.1029/2004 JE002240. [10] Buczkowski et al. (2011) Fall AGU, #U21B-05.

Additional Information: The authors gratefully acknowledge the support of the Dawn Instrument, Operations, and Science Teams. This work was funded by the Dawn at Vesta Participating Science Program.

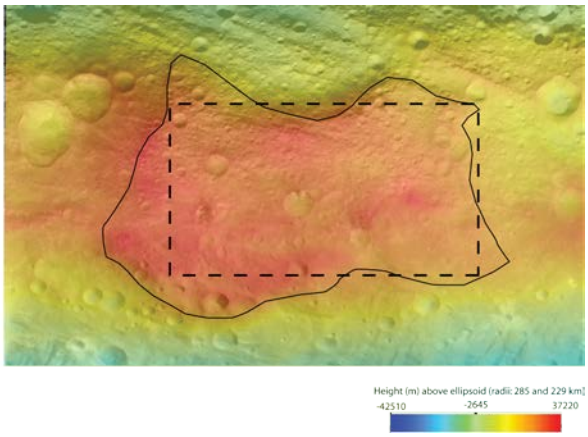

Figure 1. Global-scale topography map of Vesta centered on Vestalia Terra. Solid line marks outline of Vestalia Terra. Dashed line marks location of Av-9 quadrangle.

a)

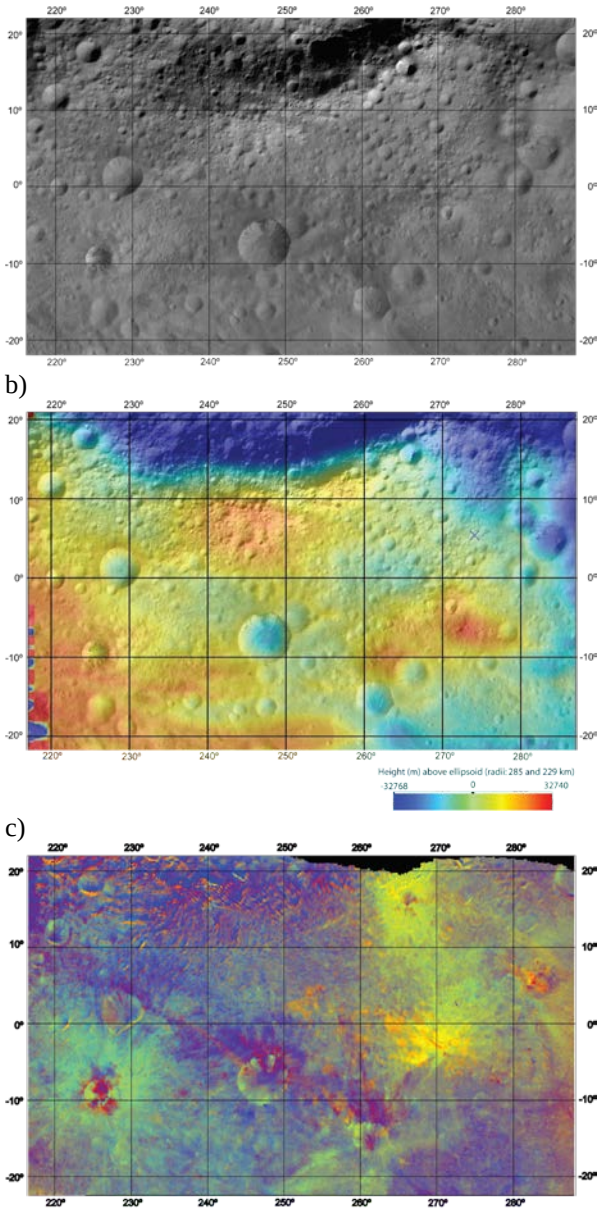

Figure 2. Data maps of Av-9 Numisia quadrangle. a) Framing Camera clear filter HAMO mosaic. b) Topography map, called to Av-9 region. c) Color ratio FC mosaic, based on Survey data. Dark ribbon and "colorful" ejecta are easily observed. Note correspondence of dark ribbon and low region on Vestalia Terra.

STATUS OF THE GLOBAL GEOLOGIC MAP OF EUROPA. M. K. Bunte[1] R. Greeley[1,*], T. Doggett[1,**], P. Figueredo[1,***], K. Tanaka[2] and D. Senske[3], [1]School of Earth and Space Exploration, Arizona State University, Box 871404, Tempe, AZ 85287 (mbunte@asu.edu), [2]U.S. Geological Survey, Flagstaff, AZ, [3]Jet Propulsion Laboratory, California Institute of Technology, Pasadena, CA, (*deceased October, 2011; **currently at Northern Virginia Community College; ***currently at the ExxonMobil Research Company, Houston, TX).

Introduction: Europa is of keen interest to astrobiology and planetary geology due to its indications of a sub-surface ocean. Knowledge of the global distribution and timing of Europan geologic units is a key step for understanding the geologic history of the satellite and for identifying areas of concern and features relevant for future study.

The first geologic map of Europa [1] was produced at a hemisphere scale with low resolution *Voyager* data. With the acquisition of higher resolution data by the *Galileo* mission, researchers identified surface units and determined sequences of events in relatively small areas of Europa through geologic mapping [2-6] using images at various resolutions acquired by *Galileo's* Solid State Imaging (SSI) camera [7]. These works [2-6] provided a local to sub-regional perspective and employed different criteria for the determination and naming of units. Unified guidelines for the identification, mapping and naming of Europan geologic units were put forth by [8] and employed in regional-to-hemispheric scale mapping [9, 10] which is now being expanded into a global geologic map [11].

Methodology: A global photomosaic [12] of *Galileo* and *Voyager* data was used as a basemap for mapping in ArcGIS, following suggested methodology of stratigraphy for planetary mapping [13]. Due caution was exercised given that the mosaic has a resolution varying from 12.6 to 0.23 km per pixel, as well as variations in illumination and viewing geometry, to avoid making distinctions between units that are functions of these variations. In areas of high resolution coverage (better than 1.7 km/px), contacts were marked as definite, and left as queried in areas of low resolution coverage.

Map Status: Attempts at global mapping have characterized geographic regions in terms of the five main surface units summarized by [8] (plains, chaos, band, ridge, and crater materials) and attempted to illustrate the surface history through four periods of formation as based on linea cross-cutting relations [14]. We are simplifying the stratigraphy to preserve the overall geologic units while outlining the structural features or *framework lineaments* that indicate the most important stratigraphic markers for formation periods.

The much debated geologic units have been defined and fully described. Full interpretations of their formation and evolution are being prepared. In order to satisfy a globally relevant origin for each unit, we have undertaken a comparison of all previously proposed formation mechanisms, the results of which will be forthcoming within several months.

To augment the basic description and interpretation of geologic units and features and to aid in our understanding of formation mechanisms so that we may appraise each model for its merit, we are examining the Galileo NIMS data to assess correlations between composition and geology or topography as in [15]. In addition, we are reviewing all photoclinometry and stereo imaging results from [16].

Acknowledgements: We graciously acknowledge the contributions to this mapping effort by E. Kolb, K. Mullins, and S. Weiser. We also acknowledge T. Hare and C. Bradbury for technological support and D. Ball of the Space Photography Laboratory for image processing assistance. This work was supported by NASA through the Planetary Geology and Geophysics Program and the Outer Planets Research Program. Additional funding to make this work possible is provided by a NASA Earth and Space Science Fellowship.

References: [1] Lucchitta and Soderblom, in *The Satellites of Jupiter*: 521, 1982; [2] Senske et al., *LPSC* XXIX, #1743, 1998; [3] Prockter et al., *JGR., 104*:16531-16540, 1999; [4] Kadel et al., *JGR*, 105, 22657-22669, 2000; [5] Figueredo et al., *JGR*, 107, 10.1029/2001JE001591, 2002; [6] Kattenhorn, *Icarus*, 157, 490-506, 2002; [7] Belton et al., *Space Science Reviews*, 60, 413-455, 1992; [8] Greeley et al., *JGR*, 105, 22559, 2000; [9] Figueredo and Greeley, *JGR*, 22629-22646, 2000; [10] Figueredo and Greeley, *Icarus*, 167, 287-312, 2004; [11] Doggett et al., in *Europa:* 727, 2009; [12] USGS, I-2757, 2003; [13] Skinner and Tanaka, *LPSC XXXIV*, #2100, 2003; [14] Doggett et al., *LPSC* XXXVIII, #2296, 2007; [15] Shirley et al., *Icarus*, 210, 358-384, 2010; [16] Schenk, *Atlas of the Galilean Satellites*, 406, 2010.

GEOLOGIC MAPPING OF ASTEROID 4 VESTA. W.B. Garry[1], D.A. Williams[2], R.A. Yingst[1], S. Mest[1], R. Jaumann[3], C.M. Pieters[4], T. Roatsch[3], F. Preusker[3], C.T. Russell[5], C.A. Raymond[6], and the *Dawn* Science Team. [1]Planetary Science Institute, Tucson, AZ (wbgarry@psi.edu); [2]ASU, Tempe, AZ; [3]DLR, Berlin, Germany; [4]Brown University, Providence, RI; [5]UCLA, Institute of Geophysics, Los Angeles, CA; [6]Jet Propulsion Laboratory, California Institute of Technology, Pasadena, CA.

Introduction: NASA's *Dawn* spacecraft arrived at the main belt asteroid 4 Vesta on July 16, 2011. *Dawn* is collecting a variety of imaging, spectral, and elemental abundance data during its one year in orbit to characterize the geology, geochemistry, shape and internal structure of Vesta. The *Dawn* Science Team has begun geologic mapping of Vesta's surface at the global [1-3] and regional scale (Fig. 1) [e.g., 4].

Geologic Setting: Vesta is an ellipsoidal asteroid with an equatorial radius of ~238 km. The southern hemisphere is dominated by two large impact structures, *Rheasilvia* and *Veneneia* (Fig. 2). Two sets of troughs and ridges are located around the equatorial region and in the northern hemisphere [5]. Several large impact basins are observed, but have been degraded by younger impacts. Bright and dark materials are exposed within impact ejecta and crater walls.

Data: *Dawn* has three instruments: the Framing Camera (FC), Visible/Infrared spectrometer (VIR), and the Gamma Ray and Neutron Detector (GRaND). FC images of variable resolution are being collected during three different mapping orbits: Survey (200 m/pixel), High Altitude Mapping Orbit (HAMO) (70 m/pixel), and Low Altitude Mapping Orbit (LAMO) (20 m/pixel). Variations in surface composition are informed by Visible and Infra-Red (VIR) hyperspectral images from Survey (700 m/pixel) and HAMO (200 m/pixel) orbits and FC color ratio images (250 m/pixel) [6] from Survey orbit. Slope and contour maps derived from the Digital Terrain Model (DTM) [7] are used to characterize geologic features and the extent of geologic units.

Global Geologic Map: A global geologic map of Vesta has been produced at 1:7M scale. The first iteration of the global map was based on Survey orbit FC images and was completed in Oct., 2011 [1]. Geologic contacts and units were refined using the HAMO FC mosaic in Mar., 2012 [2]. The surface of Vesta is subdivided into the three main geologic terrains: the *Rheasilvia Formation*, ridge and groove terrain, and heavily cratered terrain. The revised Survey-based global map was published as a figure in the *Jaumann et al.* [3] paper in the Dawn Special Issue of *Science* (11 May 2012).

Regional Geologic Maps: Vesta has been subdivided into 15 regional quadrangles (Fig. 1) with a geologic map being produced for each one at 1:500,000 scale (Fig. 3). Clear filter FC HAMO mosaics (70 m/pixel) serve as the basemaps, supplemented by LAMO, DTM, and VIR data. The northern hemisphere quadrangle maps have only been partially imaged, but current mapping shows they are heavily cratered and dominated by the northern ridge and trough terrain (e.g. *Saturnalia Fossa Formation*). The equatorial quadrangles exhibit a diversity of geologic features across the surface including ridge and trough terrain (*Divalia Fossa Formation*), impact basins (*Feralia Planitia*), relatively fresh impact craters and ejecta (e.g. *Marcia*), a broad topographic high (*Vestalia Terra Materials*) and tholus material (e.g. *Arisia* and *Lucaria Tholi*). The southern quadrangles encompass the *Rheasilvia Formation* which consists of a central topographic high surrounded by ridged and grooved terrain.

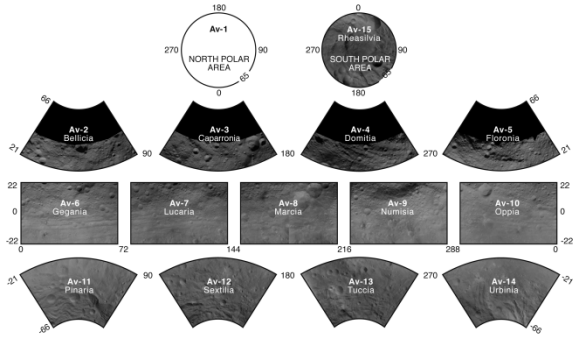

Figure 1. Layout of Vesta's 15 regional quadrangles.

Future Plans: The *Dawn* Team is working to standardize the regional geologic maps. A *Dawn* Mappers Team Meeting will be held June 5-8, 2012 at Brown University in Providence, Rhode Island to coordinate geologic contacts between maps, formalize names and descriptions for geologic units, and determine relative stratigraphy. Age dating of the surface through crater counting techniques is being coordinated by a separate subgroup. Regional geologic maps will be incorporated into peer-reviewed manuscripts that will be submitted in the Fall of 2012 to a special issue on the geology of Vesta.

References: [1] Yingst et al. (2011) Fall AGU, #P43B-0248. [2] Yingst et al. (2012) 43rd LPSC, Abstract 1359. [3] Jaumann et al. (2012) *Science* (11 May). [4] Williams et al. (2012) 43rd LPSC, Abstract 1534. [5] Buczkowski et al. (2011) Fall AGU, #U21B-05; [6] Nathues et al. (2011) Fall AGU, #U22A-01. [7] Preusker et al. (2012) 43rd LPSC, Abstract 2012.

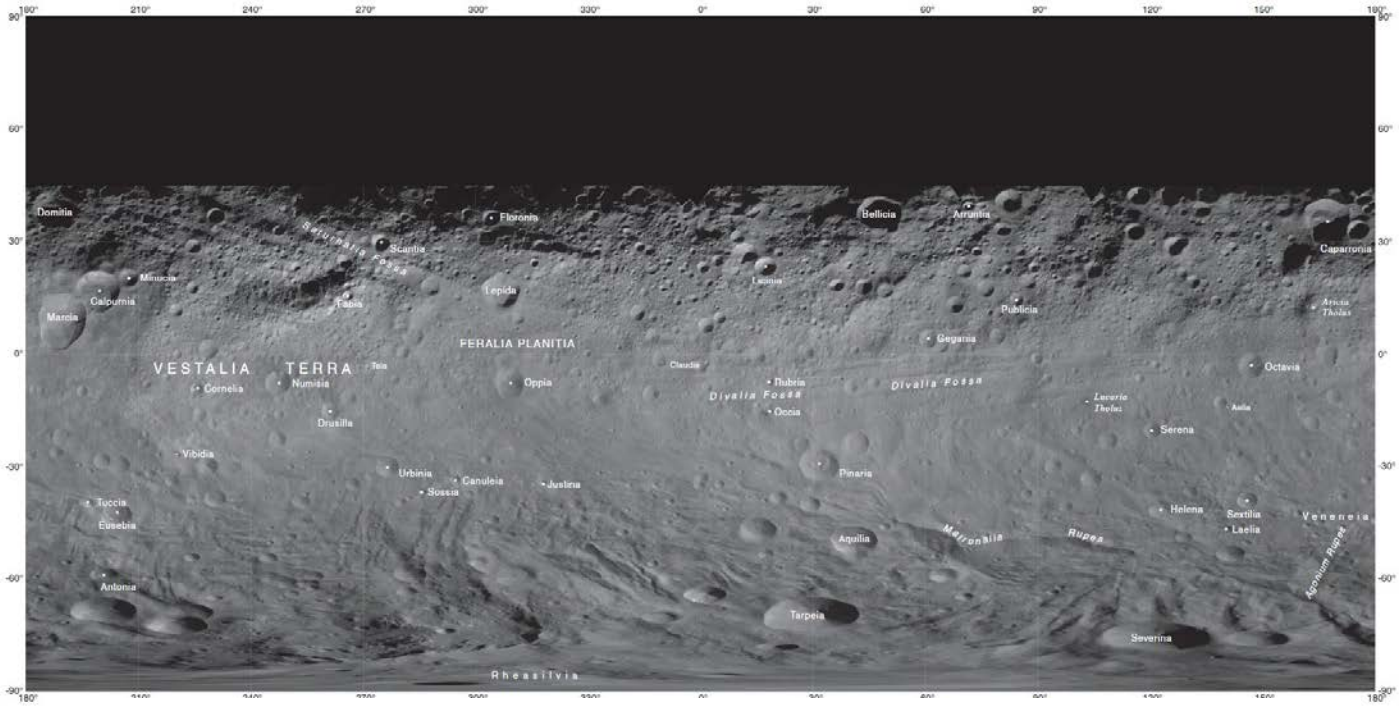

Figure 2. Global map of Vesta with named features approved by the IAU. Image Credit: NASA/JPL-Caltech/UCLA/MPS/DLR/IDA. Image from: http://planetarynames.wr.usgs.gov/images/vesta.pdf

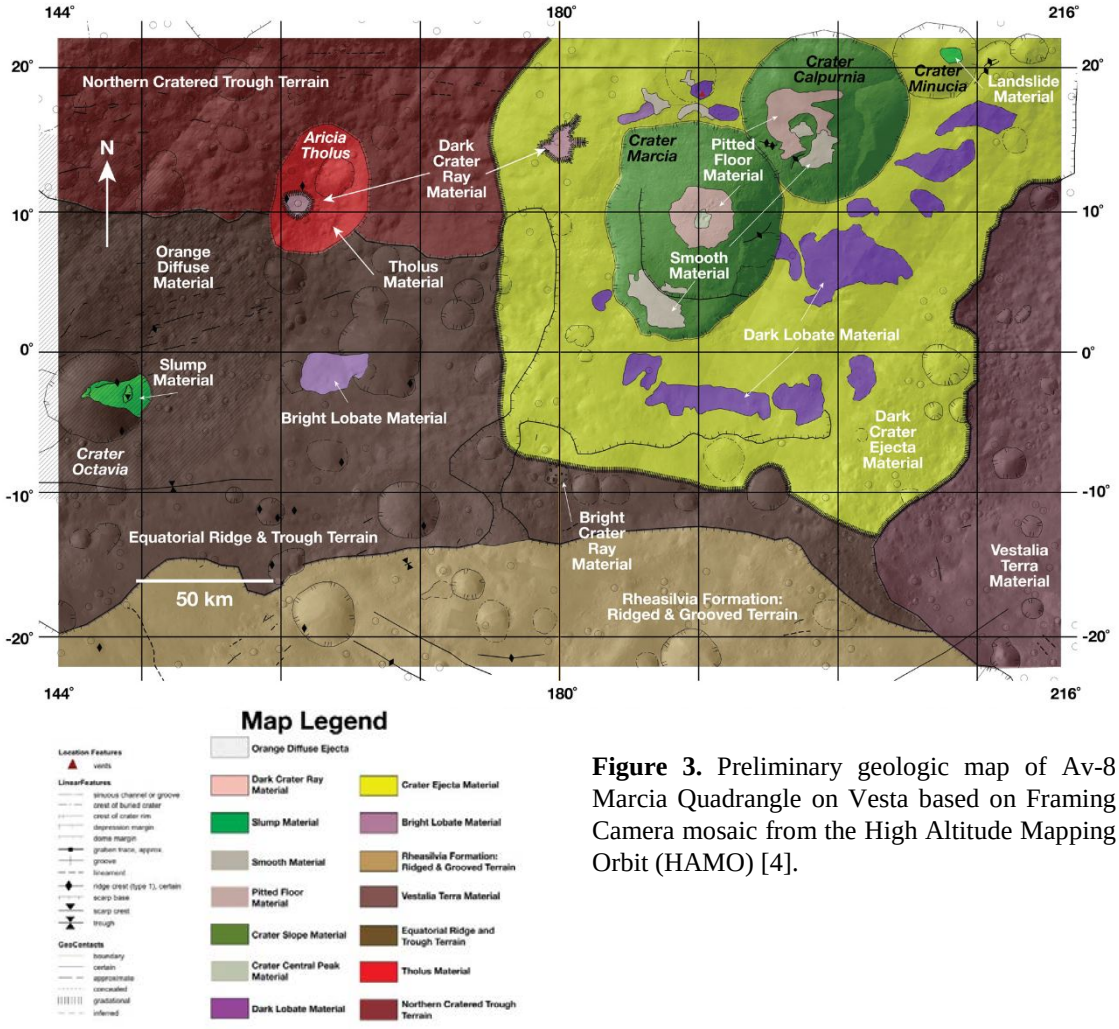

Figure 3. Preliminary geologic map of Av-8 Marcia Quadrangle on Vesta based on Framing Camera mosaic from the High Altitude Mapping Orbit (HAMO) [4].

A PRELIMINARY GLOBAL GEOLOGIC MAP OF VESTA BASED ON HIGH-ALTITUDE MAPPING ORBIT DATA. R.A. Yingst[1], S. Mest[1], W.B. Garry[1], D.A. Williams[2], D.C. Berman[1], R. Jaumann[3], C.M. Pieters[4], E. Ammannito[5], D.L. Buczkowski[6], M. De Sanctis[5], A. Frigeri[5], L. Le Corre[7], F. Preusker[3], C.A. Raymond[8], V. Reddy[7], C.T. Russell[9], T. Roatsch[3], P.M. Schenk[10], and the Dawn Team, [1]Planetary Science Institute, Tucson, Arizona, USA (yingst@psi.edu); [2]Arizona State University, [3]DLR, Berlin, Germany; [4]Brown University, Providence, Rhode Island, USA; [5]National Institute of Astrophysics, Rome, Italy; [6]JHU-APL, Laurel, Maryland, USA; [7]Max Planck Inst., Katlenburg-Lindau, Germany; [8]NASA JPL, California Institute of Technology, Pasadena, California, USA; [9]UCLA, Los Angeles, California, USA; [10]LPI, Houston, Texas, USA. #1359

Introduction: Previous maps of the asteroid Vesta were derived from albedo and elevation (Hubble Space Telescope, 38-52 km/pixel), and color data and Earth-based spectroscopy were utilized to generate mineralogic and lithologic maps [1-6]. The Dawn spacecraft has acquired images of Vesta at resolutions up to 500x higher, allowing us to advance from simple identification of the largest spatial and spectral features to complex geologic mapping of morphologic units and features, including stratigraphic and structural relationships. We have created a 1:500,000-scale preliminary global map of Vesta, based on data from the High-Altitude Mapping Orbit (HAMO). During the active phase of the Dawn mission the geologic map is refined with each improvement in resolution [e.g., 7].

Geologic Setting: Vesta is an ellipsoidal asteroid with an equatorial radius of ~283 km. It has been identified as the parent body for the Vestoids and the HED (howardite-eucrite-diogenite) family of meteorites. By dating HEDs, Vesta has been determined to be ~4.56 by old [8-10]. Previous data revealed that it has a surface composed of pyroxene-bearing minerals [e.g. 1-3]. Vesta has a heavily-cratered surface, with large basins evident in numerous locations. The south pole in particular is dominated by an impact basin so large it was identified before Dawn's arrival; this basin has been named Rheasilvia. The surface is also characterized by a system of deep, globe-girdling equatorial troughs and ridges, as well as an older system to the north. Troughs and ridges are also evident cutting across, and spiraling arcuately from, the Rheasilvia central mound [11].

Data and Mapping Procedure: We used a monochrome Framing Camera (FC) mosaic produced from the High Altitude Mapping Orbit (HAMO) data as our basemap. Images in this mosaic have an average spatial scale of ~70 m/pixel. This base was imported into ArcGIS (Geographic Information System software), and supplemented by a Digital Terrain Model (DTM) derived from Survey orbit image data [11, 12]. FC color ratio images from Survey orbit with a spatial scale of ~250 m/pixel and Visible and InfraRed (VIR) hyperspectral images from the Survey and HAMO orbits with spatial scales of 700 and 200 m/pixel, respectively, provided information on surface composition and were used to refine unit boundaries.

Geologic Units & Features: Vesta can be divided very broadly into three terrain types: heavily-cratered terrain; ridge-and-trough terrain (equatorial and northern); and terrain associated with the Rheasilvia basin. Smaller features include bright and dark material and ejecta (some defined specifically by color); and mass-wasting materials. Each of these is addressed below and shown in Figure 1.

Rheasilvia. The Rheasilvia formation is characterized by (a) bounding arcuate scarps; (b) a central mound with smoother, less cratered regions; (c) a linear set of ridges and troughs running through either side of the central mound; and (d) a more arcuate set swirling out from and around the central mound. Rheasilvia basin, centered at approximately the asteroid's south pole, stretches 60-120 degrees of latitude, and its formation undoubtedly influenced most of the geologic features on the surface and the overall shape of Vesta. [see abstracts for Av-6 to Av-14, this volume].

Ridge-and-trough terrain. Large-scale global troughs that occur at the equator cover an impressive percentage of the asteroid's 1765 km circumference and are 19 to 380 km long and up to 20 km wide. An older set of large-scale troughs is present in the northern hemisphere. The largest of these is 390 km long and 38 km wide, but shows evidence of degradation with shallower walls, rounded edges, and infilling. Mineralogical signatures of the troughs suggest the presence of howardite-eucrite, but the signatures are not homogeneous, and a region around 40°E displays shorter, deeper bands that suggest the possibility of a different composition [see abstracts for Av-2 to Av-10, this volume].

Heavily-cratered terrain. Impact structures dominate Vesta's surface. Crater morphology shows many similarities to other small, airless, rocky bodies. Small fresh craters, are characterized by sharp-crested, narrow rims and bowl shapes; larger fresh craters have flat floors and may display slumping of rim walls, some finer-textured floor fill, or visible ejecta material. All fresh craters are interpreted to be the youngest impact features on Vesta. Degraded craters, interpreted to be older, have subdued but distinct, continuous rims and

varying internal shapes. Enclosed sub-circular or ovoid regions of lower topography also exist; many of these are interpreted to be the oldest craters. Basins like Rheasilvia are characterized by high-topography rugged hills and arcuate scarps forming partial rings.

Localized features. Localities with distinct geomorphologic characteristics include regions of bright and dark materials, and areas of mass-wasting. Bright materials occur as higher-albedo ejecta, often asymmetrically distributed. Several regions of localized dark material also exist [13]. These regions are commonly characterized by lower-albedo ejecta or dark streaks within crater walls. Ejecta is commonly asymmetrically-distributed and can sometimes be tied to discrete dark layers within crater rims. Mass-wasting was a local and regional process, associated with impact-driven slumping and possibly other processes that occurred subsequent to large impact-driven shaking.

Preliminary Stratigraphy: Differentiation, fractionation and crystallization of a primary crust were followed by the formation of impact basins and craters, including at least one basin near the south pole predating Rheasilvia (this basin may be the source of the older northern ridge-and trough complex [Buczkowski et al., this volume]). Formation of Rheasilvia followed, along with associated structural deformation that formed the major ridge-and-trough complex at the equator. Subsequent impacts and mass wasting events subdued impact craters, basin rims and portions of ridge-and-trough sets, and formed slumps and landslides, especially within crater floors and along basin rims and scarps. Subsequent to the Rheasilvia formation, discontinuous low-albedo deposits formed or were emplaced; these lie stratigraphically above the equatorial ridges that likely were formed by Rheasilvia. The latest features to be formed were craters with dark rays, and those with bright rays that also display thin layers of dark material in their walls and ejecta.

References: [1] Binzel, R.P., et al., (1997) *Icarus*, *128*, 95-103. [2] Gaffey, M.J., (1983) *LPSC*, *14*, 231-232. [3] Gaffey, M.J., (1997) *Icarus*, *127*, 130-157. [4] Li, J.-Y., et al., (2006) *Icarus*, *182*, 143-160. [5] Li, J.-Y., et al., (2008) *LPSC*, *39*, 2253. [6] Degewij, J., et al., (1979) *Icarus*, *40*, 364-374. [7] Yingst et al., (2011) *AGU*, P43B-0248. [8] Nyquist, L.E., et al. (1997) *GCA*, *61*, 2119-2138. [9] Tera, F., et al., (1997) *GCA*, *61*, 1713-1732. [10] Lugmair, G.W. and Shukolyukov, A, (1998) *GCA*, *62*, 2863-2886. [11] Jaumann, R. et al. (2012) *Science*, in review. [12] Preusker, F. et al., this volume. [13] Jaumann et al., this volume.

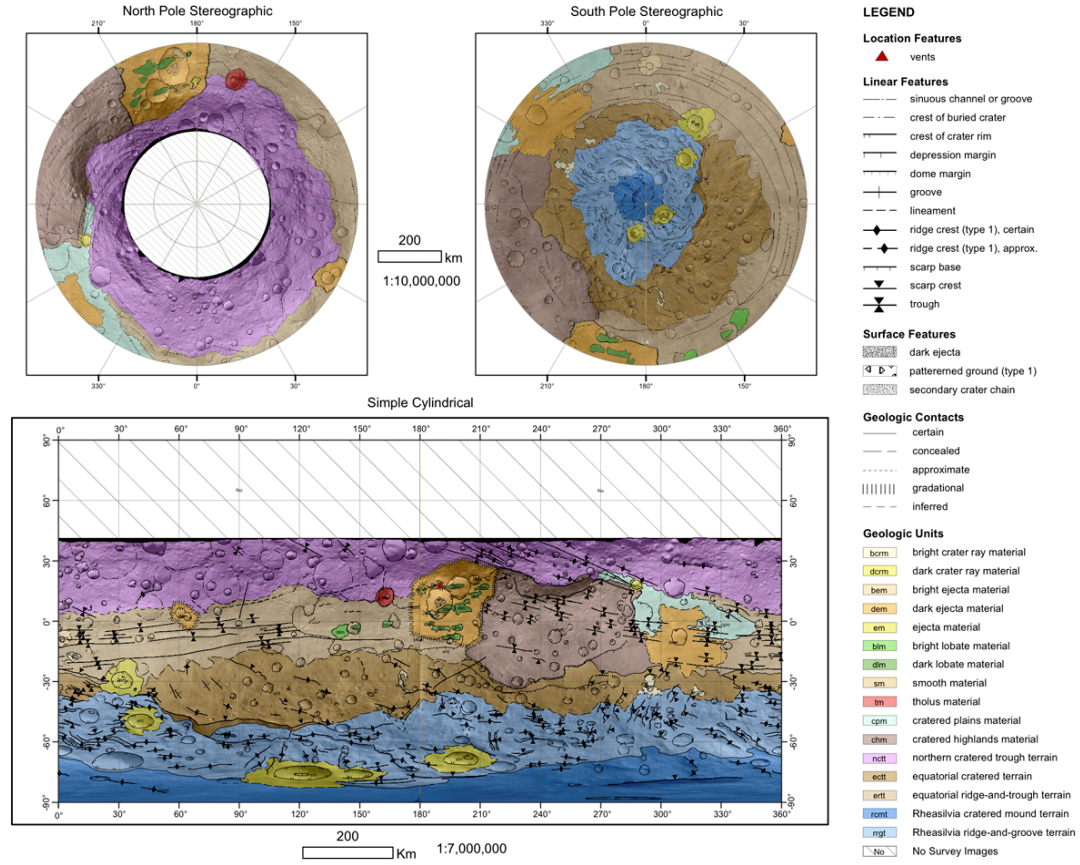

Figure 1. Geologic map of Vesta.

DIGITAL RENOVATION OF THE 1:5,000,000 LUNAR GEOLOGIC MAP SERIES. C. M. Fortezzo and T. M. Hare, U.S. Geologic Survey Astrogeology Science Center, 2255 N. Gemini Dr., Flagstaff, Arizona, cfortezzo@usgs.gov.

Introduction: In continuing support of a NASA Planetary Geology and Geophysics-funded project to digitize existing 1:5M-scale lunar paper maps and because of the increasing emphasis on lunar studies from recent orbital data returns, we have renovated the digital versions of the lunar near-, east-, and west-side, north and south pole, and the central far-side geologic maps [1-6]. The renovations used new topographic data and image mosaics to adjust the original linework and the map boundary to the current ULCN2005 and the Lunar Reconnaissance Orbiter (LRO) Lunar Orbiter Laser Altimeter (LOLA) control networks [7-8].

These maps are not a reinterpretation of the original geologic units or relationships, but a spatial adjustment to make the original work more compatible with current digital datasets. This increased compatibility allows these maps to be compared and utilized with ongoing and future lunar mapping projects.

Background: The 1:5M near-side map, released in 1971, was a synthesis of 36 1:1M maps produced from Earth-based telescopic observations and Lunar Orbiter imagery [1]. The purpose of the synthesis was to produce a coherent and consistent near-side time-stratigraphy in an Orthographic projection. The irregular boundary for the map area is due to the boundaries for the 36 1:1M maps, and narrows in broad, irregular steps as it approaches the poles.

The near-side map delineated 43 geologic units that are broken down into the following major groupings: dark materials (5 units), circum-basin materials (7 units), crater materials (20 units), and terra plain, plateau, and dome materials (11 units). The units span the pre-Imbrian to the Copernican Systems, whereas, all the remaining maps have units that span the Pre-Nectarian to the Copernican System. The only linear representations on the map are geologic contacts and basin rings. The base image was generated by the United States Air Force Aeronautical Chart and Information Center (USAF-ACIC).

The east side geologic map was generated in 1977 and includes materials grouped into crater (12), basin (7), mare and dark (3), and other (plains-5 and terra-3). The linear features include certain and queried contacts, basin rings, and buried craters. The sole hatch pattern indicates the location of the bright sinuous markings. The base image is a Defense Mapping Agency shaded-relief in Mercator projection.

The west side geologic map was generated in 1977, and includes materials grouped into plains (3), crater (6), Orientale (7), Hertzsprung (2), terra (1), mare (1), and dome (1). The linear features include contacts, mare domes and ridges, rilles, faults lineaments, large troughs, Orientale rings, older basin rings, buried craters, and crates buried by Orientale ejecta. Additionally, 2 hatch patterns indicate dark mantling material, and spectral differences in the mare. The base image is a Defense Mapping Agency shaded-relief in Mercator projection.

The lunar north pole map was generated in 1978 and delineated 34 units split into the following groups: crater materials (13), basin materials (9), other terra materials (9), and mare and other dark materials (3). The linear representations included approximate contacts, crests of buried crater rims, and certain and approximate crests of basin ring structures. The north pole map utilized a Polar Stereographic shaded-relief base map generated by the USAF-ACIC.

The central far-side map was generated in 1978 and contains materials grouped as crater (11), basin (7), and other (terra-3, plains-4, grooved-1, and mare-1). The linear features include contacts, basin rings, slope bases, and buried crater rims. The base image is a Defense Mapping Agency shaded-relief in Mercator projection.

The lunar south pole map was generated in 1979 and delineated 37 units split into the following groups: materials of primary impact and their secondary craters (13), basin materials (11), probable basin related materials (8), and mare and other dark materials (5). The linear representations included certain and queried contacts, crests of buried crater rims, certain and approximate crests of basin ring structures, fissure and narrow fault grabens, sinuous ridges, and sinuous scarps. The south pole map utilized a Polar Stereographic shaded-relief base map generated by the Defense Mapping Agency. This map included a location near the pole where there was no photographic coverage, thus no units were mapped.

Datasets: Three main orbital datasets were used to renovate the lunar maps (listed in order of utility): the LRO LOLA DTM (100 m/pix) [9], Lunar Reconnaissance Orbiter Camera wide-angle camera (WAC) mosaic (100 m/pix) [10], and the WAC-derived DEM [11]. To a lesser degree and where useful, we also used Lunar Orbiter global mosaic (~63 m/pix), Kaguya Digital Terrain Model (~2 km/pix) [12], Clem-

entine UVVIS (100 m/pix) [13], and the Clementine Mineral Ratio (200 m/pix) [13].

Methodology: These maps were originally digitized by the USGS in 2000 by tracing units on scanned versions of the maps. These original digital files were created in the orthographic and polar projections in ArcInfo Workstation and reprojected into a Simple Cylindrical projection for compatibility with global datasets standards at the time. While the vectors were not used in the current effort, the attributes from the original files were translated into the new geologic maps.

The current renovation of the digital maps adhered to strict guidelines for vector generation and used recent datasets to spatially adjust the location of the geology and linework. This adjustment did not change the original geologic framework but sought to update the locations of the contacts and geology. These adjustments resulted in the omission of some discrete units by connecting areas that were previously mapped as isolated and, vice versa, isolated previously grouped units. The sole new addition to the map was the use of both certain and approximate contacts to indicate areas where (1) the geologic relationships were unclear to the digital author and (2) where the datasets did not provide adequate information for the interpretations of the original map.

The data sets discussed above were used in combination with ESRI's ArcMap Geographic Information System (GIS) software, to draw vectors on the Lunar Orbiter global mosaic. The vectors were drawn with a consistent vertex spacing of ~3 km at 1:1.5M scale, and were smoothed using a maximum allowable offset tolerance of ~16 km. The adjustments and adherence to these guidelines resulted in a product that increased the feature location accuracy at the 1:5M scale and makes the product more cartographically appealing and consistent as a collection of maps.

We chose not to add nomenclature to the maps because of the availability of regularly updated, GIS-ready nomenclature provided by the U.S. Geological Survey's IAU Gazetteer of Planetary Nomenclature website (http://planetarynames.wr.usgs.gov). This site allows users of the map to choose which features are displayed digitally and in paper copies they generate.

Results: Subtle changes to all the maps improved the location of units, contacts, and linear features. For the south pole, the zone of "no-data" has been filled in with interpretations stemming from recent LOLA topographic coverage. This provides an update to the map that may prove helpful given the increased interest in the permanently shadowed craters at the lunar poles.

The renovated geologic maps provide the community with a means to digitally view and analyze the data from the original map. The ability of GIS to analyze data reinvigorates the 30- to 40-year-old products and makes them viable products for a new generation of planetary scientists due to an increasing reliance on digital resources. Additionally, with a new influx of lunar data, it is important to preserve and extend the capabilities of this useful heritage map.

Future Work: We are reviewing and finalizing the maps and plan to release them to the community by summer 2012.

Once all of the maps are completed, the feasibility of merging the maps will be assessed. We foresee that 5 of the 6 maps could be merged with the near-side map being the only exception due to it being a compilation of the 1:1M scale maps, its older age, and irregular shape.

To merge the maps, the first step would include creating a global stratigraphy that preserves the original interpretations of the authors based on the relative ages, descriptions, and spatial extent of the existing units. For overlapping areas, we would need to determine which contacts and units preserve the history and fit the global stratigraphy. Finding a considerate balance between lumping units and keeping valuable discrete units will determine how effectual the maps are as a complete package.

References: [1] Wilhelms, D.E. and J.F. McCauley (1971) *Map I-703*. [2] Wilhelms, D.E., et al. (1979) *Map I-1162*. [3] Lucchitta, B.K. (1978) *Map I-1062*. [4] Scott, D.H. et al. (1977) *Map I-1034*. [5] Wilhelms, D.E. and F. El-Baz (1977) *Map I-948*. [6] Stuart-Alexander, D.E. (1978) *Map I-1047*. [7] Archinal, B. et al. (2006), *Open-File Report 2006-1367*. [8] Smith, D. E. et al, (2008) NASA Goddard Space Flight Center. [9] Boyd, A.K. et al. (2012) LPSC, abs. # 2795. [10] Scholten et al. (2012) in review: JGR-Planets. [11], Becker, T.L. (2008) LPSC, abs. #2357 [12] Shin-ichi, Sobue, et al. The Result of SELENE (KAGUYA) Development and Operation, Recent Patents on Space Technology. [13] Eliason, E., et al. (1999) PDS Volumes USA_NASA_PDS_CL_4001 through 4078.

THE REGIONAL PLANETARY IMAGE FACILITY NETWORK. J. J. Hagerty[1], and RPIF Network Node Directors and Managers, [1]U.S.G.S. Astrogeology Science Center, Flagstaff, AZ 86001 email: jhagerty@usgs.gov.

Introduction: NASA's Regional Planetary Image Facilities (RPIFs) are planetary data and information centers located throughout the United States, in Canada, and overseas. The U.S. locations are funded by both NASA (via the Planetary Geology and Geophysics Program) and their host institutions [1]. A network of these facilities was established in 1977 to "maintain photographic and digital data as well as mission documentation. Each facility's general holdings contain images and maps of planets and their satellites taken by Solar System exploration spacecraft. These planetary data facilities, which are open to the public, are primarily reference centers for browsing, studying, and selecting planetary data including images, maps, supporting documentation, and outreach materials. Experienced staff at each of the facilities can assist scientists, educators, students, media, and the public in ordering materials for their own use" [2].

Since it was formally established, the network of RPIFs has expanded to nine U.S. facilities and eight facilities in other countries. The first RPIF to be established outside of the U.S. was in the United Kingdom in 1980 at University College London (UCL), and since then RPIFs have been set up in Canada, Finland, France, Germany, Israel, Italy, and Japan. Through its longevity and ability to adapt, the RPIF Network has leveraged its global reach to become a unique resource covering 60 years of international planetary science.

Historically the Network nodes have had an inward focus, providing resources to local clients, and communicating with other nodes only when the need arose. Using this methodology, the nodes of the RPIF Network, hereafter referred to as RPIFN, have combined to serve an average of ~65,000 people per year since 2000. However, with the advent of simpler and more wide-ranging forms of data transfer and sharing, it is clear that the nodes can operate together to provide the planetary science community and the public with greater access to: 1) archived mission products (e.g., maps, photographs, films, and documents); 2) mission-enabling documentation (e.g., data on previous mission design, development, implementation, and evaluation); 3) science and public research support, and 4) outreach experience and capabilities. Each node of the Network has unique capabilities that meet one or more of the above criteria; however, by linking the nodes through a centralized website and database, it is now possible to provide a wider array of materials to a wider array of clients.

Distribution of Planetary Geologic Maps: Each node of the RPIFN maintains a mixture of common and unique collections. The Regional Planetary Information Facility at the USGS Astrogeology Science Center is unique in that one of its primary functions is to serve as an archive and distribution point for planetary geologic maps. At present, the USGS RPIF has an inventory of 60,000 USGS lunar and planetary maps and now has a full inventory of all maps in the collection.

The USGS RPIF is responsible for distributing newly published I-maps to the other nodes of the RPIFN as well as to interested memebers of the planetary science community. In recent years it has become clear that the distribution process is outdated and inefficient. Given this motiviation, the USGS RPIF has been working with leaders in the planetary mapping community to increase the efficiency of the distribution process and to raise awareness of the importance of planetary geologic maps. One of our first efforts is to meet with members of the community at the Annual Planetary Geologic Mappers meeting and to begin a formal dialog regarding the importance and distribution of planetary geologic maps. We are also working to establish a web-based distribution point that will be accessible to users who are sent an invitation email with a link to the distribution page.

Future Direction: The RPIFN is making strides to better serve its customers in the coming years. In an effort to learn more about the needs and concerns of the planetary science community, the RPIFN presented an abstract [3] and operated an informational booth at the Lunar and Planetary Science Conference in The Woodlands, TX. The results of the booth indicated that the planetary science community seeks assistance in areas that the RPIFN can readily address: 1) documentation for past missions and instruments; 2) basic knowledge about current planetary mission data sets; and 3) outreach materials to engage local communities. The bulleted points below describe methods by which the RPIFN will address the needs of its clients.

- *Provide documentation for past missions and instruments*: Each node of the RPIFN will be charged with inventorying, scanning, and providing access to maps, photographs, films, reports, memoranda, and publications for past planetary missions. As current and future missions come to pass, their documentation (currently stored in mission-specific webpages) will be integrated into the RPIFN. Nodes within the network will also begin collating key mission-related science publications.
- *Provide basic information about current mission data sets*: Beginning with the most recent annual RPIF review in October 2011, RPIF managers and directors will receive training on planetary data sets, such that they can serve as local resources for

their clients. The training will provide overviews of data sets collected since the Clementine mission. The overviews will be geared toward providing basic knowledge of the mission goals, capabilities, data products, data processing tools, and science applications of the data. Several members of the RPIFN will participate in this Planetary Data Workshop.

- *Provide outreach materials*: By pooling their resources, the individual nodes of the RPIFN will have access to a wide array of space exploration materials. RPIF nodes that have unique data and/or relationships with current/future missions will share the information with the rest of the Network. Printing and distribution costs will be shared by network nodes. These materials can then be used to engage the public during facility tours, public lectures, and/or school demonstrations.

In summary, the long term vision of the RPIFN is to be a resource that provides the complete story of space exploration by providing archived data products, historical documentation of previous missions, outreach materials for engaging the public, and up-to-date knowledge and expert advice on current and future planetary missions and their data sets. The RPIFN will continually seek feedback and input from its clients via informational booths at international conferences, online surveys, and written or verbal comments.

For more information, or to request materials, please contact any of the RPIFs listed below. Additional, detailed information can also be found at http://www.lpi.usra.edu/library/RPIF

Arizona State University
Space Photography Laboratory
RPIF@asu.edu

Ben-Gurion University of the Negev
Dept. of Geography and Environmental Development
blumberg@bgu.ac.il

Brown University
Northeast Regional Planetary Data Center
Peter_Neivert@brown.edu

Cornell University
Spacecraft Planetary Imaging Facility
kline@astro.cornell.edu

German Aerospace Center
Regional Planetary Image Facility
rpif@dlr.de

JAXA
Institute of Space and Astronautical Sciences
Regional Planetary Image Facility
tanaka@planeta.sci.isas.jaxa.jp

Instituto Nazionale di Astrofisica
Southern Europe RPIF
livia.giacomini@ifsi-roma.inaf.it

Jet Propulsion Laboratory
Regional Planetary Image Facility
jpl_rpif@jpl.nasa.gov

Lunar and Planetary Institute
Center for Information and Research Services
rpif@lpi.usra.edu

National Air and Space Museum
Center for Earth and Planetary Studies
AielloR@si.edu

University College London
Regional Planetary Image Facility
p.grindrod@ucl.ac.uk

University of Arizona
Space Imagery Center
mariams@LPL.arizona.edu

University of Hawai'i at Manoa
Pacific Regional Planetary Data Center
prpdc@higp.hawaii.edu

Universite de Paris-Sud
Phototheque Planetaire d'Orsay
datamanager@geol.u-psud.fr

University of New Brunswick
Planetary and Space Science Centre
passc@unb.ca

University of Oulu
Nordic Regional Planetary Image Facility
petri.kostama@oulu.fi

U.S.G.S. Astrogeology Science Center
Regional Planetary Information Facility
RPIF-flag@usgs.gov

Acknowledgements: The U.S. nodes of the RPIF Network are supported by NASA's Planetary Geology and Geophysics program as well as by leveraging funds from host institutions.

References: [1] Shirley and Fairbridge, eds. (1997) *Encyclopedia of Planetary Sciences*, Chapman and Hall, London, 686; [2] Muller and Grindrod (2010) *European Planetary Science Congress 2010*, 883; [3] Hagerty, J. J. et al. (2012), *LPSC 43*, abstract #1548.

New Cartography of Io and Enceladus. I. Karachevtseva, L. Shishkina, M.E. Karpunkina. Moscow State University of Geodesy and Cartography (MIIGAiK), MIIGAiK Extraterrestrial Laboratory (MExLab). Gorokhovskiy per., 4, office 155, 105064, Moscow, Russia (icar2003@mail.ru; i_karachevtseva@mexlab.ru)

Results of mapping: Using new technology, developed in MIIGAiK [1, 2] for image processing of small celestial bodies the new control points and shape models of Io and Enceladus have been created [3]. For parts of the surface of these bodies for which were have been found quality stereo-images also were produced DEMs and orthoimosaic. Based on these results we have prepared new maps of the satellites using GIS-tools and new projections for three-axial ellipsoid. Here we show results (Fig. 1 a, b) of transforming data to Cylindrical Conformal projection for three-axial ellipsoid (Modified Bugayevskiy projection) which at the first time was used for Phosos mapping [4, 5]. At the meeting we will present our results for both satellites using some different projections [6] and results of 3D-modeling of the surface.

Acknowledgement: This research was funded by the Russian Government (MEGAGRANT, Project name: "Geodesy, cartography and the study of planets and satellites", contract № 11.G34.31.0021).

References: [1] Zubarev A. et al. (2012) Problems of remote sensing data processing for modeling of small bodies of the solar system, *Actual problems in ERS Journal, IKI RAS, submitted in April (in Russian).*

[2] Nadejdina I. et al. (2011), 9 *Conf. of Space Research Institute (IKI) (in Russian) http://d902.iki.rssi.ru/theses-cgi/thesis.pl?id=3025*.

[3] Nadejdina I. et al. (2012) Global shape estimates and GIS cartography of Io and Enceladus using new control point network *Geophysical Research Abstracts, Vol. 14, EGU2012-11210, EGU General Assembly.*

[4] Bugaevsky L.M. (1987) On the problem of elaborating of isometric coordinates and equiangular cylindric projection of the tri-axial ellipsoid. *Izvestiya Vuzov, ser. Geod. I Aerofot., 4, 79-90 (In Russian).*

[5] Shingareva K.B. et.al. (1992) Atlas of Terrestrial planets and their satellites, *Moscow, MIIGAiK (In Russian)*

[6] *http://geocnt.geonet.ru/en/3_axial*

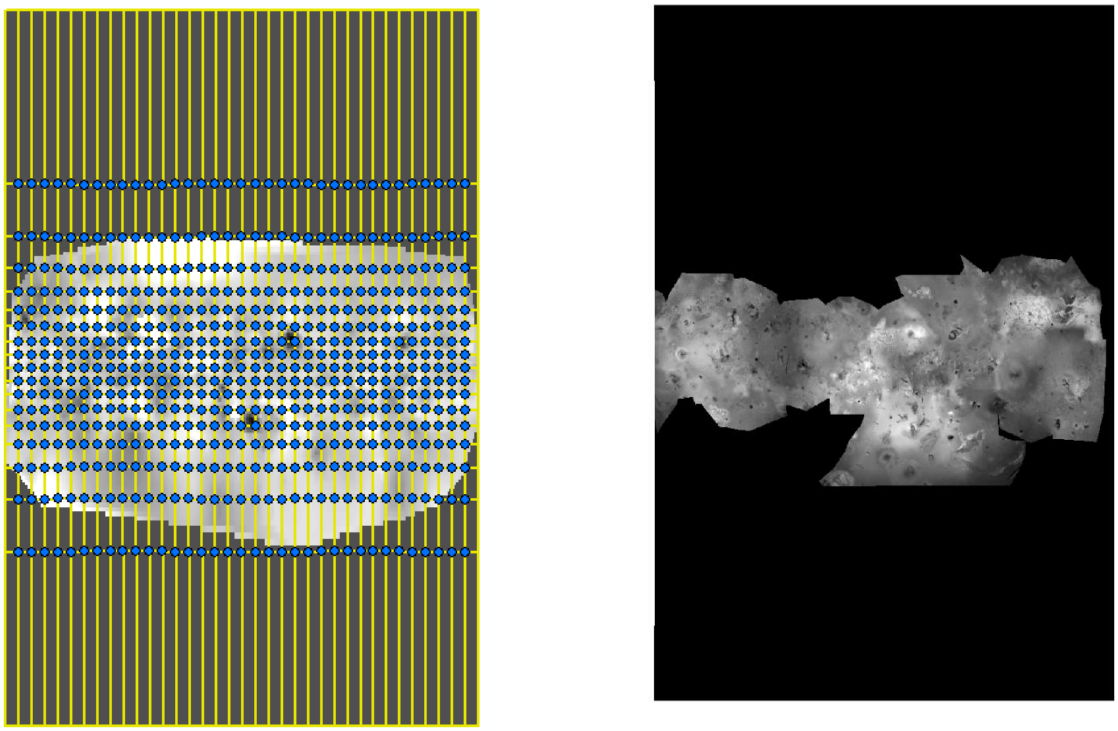

a b

Fig. 1. New Io Cartography based on projections for three-axial ellipsoid using new data: a) GIS- transforming of DEM for part of surface; b) orthomosaic for equatorial part of surface

New Phobos Cartography. I. Karachevtseva, I. Nadejdina, A. Zubarev. Moscow State University of Geodesy and Cartography (MIIGAiK), MIIGAiK Extraterrestrial Laboratory (MExLab). Gorokhovskiy per., 4, office 155, 105064, Moscow, Russia (icar2003@mail.ru; i_karachevtseva@mexlab.ru)

Introduction: We have developed geographic information system (GIS) for Phobos. Our GIS includes orthorectified images and DEM with spatial resolutions of 100 m/pxl [1, 2] as well as various thematic data sets [3]. In future we will include new data such as spectrometry analyses, modeling of gravity field as new results of studies developed in MExLab. Also we will include in GIS new DEM which contains structure of surface features: rims of craters, grooves. This DEM is a result of new Phobos control point network [4, 5].

Mapping of Phobos surface: Using the new Phobos control point network (MIIGAIK, 2012) were updates of the current Phobos shape and map models with developing newest orthomosaic [4, 5]. This recent ortomosaic was used for new Phobos cartography (Fig.1). Also for this mapping we used new projections created for triaxial ellipsoid [6].

Conclusions and Future Work: Our further activities is to make comparative analyses of latest Phobos`s DEMs using GIS-tools. Also, we anticipate to include color images, obtained by co-matching of the Mars Express images.

Acknowledgement: This research was funded by the Russian Government (MEGAGRANT, Project name: "Geodesy, cartography and the study of planets and satellites", contract № 11.G34.31.0021).

References: [1] Willner K. et al. (2010) *EPSL 294*, P. 541-546. [2] Wählisch M. et al. (2010) *EPSL 294*, P. 547-553. [3] Karachevtseva I. et al. (2011) *2M-S^3(IKI)*, P. 57-59. [4] Nadejdina I. et al. (2011), 9 *Conf. of Space Research Institute (IKI) (in Russian) http://d902.iki.rssi.ru/theses-cgi/thesis.pl?id=3025*. [5] Zubarev A. et al. (2012) Problems of remote sensing data processing for modeling of small bodies of the solar system, *Actual problems in ERS Journal, IKI RAS, submitted in April (in Russian).* [6]*http://geocnt.geonet.ru/en/3_axial*

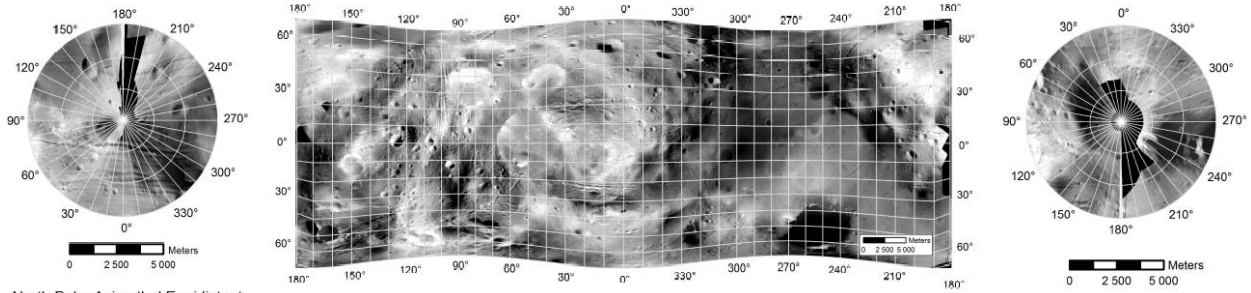

Fig. 1. New PhobosCartography using new orthomosaic and projections for three-axial ellipsoid

Mapping of Candidate Landing Sites for the Future Russian LUNA-GLOB Mission. I. Karachevtseva, A. Kokhanov, A. Bystrov. Moscow State University of Geodesy and Cartography (MIIGAiK), MIIGAiK Extraterrestrial Laboratory (MExLab). Gorokhovskiy per., 4, office 155, 105064, Moscow, Russia (icar2003@mail.ru; i_karachevtseva@mexlab.ru)

Introduction: The Russian LUNA-GLOB mission is to explore the Lunar subpolar areas. Research program was proposed by scientific team from the Russian Space Research Institute of RAS [1, 2, 3]. The general landing area for lander and rover, as well as 3 specific coordinates of landing sites have recently been proposed [4]. Our team is providing cartographic support to the mission and assessments of these candidate landing site on the basis of different types of data.

Sources: For mapping, we used images and Digital Elevation Model (DEM) of the area obtained by LRO: the WAC orthoimages and DEM "GLD 100", LOLA DEM with spatial resolution 30 m per pixel, available NAC images in the sub-polar area and also data from SELENE (Kaguya): images and DEM.

Mapping results. For characterization of the surface, we created some examples of maps using GIS techniques: slope, roughness and hill-shaded relief in various scales. On the base of the LDEM using ISIS software were created about 100 LRO NAC orthoimages, that covers the whole area of target ellipses. We use this data for creating the crater geodatabase. This catalog will allow us to calculate some parameters of lunar surface, including crater diameter, crater cumulative density and spatial density map.

Future works: For better accuracy in characterization of surface on the local level we will create new DEM with high resolution based on LRO NAC stereo images. It will be possible after new surveying of subpolar area by the LRO. New DEMs will be generated using new technology created in MIIGAiK.

References: [1] Zelenyi L. M. (2011) *The Book of Abstracts of the 2-nd Moscow Solar System Symposium (2M-S^3), Space Research Institute (IKI)*, P. 19. [2] Tretyakov V.I. (2011) *2M-S^3, IKI*, P. 116. [3] Petrukovich A.A. et al. (2011) *2M-S^3, IKI*, P. 115. [4] Basilevsky A. T. et al. (2011) *2M-S^3, IKI*, P. 70

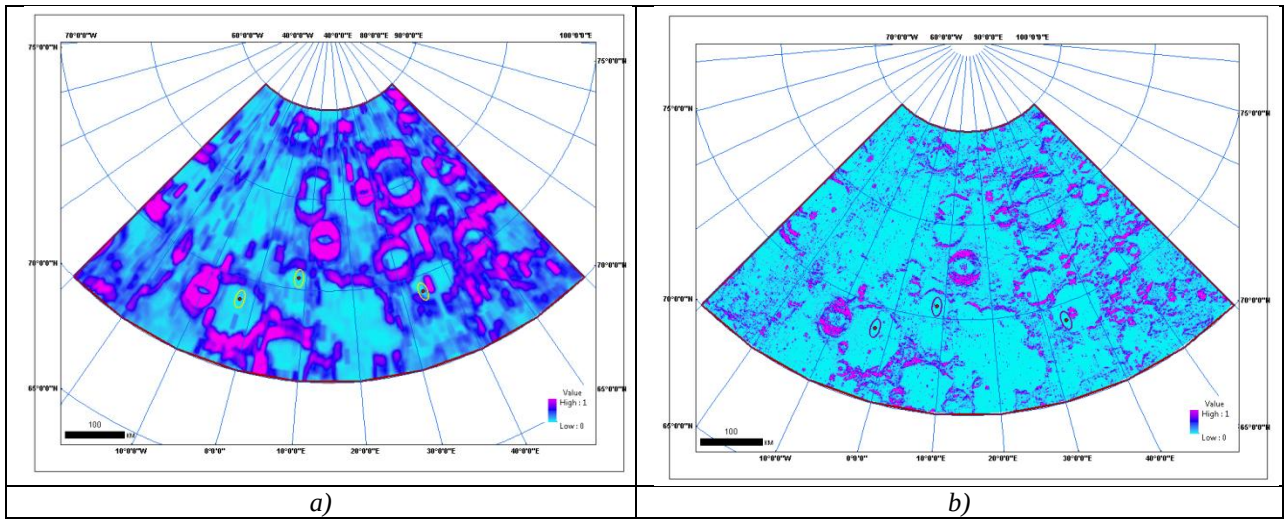

a) *b)*

Figure1. Maps of roughness calculated using different methods: a) Standard deviation of elevations: b) Area ratio (Sourse: "GLD100")

Atlas of Lunokhod-1 Landing Site. I. Karachevtseva, E. Gusakova, M. Baskakova. Moscow State University of Geodesy and Cartography (MIIGAiK), MIIGAiK Extraterrestrial Laboratory (MExLab). Gorokhovskiy per., 4, office 155, 105064, Moscow, Russia (icar2003@mail.ru; i_karachevtseva@mexlab.ru)

Sources: Based on GIS-tools we mapped the landing site of Soviet Lunar mission Luna-17 and traverse route of Lunokhod-1 [1] using new high resolution LRO NAC images and DEM.

Mapping of Lunokhod-1 area. Using GIS tools and results of geoanalyses we created various maps with different description of the Lunokhod-1 area including slopes, topographic roughness, crater spatial densities, types of craters [2]. The DEM and the orthoimage were used to map the Lunokhod-1 with various representations include colored relief, height contours and thematic data from the crater geodatabase. These maps will be present at the meeting as electronic Atlas of Lunokhod-1 (Russian and Enlish versions). Also we will discuss the new result of Lunar nomenclature dealing with Lunokhod-1 area.

Reference: [1] Barsukov V.L. et. al. (1978) Peredvijnaya laboratoriya na Lune Lunokhod-1, Vol. 2. *Nauka* (in Russian). [2] Karachevtseva I. et al. (2011) *The Book of Abstracts of the 2-nd Moscow Solar System Symposium (2M-S[3]), Space Research Institute (IKI)* P. 113-114.

Acknowledgements. This work has been supported by Ministry of Education and Science of the Russian Federation (Agreement № 11.G34.31.0021 dd. 30/11/2010)

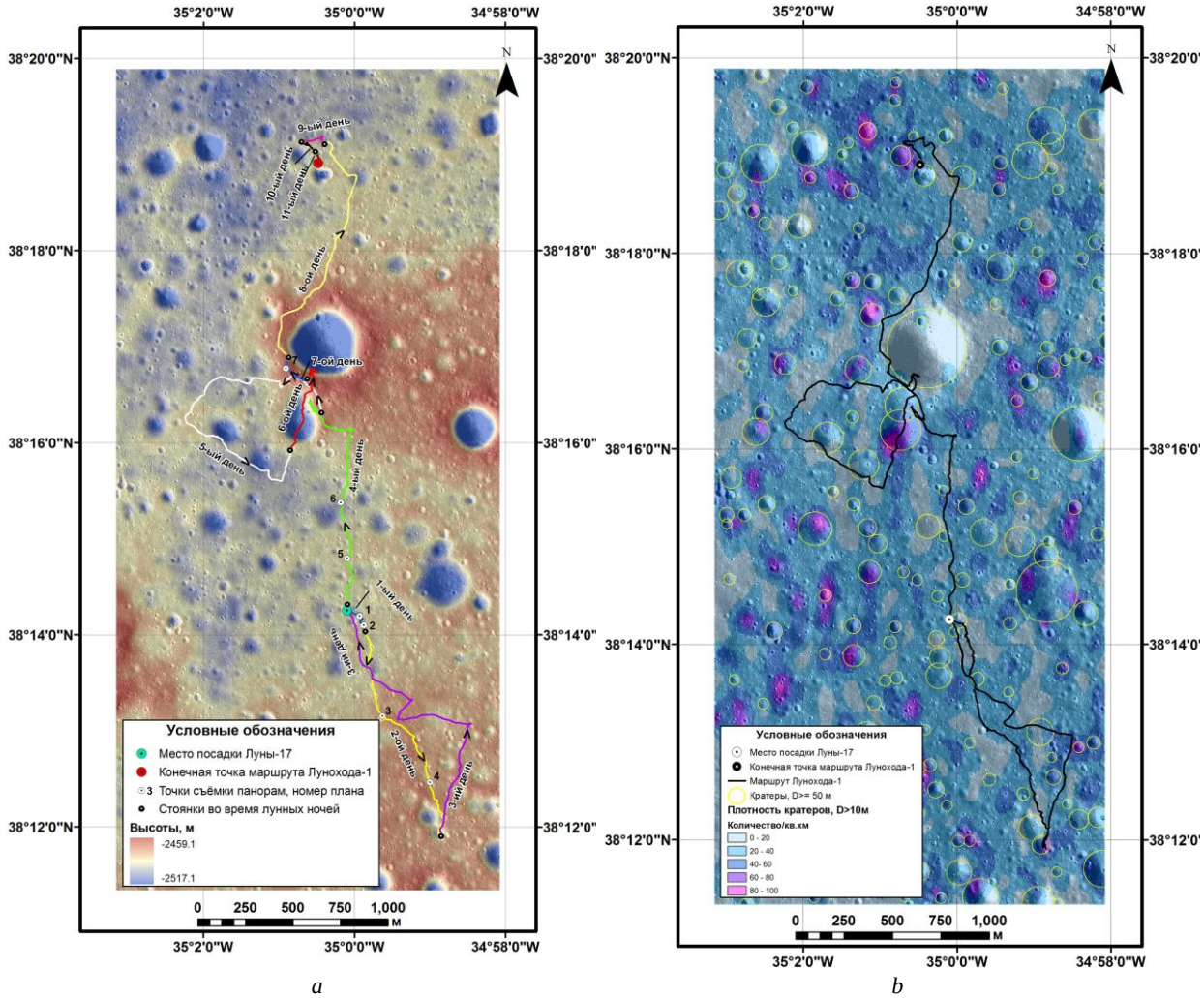

a *b*

Figure 4. Some examples of new maps from Atlas of Lunokhod-1 area : (a) Color shaded relief map; (b) Spatial crater density map (Stereographic Projection, Central meridian -35°, Latitude 38°)

Chasma Boreale: Cryptic Terrain as Indications of Sub-Surface Water and Stages of Geyser Formation

CLOUD, Jordyn, HICKLE, Sara, VIALPANDO, Ravyn, SNYDER, Richard D., Kickapoo High School, 3710 S. Jefferson Ave, Springfield, MO 65807

Morphological and spectroscopic study of geysers in polar regions, using high resolution imagery from HiRISE and CRISM instruments on the Mars Reconnaissance Orbiter, show evidence that geysers go through a series of developmental stages and that these stages can be used to indicate levels of subsurface water. To evaluate this hypothesis, we studied regions of increased geyser activity from the southern hemisphere, which we used to develop a model for the evolution of geysers on Mars. This model was applied to observations of geyser activity in Chasma Boreale to assess their stages of development.

Contrary to the model that the stages of geyser evolution is seasonal (Ness), our observations of the Inca City and Chasma Australe suggest that stage 1 is characterized by dry-venting and fan structures with definite direction; in stage 2 a mixture of ice and mud surrounds the vent and the fans no longer have a clear direction; when the central vent becomes plugged with a mud cap, the geyser has entered stage 3. Our data demonstrates that geysers will not have networks until they enter stage 3; when all venting has ceased the geyser is in stage 4. Rather than rejuvenating and resuming at stage one in the next season as is apparent by the current theory, our data proposes that the geyser will continue its progression from the previous season continue expanding its network by eroding both outwards and downwards creating the cryptic terrain.

In conclusion, our research indicates that the geysers in the northern hemisphere are in earlier stages of development than the geysers in the southern hemisphere. This is most apparent by the lack of spider networks in the former, which occur early in stage 3. The cyclical nature of our model suggests that these geysers are in stage 2 and will eventually progress into the later stages because as mud and ice collect around the opening, this mixture will eventually freeze when the temperature drops, effectively creating the mud cap that initiates stage 3 development. CRISM images show that there is an abundance of bound water and water ice surrounding these geyser formations in Chasma Boreale. Because the lack of a spider network, we conclude that they have not eroded as deep as in the southern hemisphere, and therefore have not exhausted as much of the water content stored in the sub-surface. In addition, lower albedo values in Chasma Boreale (compared to the Inca City geysers) support the hypothesis (Mitrofanov) that the water content in the northern hemisphere is higher than in the southern hemisphere.

Hebes Chasma as a Proposed Mars Mission Landing Site

Bradley Renner and Taylor Biggs, Orting High School

We propose looking for evidence of water south of the Hebes Chasma at -2.8 S, -74.62 W. Our prime science targets are to analyze areas in the channel to find mineral and microbial evidence of water. We chose this area because it looks like channels on earth that are formed by water; the area contains water formed minerals and has not been studied before.

Using the MOLA map we found differences in elevation and concluded that there would be layers exposed revealing the past geologic history of the area. Pyroxenes indicate that the lava flows from the nearby volcanoes flowed here and hardened several times and then something eroded the surface to be able to see these layers. We used the Crism map (confirmed using JCAT) to analyze browse products near our landing site. From the browse products we found that the area was fairly clear of dust which is good for landing. Also near our landing site we found hydrated aluminum phylosillicates and monohydrated sulfates. Phylosillicates are clays and are mostly formed in the presence of water. We also found sulfates which have been known to trap and preserve microbes for thousands to millions of years in salt valleys.

Due to surface scale evidence, mineral evidence and the possibility of microbial evidence, we propose Hebes Chasma as a prime research target for Mars Exploration.